Validating and improving the correction of ocular artifacts in electro-encephalography

Validating and Improving the Correction of Ocular Artifacts in Electro-encephalography

PROEFSCHRIFT

ter verkrijging van de graad van doctor aan de
Technische Universiteit Eindhoven, op gezag van de
Rector Magnificus, prof.dr.ir. C.J. van Duijn, voor een
commissie aangewezen door het College voor
Promoties in het openbaar te verdedigen
op maandag 12 november 2007 om 16.00 uur

door

Joep Johannes Maria Kierkels

geboren te Baexem

Dit proefschrift is goedgekeurd door de promotor:

prof.dr.ir. J.W.M. Bergmans

Copromotor:
dr. G.J.M. van Boxtel

Drukwerk: Universiteitsdrukkerij TUE

This work was kindly supported by the Co-operation Center Tilburg and Eindhoven Universities, (Samenwerkings Orgaan Brabantse Universiteiten).

CIP-DATA LIBRARY TECHNISCHE UNIVERSITEIT EINDHOVEN

Kierkels, Joep J.M.

Validating and improving the correction of ocular artifacts in electro-encephalography / by Joep Johannes Maria Kierkels. – Eindhoven : Technische Universiteit Eindhoven, 2007.
Proefschrift. – ISBN 978-90-386-1664-3
NUR 954
Trefw.: biomedische signaalverwerking / elektro-encefalografie / oogbewegingen.
Subject headings: medical signal processing / electroencephalography / eye.

Validating and Improving the Correction of Ocular Artifacts in Electro-encephalography

Joep Johannes Maria Kierkels

Contents

Chapter 1

Introduction

The electro-encephalogram, or EEG, reflects the electrical activity that is associated with processes in the brain [1]. These brain processes involve the activation or inhibition of neurons in the brain in order to relay relevant information to specialized parts of the brain or to other parts of the body. Associated with these activations and inhibitions are several mechanisms that involve the transport of electrically charged elements in the vicinity of the neurons. Because electrical activity of the brain is propagated throughout the body by means of volume conduction [2], it can be recorded non-invasively on the scalp of a person. The variations in electrical potential on the scalp, due to the brain activity, are referred to as the EEG.

The EEG has proven to be a valuable tool that can assist in studying the functioning of the brain. Over the past decades, it has been shown that the EEG contains relevant information for diagnosing several neural disorders [3-6], and that the EEG can be used as a means of communication, as in brain computer interfaces, BCIs [7].

Unfortunately, there are other sources of electrical activity within the human body, like muscles and eyes, whose electrical activity is also detected, on top of the EEG [8-11]. A raw EEG will thus contain electrical fluctuations caused by actual brain activity and electrical disturbances called artifacts.

1.1 Artifacts

Because the brain is always active, the EEG is an ongoing, continuous signal that is never completely silent. Similarly, artifacts will always occur because, like the brain, some other biological sources of electrical activity are never fully silent, e.g., eyes, heart and muscles. As a result, artifacts and EEG will always be recorded simultaneously and EEG research should therefore always consider signal validation, i.e., how well we measure what we want to measure [12].

In the upper part of Figure 1.1 it is illustrated how electrical activity of the brain and electrical activity of the eye is conducted to a position on the scalp. On the right a stylized impression of a corresponding EEG recording is shown.

When the EEG is being recorded, one would like to record exclusively the electrical activity of the brain. Unfortunately (from a recording point of view) it

is not possible to temporarily 'shut down' either the electrical activity of the brain or the electrical activity of the eyes during an experiment, as is illustrated by the crossed arrow going left. For this reason, other methods have been, and are being, developed to separate these electrical activities, as is illustrated by the arrow going right.

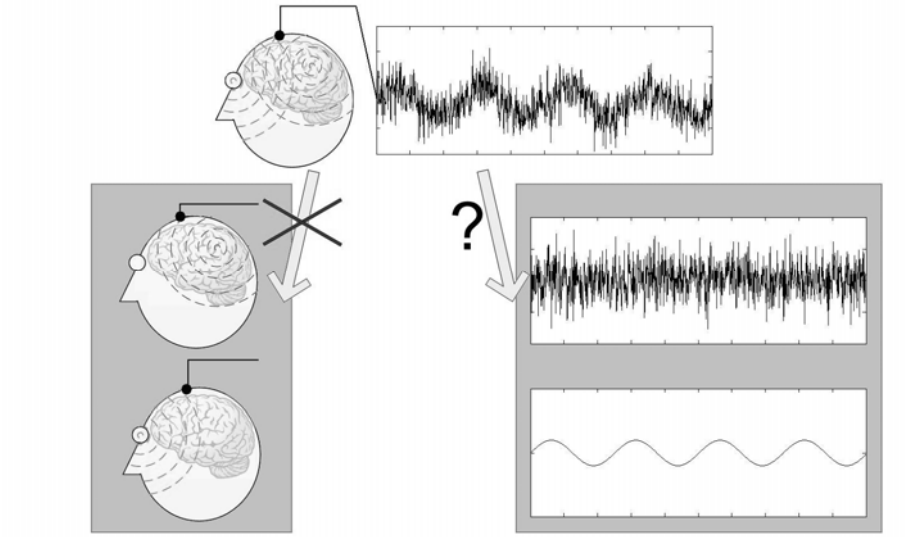

Figure 1.1: Upper part: Illustration of volume conduction of electrical activity through the head, together with an impression of the raw EEG.
Lower part: Shutting down either of the causes (eyes and brain) of the electrical activity is not possible. Therefore, alternative solutions are needed to estimate the separate effects that brain and eye activity have on the EEG.

For many EEG-based applications, artifacts can be a great nuisance in the process of extracting valuable information from the raw EEG, and therefore considerable effort has been spent on the removal of artifacts. One difficulty in artifact removal is the initial detection of artifacts. Some artifacts may have similar or smaller amplitude as the EEG itself, which can make them difficult to detect.

Among the possible sources of EEG artifacts, it is common to distinguish between non-biological sources and biological sources. The non-biological sources include amplifiers, power lines, electrode pops, and movement. The biological sources are electrically active tissues or cells in the body, other than the neurons of the brain. By carefully controlling the setup in which the EEG is recorded, the impact of the non-biological sources, as well as the impact of some of the biological sources, can be greatly reduced, e.g., by providing a comfortable chair during experiments or by providing a chin-support to reduce head movements. Unfortunately, this often involves compromising on issues like the freedom of movement of the person whose EEG is recorded.

The impact of some other biological sources, e.g., the heart, cannot be reduced by changing the recording setup. Among these sources are also the eyes. Because the eyes are located close to the brain, the electrical effects associated with eye movements and blinking are usually the major artifacts in an EEG recording. Especially for these artifacts of ocular origin, artifact removal methods are thus essential.

Currently, ever more attention is given to EEG-based applications which require that artifacts are very accurately removed prior to EEG analysis. For such applications, like single-trial based neuroscience research or brain-computer interfaces, the tolerance to artifacts is small and the need for accurate ocular artifact removal is large.

In response to this need, this thesis provides a detailed overview and comparison of existing ocular artifact removal methods and their accuracies, and develops a new method with unprecedented accuracy.

1.2 Artifact removal

Artifact removal is either done by artifact rejection or by artifact correction. Rejection implies that segments of data that contain significant artifacts are removed and excluded from further analysis. Correction implies that these segments are inspected more carefully and that the influence of the artifact is estimated and subtracted from the data. Note here that artifact detection is an element of both rejection and correction. For rejection, one needs to detect artifacts prior to being able to reject segments of data. For correction, it is equally important to determine which segments of the data require correction. Additionally, once the artifact is estimated and removed from the data, artifact detection is required to determine whether or not the estimate was accurate.

1.2.1 Artifact rejection

Assuming accurate artifact detection, rejection can ensure that all significant artifacts are removed from the data. Because artifact rejection is easy to implement, is intuitively simple, and often is sufficiently effective, it currently is the most frequently used method for handling artifacts [13].

However, for some EEG studies rejection cannot be used because the exclusion of parts of the data is unacceptable. If the relevant information in the EEG is limited to a very small period of time, rejection of this period because of a coinciding artifact is not acceptable. In BCIs for example, ultimately one would like to control a computer by a single thought. If the electrical activity related to this thought is obscured in the data by an artifact, rejecting the segment of data would delete all essential information. Furthermore, if artifacts occur very frequently, rejection may be impractical because as a result of rejection either

only a small amount of data remains, or the duration of an experiment is significantly increased in order to obtain enough usable data.

In fact, because some artifact sources, like the eyes, are never electrically silent, artifacts can never fully be avoided and rejection always involves the (subjective) selection of a threshold value regarding which artifacts are rejected and which are ignored.

1.2.2 Artifact correction

When correcting for artifacts, an ideal correction method will remove the artifact and leave the EEG unaffected. In principle, artifact correction can be used for all EEG-based studies, including the ones in which artifact rejection is unacceptable or impractical.

In this thesis, the subject of correction of ocular artifacts, for which a large number of correction methods has been developed, will be studied in detail, and several frequently used correction methods will be evaluated. In Section 1.3 a brief summary on the biophysical origin of the EEG is given, which will briefly explain why the recording of artifacts is unavoidable and why especially the ocular artifact is observed so often, and is so prominent in EEG recordings. A more elaborate overview on this can be found in [14].

Often, an electro-oculogram, EOG, is recorded simultaneously to the EEG. The EOG reflects the electrical potential as recorded on the skin very close to the eyes. It is frequently used to detect eye movements, blinks and gaze direction, but also to detect and correct ocular artifacts in the EEG.

In the following sections, existing ocular artifact correction methods will be discussed. The majority of these methods can be classified as either an EOG-based correction method or a components-based method.

The EOG-based correction methods scale EOG recordings in order to estimate ocular artifacts in the EEG.

In general, eye movements and blinks cause fluctuations in EOG recordings that are of significantly higher amplitude than the fluctuations they cause in EEG recordings. Scaling and subtraction of the EOG from the EEG is therefore frequently used in an attempt to remove the low amplitude fluctuations from the EEG. A criticism against the use of the EOG-based correction methods is the fact that EOGs will also contain artifacts and that they may be affected by brain activity. Traditionally, the fact that an EEG recording contains ocular artifacts has been named 'backward propagation' because the ocular electrical activity is conducted to the back of the head where the EEG is recorded. The term 'forward propagation' is used to indicate the opposite, i.e., cerebral electrical activity being conducted to the front of the head where the EOG is recorded. When the EOG is scaled and subtracted from

the EEG, artifacts and cerebral activity in the EOG may corrupt a corrected EEG.

The components-based correction methods are an alternative solution to the correction of ocular artifacts. These methods do not (necessarily) require recording of the EOG and also their accuracy is not (implicitly) affected by forward propagation. Under the assumption that ocular electrical activity and cerebral electrical activity are either uncorrelated or independent, components-based methods convert simultaneously recorded EEGs at different scalp positions into a set of components in which the relation between components is specified in terms of statistical dependence or correlation. Some of the components that are obtained this way turn out to reflect ocular electrical activity. By eliminating these components and then reconstructing the original signals, the artifact is removed from the recording. Currently, it is still not clear which statistical assumption results in the most accurate ocular components, and validating whether the ocular components are indeed only affected by ocular electrical activity or whether they contain cerebral activity is difficult.

Thus, both the EOG and the ocular components can be affected by electrical activity of the brain. Whereas some studies regarding ocular artifact correction accuracy argue in favor of EOG-based correction methods, [15;16], other studies indicate the opposite [17].

No ocular artifact correction method existed until recently that estimates ocular artifacts based on observations other than electrophysiological signals. The detection of eye movements and blinks is not restricted to measurement of the EOG but can also be done by camera observation, or by using magnetic coils. In this thesis, a new approach to the correction of ocular artifacts is proposed that is fundamentally different to correction by EOG-based and components-based methods. By using a non-electrophysiological method to detect eye movements and blinks, the difficulty of forward propagation and artifacts in the EOG can be by-passed which can in principle result in a better correction of ocular artifacts. The concept behind the use of the eye tracker is illustrated in Figure 1.2.

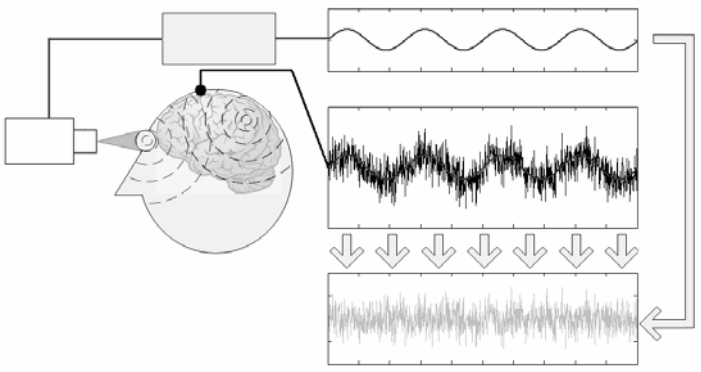

Figure 1.2: Illustration of the eye tracker solution to the correction of ocular artifacts in the EEG, with an impression of signal morphology on the right. The eye tracker only records ocular information, which can be converted to an accurate estimate for the ocular artifact. Combined with the electrode recording which contained both EEG and artifact, an accurate estimate of the EEG is derived.

With an eye tracker, eye movements and blinks can be monitored, as is discussed in Appendix A. This monitoring is expected to yield valuable information which can be used to estimate and correct the artifacts. In the following chapters it is shown that the suggested correction method consistently estimates the ocular artifact more accurately than other methods. A difficulty related to ocular artifact correction concerns the validation that correction has indeed removed the ocular artifact and has not affected the EEG. Because it is impossible to record the electrical activity exclusively related to cerebral activity, exact validation of the corrected data is impossible. So, considering that accurate correction is required for modern EEG applications like BCIs, and considering that exact correction validation on experimental data is impossible, a different way to validate correction methods should be used. In Chapter 2 of this thesis, a model for simultaneous simulation of cerebral and ocular activity is presented. The model can assist in validating correction methods because, contrary to the situation for EEG recordings, such a model enables comparing corrected data to purely cerebral activity.

The remainder of Chapter 1 will first briefly summarize the origin of electrophysiological signals in general and the EEG and the EOG in particular. Then, Section 1.5 will elaborate on several frequently used EOG-based and components-based correction methods and Section 1.6 will indicate how the accuracies of different corrections methods can be compared and evaluated. Finally Section 1.7 will preview the other chapters of this thesis.

1.3 Biophysiological origin of the EEG and the EOG

Biopotentials are electrical signals produced by living tissues. A number of cells, tissues and organs are capable of generating these electric signals. Because the body which surrounds these sources of electricity conducts these signals, their occurrence can be recorded anywhere in or on the body in the form of biopotentials. A wide range of medical applications use non-invasive recordings of these biopotentials to provide information on the processes in the body. Perhaps the best known application is the use of cardiac electrical activity in the electrocardiogram, ECG, to detect heart rate and heart rate variability.

For an adequate interpretation of the electrical activity of a specific part of the body, e.g., the brain or a specific muscle, it is required that this part's electrical activity is recorded with minimal interferences. Such interferences can be caused by external noise sources, by amplifiers or by sources of electrical activity in the body other than the desired source. When recording electrical activity of the brain in the EEG, all sources of electrical activity other than the cerebral sources are considered to be sources of interference, which deteriorate signal quality. Depending on the source of interest, a source's electrical activity may be either relevant or artifactual. Whereas cardiac electrical activity is relevant in the ECG, it is a cardiac artifact in the EEG.

The main way to focus on electrical activity of a specific source, with as little interference as possible, is to record the electrical potential on a place on the skin near the location of that source. If no other electrical sources are near to the recording site, the electric potential will generally be an adequate representation of the desired source's electrical activity. Unfortunately, if two electrical sources are close to each other or if an interference source is stronger than the desired source, the recorded signal will clearly reflect both sources. In the human head, the main electrically active sources are the neurons in the brain and the eyes.

When the electrical potential is recorded on the scalp, the potential changes due to brain activity are hard to detect because the electric signals of neurons are attenuated when they pass the skull, which has low electrical conductivity. Changes in electrical activity that are detectable on the scalp should therefore originate from sufficiently strong electrical activity in the cortex. This implies that the electrical activity of a single neuron is nearly impossible to detect on the scalp. Only combined effects of groups of synchronously activated neurons can be detected. Moreover, cerebral electrical activity should be of sufficiently long duration in order to be recordable by the EEG equipment. Action-potentials of neurons do not last sufficiently long to be detectable in scalp EEG recordings. Typically, only synaptic electrical activity at the connections between neurons has a long duration that is sufficiently long for scalp EEG recording [18]. Thus, on the scalp, only the electrical effects of groups of

parallel oriented, synchronously active neurons is sufficiently large to be detected [19].

Potential changes due to the eyes are caused by a difference in electrical charge between the cornea and the retina [14]. Electrically active cells on the retina keep a charge-difference intact, causing the cornea to be positively charged with respect to the retina. When referring to both the positively and the negatively charged parts of the eye, the term 'corneo-retinal dipole' is commonly used. The cells on the retina are sensitive to stimulation by light and therefore the difference in potential as measured across the eye also depends on the environment. When the eye is briefly stimulated by a bright flash, the (change in) electrical activity of the retina is recorded in the electro-retinogram, ERG. However, under controlled and stable lighting conditions, the difference in electrical charge between cornea and retina is fairly stable. When the eyes do not move and blinking does not occur, the stable retinal activity does will not cause any fluctuations in the EEG and the EOG.

Eye movements change gaze direction, and therefore cause the position of the cornea and the retina with respect to the rest of the head to change. This affects the ocular electrical potential. During blinking, the eyelid moves over the cornea and, as suggested in [20], 'short-circuits' the EOG electrode to the positively charged cornea. The changes in electrical potential due to eye movements and blinking are both clearly visible in the EOG. However, there is also an interaction between the causes of ocular artifacts that were just described. During blinks small eye movements occur [21], and during eye movements, especially vertical eye movements, small eyelid movements occur [22]. The electrical fluctuation in the EOG that is caused by small eyelid movement during vertical eye movements is known as the rider artifact [20].

In Figure 1.3, the effects of blinks and eye movements on an EEG and an EOG are illustrated. The upper two plots illustrate 1 s of simultaneously recorded EEG and EOG during which no significant eye movements or blinks occur. The middle two plots show the effect of two brief eye movements, at approximately 0.3 s and 0.9 s. Note that the change in amplitude that is caused by the movement is more prominent in the right plot because the EOG is recorded closer to the eyes. The lower two plots illustrate the effect of a blink, starting after approximately 0.2 s. Again the amplitude change is more prominent in the right plot.

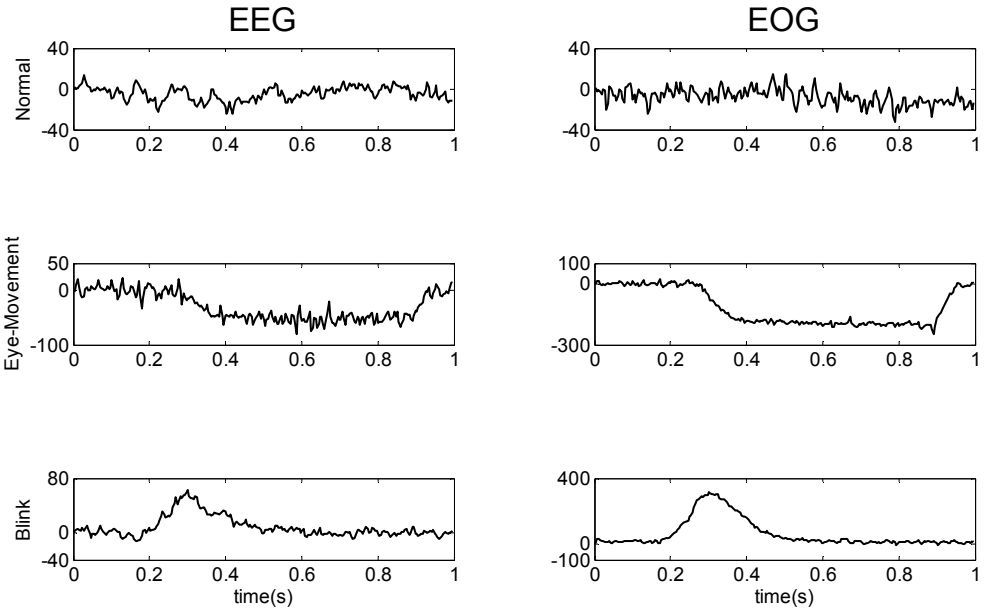

Figure 1.3: Illustration of the effects of eye movements and blinks in the EEG recording and in the raw EOG. All y-axis scalings are in μV.

The history of the EOG, as a way to detect eye movements, was described already in [23]. Currently the EOG is still often used to determine ocular orientation and gaze direction.

In the data segments of Figure 1.3, it can be seen that the artifacts have large amplitude compared to the cerebral activity, even when detected by an EEG electrode positioned not too close to the eyes. Furthermore, Figure 1.3 shows that changes in electrical potential that are caused by eye movements differ from the changes caused by blinking.

The frequency range of the cerebral activity, visible mainly in the upper two plots, also appears to differ from the frequency range of the ocular artifacts. It is well known that when different biopotentials are recorded on the surface of the body, they may span different, sometimes partially overlapping, frequency ranges, and that they may have different amplitudes. Table 1.1 summarizes some general properties of biopotentials. These properties relate to recordings on the surface of the body, closest to the biopotentials own particular electrical source, e.g., the electro-myogram, EMG, is recorded directly above skeletal muscle. When the brain is briefly stimulated e.g., by a bright flash, a loud click, or a small electrical shock, the detected response of the brain to such a stimulus is called an evoked potential, EP. Because the characteristics of such evoked potentials differ from the characteristics of EEG as recorded when no specific actions are performed during the recording, often called background EEG, the evoked potentials are mentioned separately in Table 1.1 .

Table 1.1: Characteristic properties of bio-electric signals [24]

Signal	Amplitude range	Frequency range (Hz)
EEG	2 μV–100 μV	0.5-100
EEG (EP)	0.1 μV–20 μV	1-3000
EOG	10 μV–5 mV	0-100
EMG	50 μV–5 mV	2-500
ECG	1 mV–10 mV	0.05-100

The EEG clearly has the lowest amplitude out of all these signals, making it difficult to detect. Furthermore, the frequency range of the EEG overlaps with the frequency range of other biopotentials and hence of artifacts, also making detection in the frequency domain difficult [25].

1.4 Recording the EEG

The most common standardization of EEG-electrode positioning is the 10-20 system [26].

The electrode positions in this system are based on relative distances with respect to landmark points on the scalp. The midline of the head is defined as the line running over the scalp that connects the nasion and the inion. At 20% of the distance between these points, electrode positions are defined. A similar segmentation, but with 10% distances, is defined for positioning the electrodes away from the midline. Extensions to this 10-20 system, which allow for a denser electrode positioning, are the 10-10 system [27] and the 10-5 system [28]. In Figure 1.4, a typical recording setup is shown in which EEG electrodes are positioned according to the 10-20 system, and six additional EOG electrodes are positioned around the eyes.

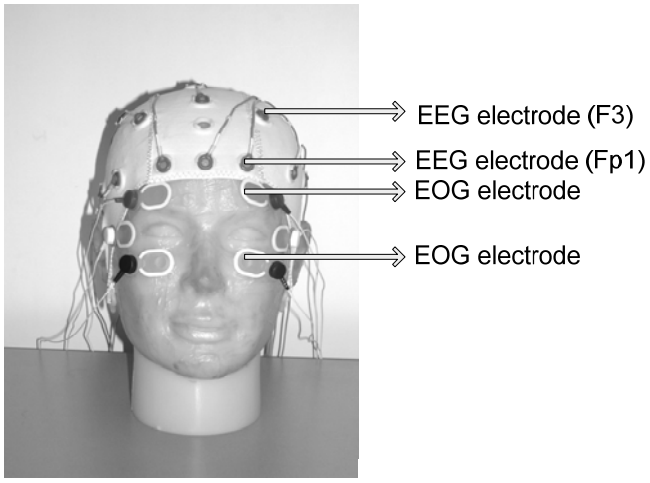

Figure 1.4: Frequently used electrode positioning. EEG electrodes are placed according to the 10-20 system, and are held in position using a special head-cap. EOG electrodes are placed around the eyes.

To record one electro-physiological signal, at least two electrodes are required, because the electrical activity picked up by one electrode, needs to be referenced against the activity that is recorded at a reference position [19]. The choice of this reference position is very important because only the difference in electric potential between the two electrodes is defined. The reference electrode is often positioned on a part of the scalp that has almost no electrical activity and thus is far away from brain, eyes and muscles. An electrode attached to the earlobe or the mastoid can be used for this. To focus on local differences in electrical activity, the reference electrode can instead be placed close to the other electrode. Frequently used references include averaged reference and common reference. In average referencing, the electrical activity as picked up by a specific electrode is referenced against the average electrical activity of multiple simultaneously recorded electrodes, including that specific electrode. For common referencing, all electrodes are referenced to the same specific electrode, e.g., a single mastoid electrode or a specific electrode positioned at Cz. A closely related common reference is the linked mastoid reference. For this reference, two electrodes attached to both mastoids are connected, which forces the electrical potential at both mastoids to be the same. Theoretically such a link between electrodes has been found to affect the potential distribution over the whole scalp [19], but in practice such effects on potential distribution were proven to be negligibly small [29-31]. The averaged mastoids reference is an alternative to the linked mastoids reference that does not physically link to mastoid electrodes, but 'digitally links' them using signal averaging.

Because the effect of the choice of reference on EEG recordings is beyond the scope of this thesis, all EEG recordings and simulations will be referenced to

averaged mastoids as this is a frequently used reference with little electrical activity. Note however that if the EEG is recorded using any common reference, including averaged mastoids, the recorded signals can be re-referenced afterwards to any other reference position or to average reference. An elaborate discussion on the optimal location of a reference electrode is given in [32].

Most of the power in the frequency spectrum of an EEG is restricted to frequencies of up to 50 Hz. When recording an EEG, the frequency spectrum of the recorded signal should be considered prior to digitization. To detect relevant brain activity while avoiding aliasing, a low pass filter is often applied with a cut off frequency around 50Hz. The sampling frequency of the EEG should then be at least 100 Hz. Suggestions have been made to record the EEG at much higher frequencies [33]. For certain types of EEG recordings, this is already common practice as the frequency spectrum of evoked potentials can contain frequency components up to some kHz. The DC value of an EEG recording depends on many things, including the impedances of the signal- and the reference electrode. These impedances are not indicative of brain activity and therefore the DC of EEG recordings is usually removed prior to further signal processing.

1.4.1 Trial-based EEG

EEG-based experiments are used in a wide range of studies, both clinical and fundamental. Studies include the diagnosis of sleep disorders and attention deficiency disorders, the detection of epileptic seizures, and the cortical mapping of the brain and the search for neuronal connections within the brain.

In some of these studies, special 'events' are presented to a participant during the recording. Examples of such events are clicks, flashes or electric shocks that stimulate respectively the auditory, the visual and the sensory part of the brain. Usually, a sequence of multiple, often similar, events occurs during one recording session. Often, however, a visual inspection of the raw EEG does not reveal fluctuations that are clearly caused by the event. On first sight the raw EEG of studies with events may thus appear similar to the raw EEG of studies without events. This is because the major contributor to the electrical fluctuations in the raw EEG is the ongoing brain activity which is not related to any specific stimuli. The part of the raw EEG that is caused by this ongoing brain activity is commonly referred to as the background EEG.

To inspect more thoroughly whether or not an event causes detectable fluctuations in the raw EEG, a common technique is to average over multiple segments of the raw EEG. These segments (or trials) are extracted from the raw EEG in such a way that they are aligned with respect to the event, which is usually done by selecting segments that start (and end) at fixed intervals

prior to (and after) the event occurrences. As a result of this segmentation, each single event will occur in only one trial.

When averaging over multiple trials, it is generally assumed that each separate trial contains two different sorts of electrical fluctuations. The first sort is the electrical fluctuation which is the result of the stimulus. The second sort is the electrical fluctuation which is the result of other brain activity. Usually, only the stimulus-related electrical fluctuations are considered to be relevant when analyzing the brain response to a stimulus. If multiple trials are averaged, it is often assumed that the stimulus-related brain activity is deterministic and fluctuations of exactly the same shape and amplitude can be seen in the EEG each time a stimulus is presented. The other electrical fluctuation which is recorded in each trial is, by definition, not related to the event. If the averaged trial shows electrical fluctuations that do not decrease in amplitude if more trials are used for averaging, then this is evidence that the event does indeed cause detectable fluctuations in the raw EEG. Clearly, such fluctuations are best detectable in the raw EEG that is recorded closest to the region of the cortex that processes the event. The exact shape of the waveform that can be seen in the averaged trial varies with event properties. To illustrate this, a brief example is used.

If a participant hears a series of identical clicks, a common assumption is that these clicks result in trials with identical click-related brain responses and EEG waveforms. Averaging over all trials would result in an estimate of the click-related brain response. If instead, a series of identical clicks with different loudness was heard, it is expected that the click-related brain response of this second series would differ from the first series simply because the brain is processing different stimuli. When a series of clicks is heard in which one single click differs in loudness from all other clicks, the 'deviant' click has a different click-related brain response. However, this difference is not only caused by the different click loudness, but also by the fact that the participant will notice that this click is deviant. As a result, the brain response and the corresponding EEG waveform for the deviant click are not only expected to differ from the responses for clicks of other loudness, but are also expected to differ from the brain responses corresponding to a series of such deviant clicks[1]. The difference between the waveform that corresponds to the deviant response and the averaged waveform for a series of such deviant responses is usually attributed to the mental process of recognizing deviancies.

[1] Note that this example overlooks the fact that even in a series of identical clicks, the brain response may differ between consecutive clicks [142]. Like the deviant click in the example, a click which follows a click of equal loudness may also trigger a mental process of recognition, now detecting that the click was identical.

The click-related waveforms will thus contain a component that is determined exclusively by event-properties, e.g., click loudness. These components are usually called evoked potentials, or EPs. Furthermore, waveforms may contain an additional component that is caused exclusively by an internal event, e.g., the recognition that a click was different from previous clicks. These latter components are called event related potentials, or ERPs.

Table 1.1 indicated that the amplitude of evoked potentials is low compared to the amplitude of background EEG. This low amplitude is what makes detection of EPs (and ERPs) in the raw EEG difficult.

Differences in shape, amplitude and timing of EPs and of ERPs are known to exist between different trials, and methods to compensate for these differences in the trial-averaging process have been developed. However, ultimately each event produces a unique event-related potential, and averaging over multiple events will not fully succeed in extracting the exact EEG response to this unique event. Extracting the event-related potential that results from a unique event should thus be performed on a single-trial basis.

Making a distinction between what is an event-related potential and what is background EEG in a single trial is a difficult and highly challenging problem, even without ocular artifacts. Therefore, it is crucial that any ocular artifact that coincides with the event-related potential is accurately removed.

1.5 Correction methods

A great number of ocular artifact correction methods have been described in literature.

As a yardstick to see how often correction methods were used in EEG-based research, a scan of all articles which appeared in Clinical Neurophysiology over a 22 month period, from January 2005 to October 2006, was performed. Articles which relate to detection of evoked potential, EPs, or event-related potential, ERPs, were marked because in principle these require accurate artifact removal [34]. For these marked articles, 73 in total, it was checked whether or not ocular artifacts are mentioned, whether data with artifacts is corrected or rejected and when appropriate, which correction method is used. Results of this scan are shown in the left pie-chart in Table 1.2. The right pie-chart indicates which correction methods were used in case artifact correction was applied.

Table 1.2: Two pie charts showing how frequently some ocular artifact handling techniques are used. Data are obtained from all EP/ERP related articles in "Clinical Neurophysiology" over a 22 month period from January 2005 to October 2006. Left: distinction between correction/rejection. Right: Distinction of methods within the correction slice of the left plot. The abbreviations for these methods and their algorithms are explained in Section 1.5.3 and Section 1.5.4.

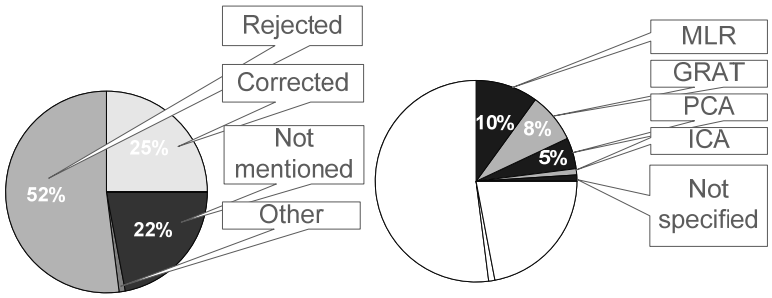

From this brief scan, the first somewhat striking result is that despite the attention that ocular artifact correction has received in literature, artifact rejection is still often preferred. This can, most likely, be explained by the fact that rejection is the most straightforward way to handle ocular artifacts. If this way of handling artifacts provides the accuracy that an author considers sufficient, and if the consequences of losing data and trials are acceptable, then artifact removal is often used. A second result is that amongst the studies that do correct for artifacts, older methods like multiple linear regression, MLR, and the Gratton method [35], GRAT, are more popular than younger methods like Principal Components Analysis [36], PCA, and Independent Components Analysis [37], ICA. On the one hand this may indicate that researchers are reluctant to replace familiar correction methods for new ones, but on the other hand this may also indicate that no new correction method has managed to fully convince the general users of its added value. A third overall result from this scan clearly is that no one correction method exists, either young or old, that satisfies all general users.

Sections 1.5.3 and 1.5.4 will explain the principles behind the correction methods that are found in this scan, and stress what their key distinctions are. Apart from the methods observed in the scan, two more correction methods will also be discussed. These two additional correction methods both consider and use the time structure that is observed in EEG recordings, whereas the methods from the scan do not (specifically) consider this structure.

1.5.1 Calibration

Some ocular artifact correction methods can only be used if the experiment is preceded by a calibration period. During this period, the EEG (and the EOG) is recorded, and eye movements and blinks occur.

Many of the correction methods that require a calibration period also require that during this calibration period, eye movements are made in a predetermined fashion. This can easily be achieved by having a subject focus at different points on a screen that is placed in front of him. Similarly, a subject can be instructed to blink frequently and regularly.

From the ocular artifacts that are observed during the calibration period, the effects of blinks and eye movements on the EEG are estimated. Under the assumption that these effects are identical during the calibration and during the subsequent experiments, the data of experiments can be corrected for artifacts.

The requirement of a correction method that a calibration period precedes the experimental protocol has the advantages that

- after calibration, the experimental data can, in principle, be corrected online and in real-time,
- the influence of background EEG on artifact correction can be reduced by aligning identical eye movements and averaging them in a way similar to the alignment of trials as described in Section 1.4.1, and
- the experiment-related brain activity does not occur during the calibration period and therefore also cannot affect ocular artifact correction,

but also has the disadvantages that

- it limits the possible studies for which the method can be used, as such a calibration period is for example hard to include in sleep studies,
- the ocular artifacts that are the result of compulsory eye movements and blinks may differ in amplitude and morphology from the voluntary ocular artifacts that are observed during experiments,
- the correction method can only be used on data with the required calibration period, whereas many (previously recorded) data may not contain such a calibration period.

Other correction methods do not require such a calibration period, and still others can be used either with or without calibration period

1.5.2 Modeling the raw EEG

The raw EEG, $r(t)$, at time instant t is modeled as a combination of ocular and cerebral sources. The 'mixing' of ocular and cerebral activity is linear because

the electrical field due to two electrical charges is merely the sum of the two separate electrical fields. Because the total number of neurons in the brain is very large, the part of $r(t)$ which is caused by cerebral activity (combined over all neurons) is commonly modeled by one term, $c(t)$. As a result $r(t)$ is modeled as

$$r(t)=\sum_{k=1}^{K}\gamma_k \cdot \varepsilon_k(t) + c(t), \qquad (1.1)$$

with K the number of ocular artifact sources and γ_k determining the contribution of the k^{th} ocular source to $r(t)$.

The K parameters γ are denoted in (1.1) as time-invariant. However, physiological factors can change the conductive properties of human tissues, e.g., body temperature changes and sweating. Changes in these physiological factors are mainly only slowly varying during EEG recordings and are therefore generally assumed piecewise constant. This implies that the parameters γ can be considered constant for a limited period of time. The length of this period varies, however, greatly between different studies. When estimating the parameters γ, an alternative to the assumption of piecewise constant parameters is adaptive parameter tracking in which changes in parameter value can be estimated adaptively, and changes over time are tracked. Such will be used in this thesis.

Often, as in (1.1), it is assumed that measurement noise is very small and can be neglected. To meet this assumption, adequate EEG recording equipment is used, with peak-to-peak noise for low frequencies (coinciding with the EEG frequency content) below 1 μV.

1.5.3 EOG-based correction Methods

Many of the existing correction methods, especially the older ones, use one or more EOG recordings in combination with regression as a reference on what part of $r(t)$ to remove [38;39]. Such methods will be referred to as EOG-based correction methods. Key differences between these correction methods relate to the EOG electrode positioning and to assumptions regarding the spectrum of the EEG. The block diagram in Figure 1.5 illustrates this and highlights some of the main differences.

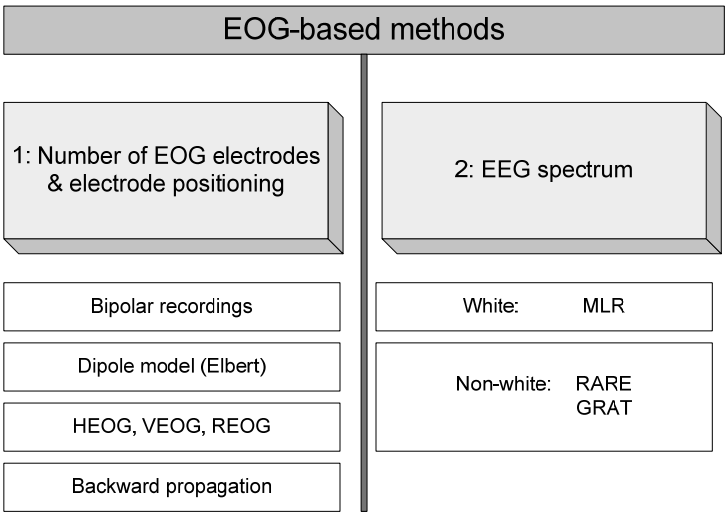

Figure 1.5: Block diagram illustrating key issues for EOG-based correction methods.

Regarding electrode positioning, several studies have examined how, and how many, EOGs should be recorded to get an optimal ocular artifact correction [39]. It was shown analytically [40] that using three EOG recordings is optimal to get an accurate estimate of the ocular artifact. Under the assumption that the source of ocular artifacts can be modeled as a dipole, [40] shows that three EOG recordings are needed to capture all degrees of freedom for dipole rotation. The assumption that dipole strength remains constant does not reduce this number of EOGs, because each EOG is only an adequate measure for changes in dipole orientation and not a direct measure for dipole orientation. In contrast to this analytic result, many of the current EOG-based correction methods only use two EOG recordings, as this appears to be sufficient for many applications. EOGs are commonly displayed as the difference in electrical potential between two electrodes that are both close to the eyes. This means that the reference electrode, as discussed in Section 1.4, for an EOG usually is close to the other electrode. By using this electrode positioning, the effect of the eye movement is accentuated because eye movements cause changes in electrical potential that are of opposite polarity on both sides of the eye. Furthermore, small artifacts in the EOG may be reduced if these artifacts are recorded on both electrodes. Recordings with both electrodes close to each other are commonly referred to as bi-polar, whereas recordings with a distant reference electrode are referred to as mono-polar. As a result of the bi-polar EOG recordings, two EOG electrodes are required to monitor one EOG recording. The difference in potential between two electrodes that are positioned above and below one eye is commonly referred to as the vertical EOG, VEOG. In the VEOG, blinking and vertical eye movements are very prominent. Perpendicular to the imaginary line that connects the two VEOG electrodes is a line that connects two other EOG

electrodes, positioned next to the eyes. The difference in potential between these electrodes is referred to as the horizontal EOG, HEOG. Contrary to the VEOG, the HEOG is hardly affected by blinking and vertical eye movements, but prominently shows horizontal eye movements. Accurate EOG electrode placement is essential for acquiring accurate HEOG and VEOG recordings, as is discussed in [41].

Recording of the HEOG and the VEOG thus provides two essentially orthogonal representations of eye movements. If a third EOG is added, it should contain extra information that is lacking in the HEOG and the VEOG. The radial EOG, REOG, is suggested for this in [40] and is implemented in [42]. The REOG can be obtained as the average of the EOG recorded above and below the eye and in principle, as suggested in [42], records the difference in potential along a third line that is perpendicular to both the VEOG and the HEOG lines. The key motivation behind this is that two electrodes which are placed perpendicular to the plane of horizontal dipole rotation are affected differently by vertical and radial changes in dipole orientation. A change in vertical orientation will cause potential changes of opposite polarities on both electrodes and is therefore highlighted in the VEOG and eliminated in the REOG. A change in radial orientation will cause potential changes of equal polarity on both electrodes and will therefore be highlighted in the REOG and eliminated in the VEOG. Whether or not this third EOG is essential for correction is discussed in [43]. It has been suggested that the REOG should be used for "follow-up" correction. After correction using HEOG and VEOG, the resulting EEG is almost clean of artifacts. The follow-up correction uses the REOG to correct the HEOG-VEOG corrected signal again [42].

The negative effect that forward propagation, as introduced in Section 1.2.2, allegedly has on correction accuracy is often used as a motivation for using other, non EOG-based, correction methods. However, a study that (for the first time) attempts to quantitatively estimate these negative effects, [44], claims that although such effects are detectable, they do not substantially affect correction accuracy and that these effects thus do not make an argument against using EOG-based correction methods.

The study in [44] assumes that only a single region of the cortex is involved in processing a specific stimulus. This region is subsequently considered to be the sole source of electrical activity in the forward propagation. The negative effect that forward propagation has on EOG-based correction is estimated based on the ratio between forward and backward propagation that is estimated for this region of the cortex. However, often it will not be true that only a single region of the cortex is activated by a stimulus. For many fundamental studies it is a priori unknown which and how many regions of the cortex will respond to a stimulus, and therefore the effects of

forward/backward propagation when using EOG-based correction methods are hard to predict. If two different regions in the cortex, e.g. one located frontally and a second one occipitally, respond to the same stimulus, both activities are time-locked to the same stimulus, but their EEGs are not necessarily of similar shape, duration and amplitude. When considering the effect of EOG-based correction for the occipital site, the ratio between forward and backward propagation as determined in [44] does not consider forward propagation of the frontal cerebral sources.

In general, the frontal cortex will be always active during EEG recordings and will contribute to the background EEG. Fortunately, it is often irrelevant whether or not the background EEG as recorded at an (occipital) electrode reflects only ongoing electrical activity of neurons close to this electrode or whether the background EEG is disturbed by ongoing electrical activity of more distant neurons whose activity is easily propagated to the EOG.

1.5.3.1 Multiple Linear Regression (MLR)

Regression intends to quantify the relation between one signal $y(t)$ and another signal $x(t)$. The time series corresponding to these signals can be written as (Tx1) vectors $\underline{y}$ and $\underline{x}$. The residual part of $\underline{y}$, i.e. the part which cannot be explained by the relation with $\underline{x}$, is denoted as a noise vector $\underline{n}$, which is assumed to be zero mean, white, of normal distribution, and independent of $\underline{x}$.

For linear regression, the structure of the relation is assumed to be

$$\underline{y} = \alpha \cdot \underline{x} + \underline{n}, \qquad (1.2)$$

in which α is the 'propagation factor' that expresses which fraction of $x(t)$ is detected in (or propagates to) $y(t)$.

The goal of regression is to estimate an optimal value for α, denoted as $\hat{\alpha}$, given the measurements for both $\underline{x}$ and $\underline{y}$ over a period $t = [1,2,...,T]$.

In multiple linear regression, MLR, the vector $\underline{y}$ depends on the value of multiple, e.g., three, other vectors, $\underline{x_1}, \underline{x_2}, \underline{x_3}$, and on noise $\underline{n}$, as is illustrated in Figure 1.6.

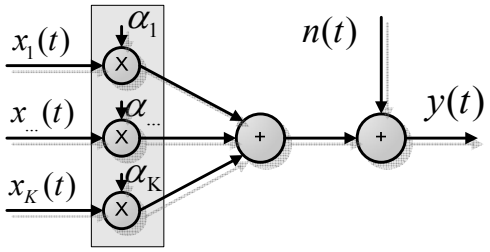

Figure 1.6: Schematic representation of the assumptions of MLR. The recorded signal $y(t)$ is a linear superposition of several reference signals $x(t)$, each with its own propagation factor α. The difference between $y(t)$ and this linear combination is a stochastic, white noise signal $n(t)$.

This leads to

$$\underline{y} = \underline{\underline{X}} \cdot \underline{\alpha} + \underline{n}, \tag{1.3}$$

with $\underline{\underline{X}} = [\underline{x}_1, \underline{x}_2, \underline{x}_3]$ and $\underline{\alpha} = [\alpha_1, \alpha_2, \alpha_3]^T$. MLR provides an estimate $\hat{\underline{\alpha}}$ for $\underline{\alpha}$ in the manner shown in Appendix B1.

The similarity between (1.1) and (1.3) is obvious and MLR can be used for artifact correction. An additional subscript i is used to denote a specific electrode. Using $\hat{\gamma}_{ik}$ as an estimate for γ_{ik} in (1.1), an estimate of $c_i(t)$ is defined as

$$\hat{c}_i^{MLR}(t) = r_i(t) - \sum_{k=1}^{K} \hat{\gamma}_{ik} \cdot \varepsilon_k(t). \tag{1.4}$$

For $\varepsilon_k(t)$, it is common to use the raw EOG. The number of EOGs, *K*, that is used in (1.4), affects the accuracy of the estimation and should be selected with care [39], as discussed above.

Some of the assumptions for optimal performance of MLR are not completely valid. The most significant violation of assumptions is that in $c_i(t)$, consecutive samples clearly are correlated, whereas MLR models cerebral electrical activity as white noise. Also, EOG electrodes do not only record ocular activity but also record some electrical activity of the brain due to forward propagation, which will be (erroneously) subtracted from $r_i(t)$. Furthermore, because the brain is involved in controlling the movement of the eyes, there will be some correlation between $\varepsilon_k(t)$ and $c_i(t)$ which is overlooked by regression. Despite these violations, MLR is a frequently used correction method, mainly because of simplicity. Moreover, the consequences for correction accuracy of these violations are often tolerable.

1.5.3.2 Regression with an auto-regressive error signal (RARE)

Typically an EEG is a time series in which rhythmical patterns are sometimes visible when the brain is at rest, and in which consecutive samples are

correlated. With the MLR method, this time structure in the EEG is ignored and the cerebral signal, $c_i(t)$, is assumed to be a white, random process.

The regression with auto regressive error signal (RARE) correction assumes a structure of the relation between $\underline{y}$ and $\underline{x}$ that is closely related to (1.2), but extends the structure of noise vector $\underline{n}$. Each new element of vector $\underline{n}$ is modeled as a combination of the D past elements of $\underline{n}$ and some noise $\eta(t)$,

$$n(t) = \sum_{\tau=1}^{D} \mu_\tau \cdot n(t-\tau) + \eta(t) \; . \qquad (1.5)$$

The time series of signal $\eta(t)$ can also be represented as a (Tx1) vector $\underline{\eta}$. Here, $\underline{\eta}$ is zero mean, white, of normal distribution, and independent of $\underline{x}$. The scaling parameters μ_τ determine the auto correlations between elements of vector $\underline{n}$, as illustrated in Figure 1.7.

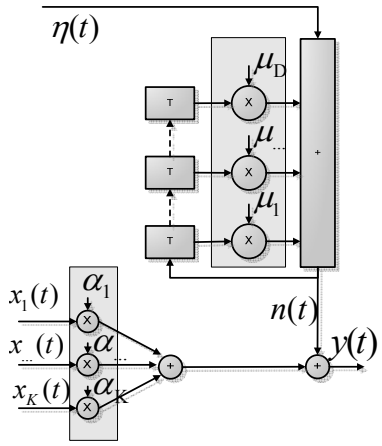

Figure 1.7: Schematic representation of the assumptions of RARE. Except for the noise assumptions this figure is similar to MLR and Figure 1.6. RARE assumes that the noise at time t is a scaled linear combination of its own past values and some stochastic, white noise η(t). Scaling factors are labeled μ, and the total number of relevant past values is labeled D.

As defined in (1.5), $\underline{n}$ has an auto-regressive structure, hence the name regression with auto regressive error, RARE.

The similarity between (1.1) and (1.3) suggests that the EOG can be used to correct the raw EEG. The cerebral electrical activity $c_i(t)$ is now modeled as an auto-correlated process. For this process all parameters γ_i and μ_τ have to be estimated. By minimizing $\underline{\eta}^T\underline{\eta}$, the parameters $\hat{\mu}_\tau$ and $\hat{\gamma}_i$ are optimized. Note that this reflects the difference with MLR where $\underline{n}^T\underline{n}$ is minimized.

The estimated cerebral electrical activity using RARE is given by

$$\hat{c}_i^{RARE}(t) = r_i(t) - \sum_{k=1}^{K} \hat{\gamma}_{ik} \cdot \varepsilon_k(t), \qquad (1.6)$$

which appears similar to (1.4), but differs because $\hat{\gamma}_{ik}$ is estimated differently as described above.

In literature, the EEG is often described as an autoregressive process, but there is some controversy about the order of autocorrelation, D [45-47]. When compared to MLR one would expect that RARE will remove ocular artifacts more accurately because of the detailed structure that is used to model the EEG. For simulated data, a direct comparison of MLR and RARE in [48] suggests that RARE indeed corrects more accurately. However, when the same study evaluated correction on experimental data, a visual inspection of the corrected data suggested that MLR was more accurate. Finally, no conclusive results were drawn as to which method was more accurate, as this turned out to depend greatly on the data at hand and on whether or not the EEG contained brief periods with deterministic signals like ERPs.

1.5.3.3 The Gratton method (GRAT)

The Gratton method, GRAT, was introduced in 1983 [35] as a method to correct offline for ocular artifacts in trial-based EEG data.

For such data, GRAT does not require a calibration period yet it provides a way to copy some of the advantages of using a calibration period, as discussed in Section 1.5.1

The most important new feature of GRAT is that prior to estimating the propagation of EOG to EEG it removes any deterministic experiment-related brain activity, EPs or ERPs, from both EEG and EOG. By doing so, it reduces the possibility that this activity affects the estimation of propagation factors. This is done on the trials that are recorded during the experiment.

Also, GRAT separates trials that contain blink artifacts from trials that do not. Because the biophysiological cause of blink artifacts differs from the cause of eye movement artifacts, as was discussed in Section 1.3, GRAT determines different propagation factors for the blink artifacts and for eye movement artifacts. Later in an extension to the original method, the method was slightly altered [38] to use different propagation factors for horizontal and vertical eye movement artifacts as well. Averaged propagation factors are estimated based on all relevant trials e.g., all trials with blink artifacts for the blink propagation factor. This has the advantage that the influence of background EEG on the estimation of the propagation factors is reduced. The blinks in the experimental data are detected based on a pattern recognition algorithm.

Although the above-mentioned features have made GRAT one of the most frequently used correction methods for trial-based EEG data, GRAT also has a serious limitation. Because GRAT relies on averaging trials (in order to

remove ERPs and EPs) prior to determining the propagation factors, its performance depends on the number of trials that contain these EPs and ERPs. For single-trial experiments and for experiments with only few identical trials, the GRAT method is thus less suitable. More information on GRAT can be found in [49] and [50].

1.5.4 Components-based correction Methods

Components-based correction methods exploit the information contained in many electrode recordings simultaneously in order to get an estimate of the ocular artifact. These electrode recordings include multiple EEG recordings and sometimes also EOG recordings. Components analysis techniques are powerful mathematical tools for the purpose of multivariate data analyses.

Basically, components analysis merely transforms data and provides an alternative way of representing data, as will first be explained. Further on, it will be shown how this alternative representation can be used to remove artifacts from EEG recordings.

Each electrode records a signal $y_i(t)$, with $i = [1,...,N]$, over a period $t = [1,2,...,T]$. These recordings are combined in vectors $\underline{y}_1,..,\underline{y}_N$ of size (Tx1), and these vectors are (again) combined in a matrix $\underline{\underline{Y}}$ of size (TxN).

Components analysis assumes that the data in $y_i(t)$ are linear mixtures of several components $z_i(t)$, with mixing coefficients w,

$$\begin{aligned} y_1(t) &= w_{11}z_1(t) + w_{12}z_2(t) + ... \\ y_2(t) &= w_{21}z_1(t) + w_{22}z_2(t) + ... \\ &... \\ y_N(t) &= w_{N1}z_1(t) + w_{N2}z_2(t) + ... \quad . \end{aligned} \tag{1.7}$$

After combining the different mixing coefficients in a mixing matrix $\underline{\underline{W}}$, and combining components in a matrix $\underline{\underline{Z}}$ (TxN), (1.7) changes to

$$\underline{\underline{Y}}^T = \underline{\underline{W}} \cdot \underline{\underline{Z}}^T. \tag{1.8}$$

The alternative representation of the data matrix $\underline{\underline{Y}}$ as provided by components analysis is thus contained in the two matrices $\underline{\underline{W}}$ and $\underline{\underline{Z}}$. Equation (1.8) can be used to get

$$\underline{\underline{Z}}^T = \underline{\underline{W}}^{-1} \cdot \underline{\underline{Y}}^T, \tag{1.9}$$

provided that matrix $\underline{\underline{W}}$ is invertible. Appendix B2 explains how orthogonal components and an invertible matrix $\underline{\underline{W}}$ can be obtained.

In Figure 1.8, an illustration of equation (1.9) is shown. The left box illustrates matrix $\underline{\underline{Y}}$ in which the single electrode recordings $y_i(t)$ define the column contents. Following the arrows in the upper part of Figure 1.8, this matrix is

transposed, multiplied by $\underline{\underline{W}}^{-1}$, and transposed again, leading to matrix $\underline{\underline{Z}}$ in which separate components define the column contents.

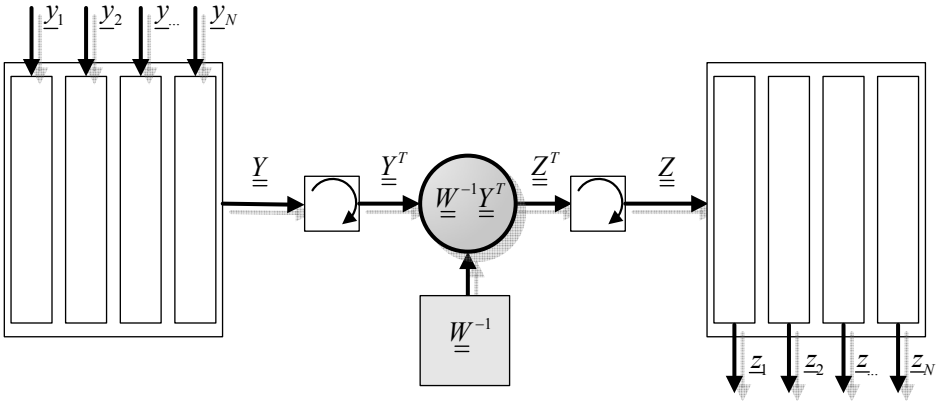

Figure 1.8: Schematic representation of components analysis.
Recorded signals $\underline{y}_1,..,\underline{y}_N$ are grouped in $\underline{\underline{Y}}$ and converted to their component matrix $\underline{\underline{Z}}$ by the inverse of matrix $\underline{\underline{W}}$.

A priori $\underline{\underline{W}}$ is unknown and should be estimated. Once $\underline{\underline{W}}$ is estimated, $\underline{\underline{Z}}$ is obtained from (1.9). For the estimation of $\underline{\underline{W}}$, it is necessary to apply certain restrictions to matrices $\underline{\underline{Z}}$ and/or $\underline{\underline{W}}$. Otherwise the number of possible solutions is infinite, and even the trivial conversion with $(\underline{\underline{Z}} = \underline{\underline{Y}}) \wedge (\underline{\underline{W}} = \underline{\underline{I}})$, with $\underline{\underline{I}}$ the (NxN) identity matrix, is a possible solution to (1.8).
The way in which $\underline{\underline{Z}}$ and $\underline{\underline{W}}$ are restricted, leads to different solutions. Therefore, the different ways to restrict $\underline{\underline{Z}}$ and $\underline{\underline{W}}$ are considered to be different components analysis techniques. In the next subsections some of these restrictions will be specified, but first it will be explained how components analysis can be used to correct EEG recordings.

The restrictions imposed on matrices $\underline{\underline{Z}}$ and $\underline{\underline{W}}$ usually reflect a property of the ocular artifact and/or of the EEG itself. As a result, some of the components $\underline{z}_1, \underline{z}_2,..., \underline{z}_N$ resemble the artifact and some resemble the EEG. When components analysis is used for artifact removal, the components that resemble ocular artifacts should be removed from the data. For this purpose a new mixing matrix $\underline{\underline{W}}^{\#}$ is used which is equal to $\underline{\underline{W}}$, with the exception that the mixing coefficients in $\underline{\underline{W}}^{\#}$ are set to zero for the components that resemble an artifact. The matrix $\underline{\underline{\hat{C}}}$ that is obtained using $\underline{\underline{W}}^{\#}$ along the lines of (1.8), contains N vectors $\underline{\hat{c}}_1, \underline{\hat{c}}_2,.., \underline{\hat{c}}_N$ that estimate the cerebral electrical activity recorded at the N different electrodes, as shown in Figure 1.9.

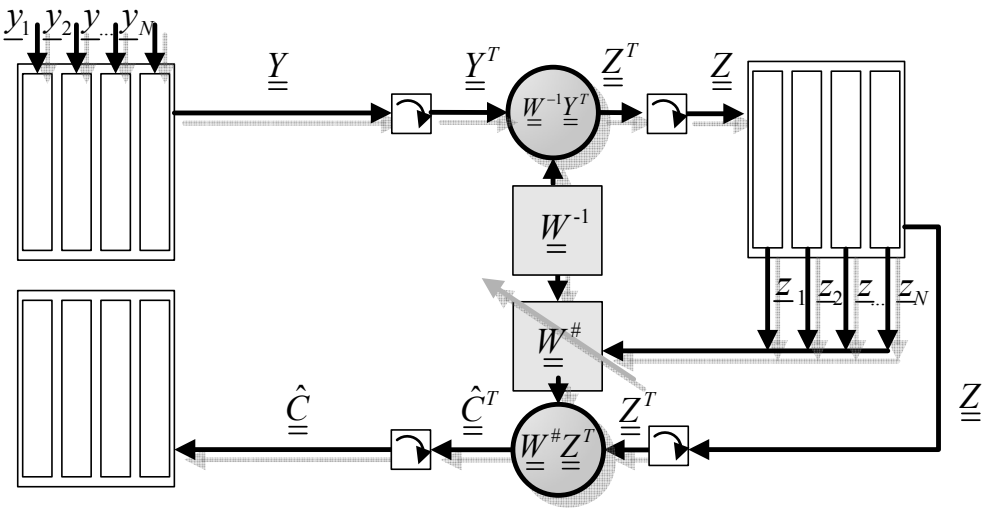

Figure 1.9: Schematic representation of signal reconstruction with artifact removal. Compared to Figure 1.8, the matrix $\underline{\underline{W}}$ is now changed prior to reconstructing the signal. By changing $\underline{\underline{W}}$ to $\underline{\underline{W}}^{\#}$ based on the components that resemble artifacts, these artifacts can be removed from the original data, and therefore $\hat{\underline{\underline{C}}}$ differs from $\underline{\underline{Y}}$.

Obviously, the ocular artifact at each electrode can be estimated as

$$\hat{\underline{\underline{E}}} = \underline{\underline{Y}} - \hat{\underline{\underline{C}}}, \qquad (1.10)$$

with $\hat{\underline{\underline{E}}}$ (TxN) containing the vectors $\hat{\underline{e}}_1, \hat{\underline{e}}_2, \ldots, \hat{\underline{e}}_N$ that estimate the ocular artifact at each electrode position. To return from $\underline{\underline{Z}}$ to $\underline{\underline{Y}}$ without removing any artifacts, matrix $\underline{\underline{W}}^{\#}$ should be equal to matrix $\underline{\underline{W}}$.

A drawback of using components-based correction is that the components in $\underline{\underline{Z}}$ are derived based on purely mathematical recipes, and that as a result objective verification whether these components only reflect the artifact is not possible. Usually either a visual inspection of $\underline{\underline{Z}}$, or determining the cross correlation between components and the EOG, is used to identify components with ocular artifacts.

1.5.4.1 Principal Components Analysis

In Principal Components Analysis, PCA [36], the main restriction for estimating matrices $\underline{\underline{W}}$ and $\underline{\underline{Z}}$ is that different components are orthogonal, resulting in the requirement

$$E\{\underline{z}_i(t) \cdot \underline{z}_{j\neq i}(t)\} = 0 \quad \forall\ t = [1:T]\ \ i,j = [1:N]. \qquad (1.11)$$

As a result, $\underline{\underline{Z}}^T\underline{\underline{Z}}$ is an (NxN) diagonal matrix.

Subscripts will be added to matrices, e.g., $\underline{\underline{W}}_{PCA}$, to indicate the specific components analysis method (here PCA) that is used to derive it. Further on,

more subscripts will be defined. The transformation of data matrix $\underline{\underline{Y}}$ into component space $\underline{\underline{Z}}_{PCA}$ by means of matrix $\underline{\underline{W}}_{PCA}$ is described in more detail in Appendix B2.

1.5.4.2 Sphering

The PCA transformation described in the previous section and Appendix B2 results in matrices $\underline{\underline{W}}_{PCA}$ and $\underline{\underline{Z}}_{PCA}$. The components in $\underline{\underline{Z}}_{PCA}$ are orthogonal and a common standardization step, called sphering, is frequently used in literature to scale them in order to obtain orthonormal components.

For this standardization, a scaling matrix $\underline{\underline{A}}$ is used whose elements are (indirectly) derived from matrix $\underline{\underline{Z}}_{PCA}$, as is derived in Appendix B3. The matrix $\underline{\underline{W}}_{\mathrm{PCA}_2}$ that results in orthonormal components is defined as

$$\underline{\underline{W}}_{PCA_2} = \left(\underline{\underline{A}}\,\underline{\underline{W}}_{PCA}{}^{-1}\right)^{-1}. \tag{1.12}$$

1.5.4.3 Second Order Blind Identification

The motivation behind applying RARE instead of MLR is that in $c_i(t)$ consecutive samples are correlated. When using PCA, such temporal correlation is ignored[2], just as for MLR.

Second order blind identification, SOBI, is a components analysis technique that, like PCA, extracts uncorrelated sources, but also like RARE assumes some temporal correlation in the EEG [51]. The SOBI mixing matrix will be referred to as $\underline{\underline{W}}_S$, and the SOBI-component space as $\underline{\underline{Z}}_S$.

Like PCA, SOBI assumes that the components in $\underline{\underline{Z}}_S$ are uncorrelated between different electrodes, as in (1.11). Moreover, SOBI also states that components should be uncorrelated when different moments in time are considered, as

$$E\left\{\underline{z}_i(t)\cdot\underline{z}_{j\neq i}(t+\tau)\right\} = 0, \tag{1.13}$$

with $\tau \in [1-t : T-t]$ indicating the specific delay between the components.

This extra statement only holds for correlations between different components. SOBI does allow correlation in time within one component, as

$$E\left\{\underline{z}_i(t)\cdot\underline{z}_i(t+\tau)\right\} = \rho_i(\tau), \tag{1.14}$$

where $\rho_i(\tau)$ is used to indicate the auto-covariance of the i^{th} component at delay τ.

SOBI estimates one matrix $\underline{\underline{W}}_S$, in accordance with (1.13), based on minimization of the sum of $\underline{z}_i(t)\cdot\underline{z}_{\neq i}(t+\tau)$ for multiple delays and for multiple

---

[2] Note from Appendix B2 that $\frac{1}{T}\underline{\underline{Y}}^T\underline{\underline{Y}}$ and $\frac{1}{T}\underline{\underline{Z}}^T\underline{\underline{Z}}$ will not change if matrix $\underline{\underline{Y}}$ is randomly permutated over its rows

electrodes. A way to iteratively estimate this minimum, and find the matrix $\underline{\underline{W}}_S$ is given in [51].

To allow for faster computations or for specific time structures in the component-space, often not all possible values for τ are included when determining the set of matrices for which the sum of off diagonal elements is minimized. The matrix $\underline{\underline{W}}_S$ depends on the selected delays τ [52].

1.5.4.4 Independent Components Analysis

Independent Components Analysis, ICA, originated in 1991 [37] and was used to minimize statistical information between components. Whereas PCA assumes that components that underlie a recorded signal have to be uncorrelated, ICA assumes the components to be independent. Independence is a much stricter statistical requirement than uncorrelatedness.

Probability theory can be used to define independence. N vectors $\underline{z}_1$, $\underline{z}_2$,.., $\underline{z}_N$ are independent if

$$\text{prob}(\underline{z}_1, \underline{z}_2, .., \underline{z}_N) = \text{prob}(\underline{z}_1) \cdot \text{prob}(\underline{z}_2) \cdot ... \cdot \text{prob}(\underline{z}_N). \qquad (1.15)$$

To illustrate the difference between PCA and ICA, a simple example in an N=2 subspace is used, following the illustration as given in [53].

By way of illustration, two signals $\underline{y}_1$ and $\underline{y}_2$ are simulated as a linear combination of two underlying source signals $\underline{s}_1$ and $\underline{s}_2$, combined in a matrix $\underline{\underline{S}}$. These source signals are stochastic and are randomly drawn from a uniform distribution.

The mixing process is defined by mixing matrix $\underline{\underline{V}}$, with

$$\underline{\underline{Y}}^T = \underline{\underline{V}} \cdot \underline{\underline{S}}^T,$$

$$\underline{\underline{V}} = \begin{bmatrix} 0.75 & 0.23 \\ 0.44 & 0.80 \end{bmatrix}$$

Both ICA and PCA estimate the mixing matrix and transform $\underline{y}_1$ and $\underline{y}_2$ into a component subspace. Ideally, $\underline{\underline{W}}^{-1} \cdot \underline{\underline{V}}$ should result in a diagonal matrix because each component should reflect a single source signal. If the mixing process is known, as it is for simulated mixing, the accuracy of finding the components can be determined by an inspection of the off-diagonal elements of this matrix [54]. These off-diagonal elements indicate whether the components are mixtures of multiple source signals or not. For experimentally recorded signals, the matrix is $\underline{\underline{V}}$ unknown and this way of correction validation cannot be used.

After performing a PCA, the estimated components are uncorrelated and have equal variance due to the sphering operation. After performing an ICA, the estimated components are independent. Figure 1.10 illustrates this. Note that for the example in this plot, the extracted principal components are denoted

PC_1 and PC_2 instead of $\underline{z}_1$ and $\underline{z}_2$, and the extracted independent components are denoted IC_1 and IC_2, to differentiate between PCA and ICA.

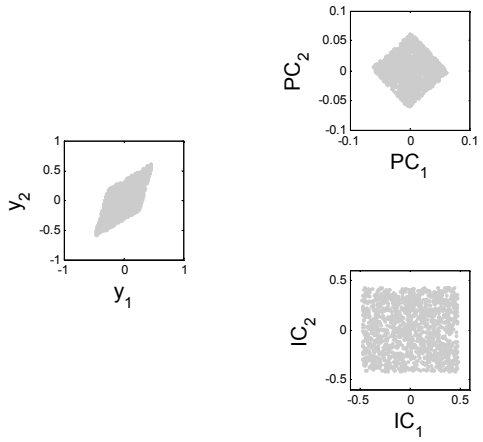

Figure 1.10: Two-Dimensional illustration of the difference between PCA and ICA. Two signals $\underline{y}_1$ and $\underline{y}_2$ are decomposed into a principal components subspace (upper right) and an independent components subspace (lower right).

The scatter plot on the left shows the simulated data. The upper right scatter plot shows the component space after PCA. In this scatter plot the expected value of PC_2, clearly depends on the value of PC_1. The lower right scatter plot shows the component space after ICA, in which this dependence has disappeared.

Many ICA methods and SOBI, do not use $\underline{\underline{Y}}$ as a starting point. They first apply PCA and sphering as in Section 1.5.4.2 to obtain $\underline{\underline{Z}}_{PCA_2}$.

For ICA there is no direct calculation of a matrix $\underline{\underline{W}}_{ICA}$ that results in independent components as there is for $\underline{\underline{W}}_{PCA}$ and the principal components. ICA methods require a measure of statistical dependence between signals and then maximize the independence. Numerous papers on how to implement ICA, what measure to select and how to maximize it, have appeared during the past two decades, including [54-69], as well as numerous papers that focus on applying ICA to biopotentials such as the EEG, [67;70-79]. Comparisons and links between ICA methods are given in [80].

One measure of independence that is used in several ICA methods is Gaussianity. If two Gaussian signals have zero covariance, this implies that they are independent. A way to find independent components is to maximize the non-Gaussianity of the components in $\underline{\underline{Z}}_{ICA}$. The fourth-order cumulant of a signal [81], closely related to its kurtosis, is known to reflect a signal's non-

Gaussianity. The information contained in fourth-order cumulants of a set of signals is exploited by the joint approximate diagonalization of Eigen-matrices, JADE, method [59]. The fourth-order cumulants of (sphered) EEG data are stored in set of matrices and then a matrix $\underline{\underline{W}}_{JADE}$ that jointly optimizes independence is determined.

1.5.5 Other ocular artifact correction methods and surveys

Some interesting other methods will be mentioned briefly in this section. These will not be used in the remainder of this thesis. Most of the methods in this section are seldom used for ocular artifact correction.

- Wavelet-based artifact correction has more recently been introduced for correcting ocular artifacts [82-84]. One survey of ocular artifact correction techniques already covers this type of correction and labels it as "superior to existing techniques" [85]. However, this statement is based mainly on the assumptions that underlie the method instead of on experimental or simulated results, and more thorough evaluation is needed.
- Auto-regressive moving average modeling of the EEG, [86]. This method is basically an extension to RARE in which the assumed EEG structure is auto-regressive moving average.
- Dipole modeling for correction, [87;88]. These methods estimate dipole properties, i.e., location, orientation and/or strength, in a volume conductor based on the recorded EEG signals. Dipole modeling correction methods are mainly used for source localization studies.
- Adaptive band-pass filtering, [89;90].
- Neural network-based correction, [91;92].
- Correction based on third-order cumulants, [93].

Several reviews include a comparison of correction methods based on the assumptions underlying them [85;94;95]. Other reviews, such as those in the following section, use a more quantitative comparison.

1.6 Validation of correction, use of models

To validate if and to what extent correction methods are successful in removing ocular artifacts, performance measures are needed. One frequently used performance measure is related to the mean squared error between $\hat{c}$ and c [16;39;48;96;97]. Intuitively such a measure appears appropriate because it is directly related to c, the clean EEG. Similarly, a squared error performance measure is also used in the frequency domain, based on spectral power in recorded and in clean frequency bands [16;97]. For the components-based

methods it is also possible to use a similar squared error between the estimated components and the sources that were used for simulation [98]. However, in an experimentally recorded EEG, $c(t)$ is unknown. The squared error performance measure is therefore unsuited for use with experimental data and can only be applied to simulated data in which $c(t)$ is known. Accordingly, validation on experimental data is often restricted to a visual inspection of $\hat{c}(t)$ and/or $\hat{e}(t)$. Comparisons between correction methods, reviews and surveys can be found in many studies, including [8;13;15;16;22;38;39;43;48;50;85;94;96-100].

Imagine two different correction methods applied to the same raw EEG, and resulting in two different corrected EEGs. If neither of the corrected EEGs still contains high-amplitude artifacts, it is easy to conclude that both methods succeeded in removing the high amplitude artifacts, but it is difficult or impossible to tell which of the corrected EEG is best. Without knowing *c*, this question cannot be conclusively answered, and therefore, to by-pass this difficulty, models can be used that simulate raw EEG. As opposed to experimental data, for simulated data the EEG, i.e. $c(t)$, is known and can be used to determine which correction method is more accurate, even for low-amplitude artifacts.

Modeling of an EEG begins with finding a suitable simplification of the sources of electrical activity and of the human head that conducts the electrical activity.

For the human head, a variety of simplifications have been used in the past. In a very basic form, the head can be modeled as a sphere with conductive properties that is surrounded by non-conductive air. This simplification overlooks several important issues, including the fact that a head consists of multiple sorts of biological tissues, with different conductivities. A slightly more elaborate model of the head is the concentric spheres model, which can represent different tissues, but lacks realistic morphology of these tissues. By implementing such a model, [40] showed that three EOGs are theoretically required to fully estimate ocular artifacts due to rotations of the corneo-retinal dipole. Imaging techniques, like MRI, can provide additional data on the morphologies of tissues and the resulting images of the head can be used for modeling the head as a number of compartments (tissues), with different morphologies and different conductive properties [101].

A simplification of the sources of electrical brain activity that can be used in combination with the head models is the current dipole. Dipoles are simplified representations of localized neuronal activity in the brain as is explained in [19]. Other simplifications of the neuronal sources include the use of multiple dipoles of quadrupoles, and of dipole layers to model the electrically active areas in the brain. Dipoles are frequently used for modeling localized neuronal activity, such as the activity involved in the generation of ERPs.

When simplifications for both the head and sources are chosen, a mathematical tool is required that calculates electrical potential on the simplified head as a result of the simplified sources. Two common tools for this are the Boundary Element Method, BEM, and the Finite Element Method, FEM. Both these methods divide the volume into elements. The electrical potentials on the head can be derived from potentials in/on these elements. The main difference between these two methods is that the FEM divides the complete head into elements, whereas the BEM only divides the boundaries between tissues into elements. An advantage of the BEM is that it is computationally less demanding, whereas an advantage of FEM is that anisotropic properties of tissues are easier to model. Once the simplifications of head and sources, and a mathematical tool are selected, an EEG can be simulated at any position of the modeled head.

A drawback of using models and simulated data for the purpose of validating correction methods is that a model is never fully accurate in its approximation of reality. Certain parts of reality are excluded in a model because they seem to be of lesser importance. The consequences of the omission of such parts cannot be studied with the same model, and interpretation of simulated results should consider the limitations of the model. Especially when using models for validation, it is essential to know whether inaccurate correction is either due to flaws of a correction method or due to flaws of the modeling assumptions, as was argued in [50]. An alternative to the use of models is to use experimentally recorded data and manipulate this in such a way that flaws of artifact correction methods are accentuated. Possible schemes of this type are given in [50] and [13]. The first scheme, in [50], requires recordings in which eye movements and blinks are intentionally made by the participants, whereas the second [13] does not require intentionally made eye movements and blinks. In Chapter 5, a validation on experimental data is used which is essentially similar to the scheme in [13].

1.7 Preview of thesis contributions

From the past sections and the existing literature on ocular artifacts it becomes clear that gaze direction and eyelid movement are key sources of ocular artifacts.

Several issues concerning ocular artifact correction, e.g. the forward/backward propagation issue, the number of EOG recordings, and the statistical assumptions regarding component extraction, are still widely debated. What is proposed in this thesis is to go beyond these issues and develop an ocular artifact correction method that is different from existing methods, and

fundamentally more accurate. To this end, a reference on gaze direction and eyelid movement will be used that does not involve recording biopotentials, but rather tracks the eye with a camera. This extra reference provides clean information on the occurrences and morphologies of any ocular artifacts that is highly valuable for accurate artifact correction.

In Chapter 2, a model of the human head is introduced that can simultaneously simulate brain- and ocular electrical activity. The model will be used to objectively determine how well a selection of eye movement artifact correction methods succeed in correcting simulated eye movement artifacts. Because the performance of correction methods may depend on the number of simultaneously recorded EEGs/EOGs, the correction methods in this chapter will correct several sets of data with different numbers of electrodes and different electrode positioning. Chapter 3 introduces the use of eye tracker recordings as a reference signal in a new adaptive correction method for eye movement artifacts. With the model of Chapter 2, datasets are again simulated, and it is shown that the new correction method consistently outperforms existing correction methods on this simulated data. A key feature of the new correction method is the parameterization of the relation between ocular artifact and pupil position as recorded by and eye tracker. The structure of this relation is derived from experimental recordings and turns out be adequately represented by a second-order equation. The fine-tuning of the parameters that are involved in this relation is made adaptive, which has the advantages that parameter value changes can be tracked, and that initialization of parameters does not require additional prior knowledge regarding volume conduction properties.

Chapter 4 extends the functionality of the new correction method. By monitoring eyelid position and adding eyelid movement effects to the relation between artifact and pupil positions, the new correction method is altered in a way that allows it to correct for both blink and eye movement artifacts. Because most eye trackers do not estimate eyelid position (yet), it is shown how the use of an EOG electrode can provide an adequate alternative.

The resulting eye tracker-based correction method, dubbed EYE, is then applied to simulated data, and its correction accuracy is compared against that of several other methods. EYE proves to be superior to both the EOG-based and the components-based correction methods on these simulated datasets. Chapter 5 stresses that correction method accuracy should not only be derived from simulated data. An experiment is set up that is expected to generate low-amplitude ERPs, located mostly at frontal electrode positions. For this type of data, it is essential that ocular artifacts are adequately removed. A yardstick for the accuracy of the correction methods is derived based on the power of

background EEG. Accuracy, as estimated by this yardstick, turns out to comply very well with accuracy as found on the simulated data in Chapter 4.

In summary, the key contributions of this thesis are the development of a realistic model that assists in the validation of ocular artifact correction methods, the introduction of a highly powerful new approach to ocular artifact correction based on the use of an eye tracker, and the validation of this new method on experimental data.

Several chapters of this thesis have appeared as journal publications over the past years, including

- Chapter 2 as [102], and
- Chapter 3 as [103].

Chapter 2

A model-based objective evaluation of eye movement correction in EEG recordings

2.1 Abstract

We present a method to quantitatively and objectively compare algorithms for correction of eye movement artifacts in a simulated ongoing EEG. A realistic model of the human head is used, together with eye tracker data, to generate a data set in which potentials of ocular and cerebral origin are simulated. This approach bypasses the common problem of brain-potential contaminated EOG, when monitoring or simulating eye movements. The data are simulated for five different EEG electrode configurations combined with four different EOG electrode configurations. In order to objectively compare correction performance for six algorithms, listed in Table 2.3, the signal to noise ratio of the EEG before and after artifact correction is determined. A score indicating correction performance is derived, and for each EEG configuration the optimal correction algorithm and the optimal number of EOG electrodes are determined. In general, the Second Order Blind Identification, SOBI, correction algorithm in combination with 6 EOG electrodes performs best for all EEG configurations evaluated on the simulated data.

2.2 Introduction

This chapter introduces a method to objectively assess the performance of eye movement artifact correction algorithms used in electroencephalographic (EEG) measurements. The EEG is a recording of potential changes on the scalp caused by brain activity. It is often used in clinical situations, for instance to diagnose sleep disorders or epilepsy, because it reveals important information about a person's mental condition. The EEG can be distorted by numerous other sources of electrical activity, called artifact sources. Before the information in the EEG can be retrieved, however, any artifacts should be removed. Eye movement artifacts can have a large disturbing effect on EEG

JJM Kierkels, GJM v. Boxtel and LLM Vogten, IEEE TBME, 52(2), pp246-253, 2006

recordings because the eyes are located close to the brain. The front of the eye (cornea) is positively charged with respect to the back (retina), and thus the eye can be seen as a dipole [104]. Rotation of this dipole, caused by eye movements, changes the electric field in the tissues surrounding the eye. This change in electric field will be picked up by EEG electrodes as a change in electric potential. The magnitude of this potential change can be as much as ten times the change due to brain activity at frontal electrodes. Eye blinking also causes artifacts. When the eyelid is moved during blinking, the electric field surrounding the ocular dipole changes and the EEG electrodes record blink artifacts. In this chapter blinks will not be examined because the model that is needed to simulate the blink artifact is different from the model for eye movement artifacts. The blink model would be an extension of the model presented here. The data we recorded for this study did contain blink artifacts but for performance validation we only selected intervals without blinks.

An EEG electrode is positioned near some part of the brain and mainly, but not exclusively, records cerebral signals. The EEG electrode also records some ocular signals. Likewise, an electro-oculographic (EOG) electrode is positioned close to the eyes and mainly, but not exclusively, records ocular signals. It also records small cerebral signals. This 'double signal' recorded at every electrode, called cross-over, is the main reason why artifact correction is so difficult. An electrode, positioned anywhere on the scalp, will record a signal $r(t)$ that is a combination of a brain-related potential $c(t)$, an artifact-related potential $e(t)$ and electrode-noise $n(t)$ that is assumed here to have a white spectrum.

Since the volume conduction in biological tissues can be considered instantaneous [105], the summation of $e(t)$, $c(t)$ and $n(t)$ is also instantaneous.

Because it is not possible to 'turn off' either the ocular sources or the cerebral sources it is not possible to record either $c(t)$ or $e(t)$ alone. The eye movement artifact thus has to be removed from the combined recording by means of signal processing. This has led to the development of several correction algorithms. A description of the differences between these algorithms can be found in reviews [8;38;98;106]. Which of these algorithms performs best is difficult to determine because 'clean' $c(t)$ and $e(t)$ signals are not available. Once the recorded signal is corrected optimally, the corrected EEG, $\hat{c}(t)$, should be the same as $c(t)$. But $c(t)$ cannot be measured, so there is no performance measure that can validate the results of a correction algorithm applied on real data. Several papers have therefore made a comparison between some of the algorithms based on data simulated by (randomly) mixing simulated sources. Recently EOG-based algorithms, the Principal Components Analysis (PCA) algorithm and the Independent Components Analysis (ICA) algorithm were evaluated in [16]. Results of that study showed that PCA and EOG-based methods are favored over ICA methods.

By using the conductivity properties of the human head and eye tracker data to simulate ocular movements we are able to simulate ocular movement related artifacts, $e(t)^s$, in the EEG. These artifacts will be superimposed on the simulated, artifact-free, EEG, $c(t)^s$. The use of the eye tracker gives the unique opportunity to have a very realistic eye movement in our simulations. Moreover the eye tracker does not pick up any brain related potentials and therefore is very useful to simulate clean $e(t)^s$ data. Since we are now able to simulate $e(t)^s$ and $c(t)^s$ separately and without artifacts, we can use them as references when evaluating how well a correction algorithm has removed eye movement artifacts. The simulations in this chapter make use of the boundary element method (BEM) [107]. The BEM can be used to numerically estimate the electrical potential at different positions on the scalp. For this, the head is assumed to be a conductor that can be modeled as compartments with constant, isotropic conductivity. The different conductivities of tissues in the head can be modeled by assigning a different conductivity value, σ, to each tissue. Brain activity and ocular activity can be modeled separately. The method we propose can be used to evaluate objectively which algorithm performs best in a specific electrode configuration. We use a signal to noise ratio (SNR) measure to determine the performance of the algorithms for various EEG and electro-oculographic (EOG) electrode configurations. On real data, the correction performance might deviate from the results shown here for simulated data. Any possible deviancies are due to features from reality that were omitted in the model and thus refining the model can minimize this deviance, but at the cost of more complexity.

2.3 Simulations

A requirement in choosing a simulation model for this study is that the model should be able to simulate separately $c(t)^s$ and $e(t)^s$. Also electrode-noise, $n(t)^s$, should be simulated. A model should thus simulate the cerebral and ocular sources and also the transfer from source to electrode resulting in $c(t)^s$ and $e(t)^s$. As mentioned before, $c(t)^s$ and $e(t)^s$ originate from electrically active tissues inside the head, either brain or eye. In the model such a structure is called a 'source-dipole'. Each source-dipole has a specific location, determined by the position in the head, and a specific activity determined by the electrical activity it generates. For the calculation of the potential at the electrode positions the BEM, as described in [107], is implemented in MATLAB 6.5. The BEM, often used in biopotential studies [108], calculates the potential at any position in an arbitrarily shaped volume. If there are multiple electrical source-dipoles in that volume, the calculated potential is affected by all the source-dipoles. In Figure 2.1 details are shown of our model to simulate the

$c(t)^s$, $e(t)^s$ and $n(t)^s$. The blocks in Figure 2.1 will be explained in this paragraph.

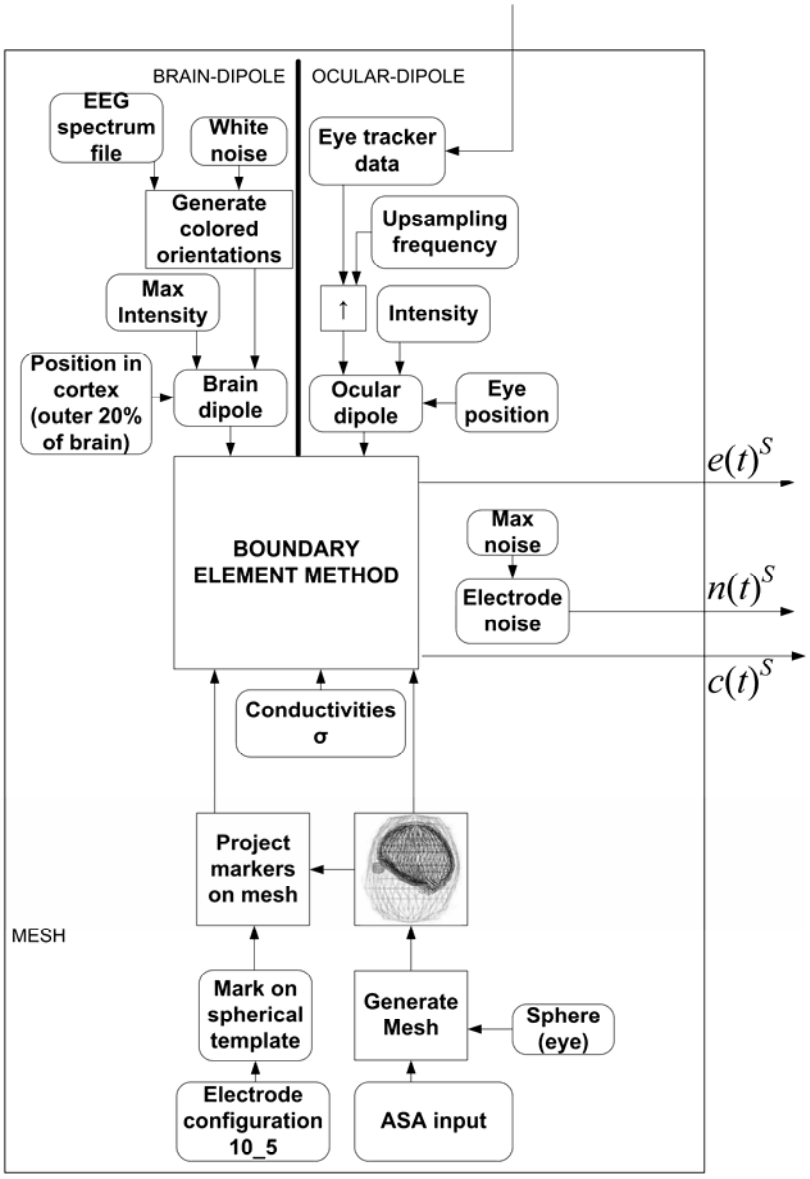

Figure 2.1: Model used to simulate $e(t)^s$ and $c(t)^s$. Input of the model is eye tracker data. Other important parameters are: EEG spectrum, volume specification (mesh), electrodes positions and conductivities. The upper part of the figure models the dipole properties, the lower part models the volume. These are combined in the BEM to simulate the output $c(t)^s$, $n(t)^s$ and $e(t)^s$.

The lower part of Figure 2.1 illustrates the steps needed to obtain a mesh of the boundaries between different tissues in the head. Such a mesh is required as an input for the BEM. For this mesh we simplify the head to 4 different tissues: scalp, skull, brain and eye. Conductivity values of these tissues are taken from

literature, with σ= 0.3, 0.04, 0.25 and 1.0 ($\Omega^{-1}m^{-1}$) respectively [109;110]. Points that specify the boundaries between these tissues are imported from the "ASA 3.0.0.7. Signal & Source" software package [111]. By linking these points systematically, a closed triangular mesh is generated. For the mesh generation, points are grouped in transversal slices according to their coordinates. Each point is clustered with the nearest clockwise point in that group, and with the nearest points from the groups both below and above the transversal slice of the group. The resulting cluster contains two triangles that are part of the triangular mesh. On the top and the bottom of the head, one point is added to assure the full triangular mesh represents a closed surface. The number of points, listed in Table 2.1, determines the complexity of this mesh.

Table 2.1: Number of points on the boundaries between tissues used in this study

Boundary	Number of points
Skull-Brain	860
Scalp-Skull	616
Air-Scalp	510
Scalp-Eye	151

The boundary between scalp and eye is not obtained from ASA, because no eye boundaries are described in this package. This boundary is added by sampling a sphere, with a radius equal to an eye, and positioning these samples in the other meshes. This eye positioning is done based on an MR cross-section of a head. Landmark points are marked in this image and angles and (relative) distances between the eyes and these landmark points are determined and subsequently used to position the eyes in the model. It should be noted here that in the mesh, the eye compartments are fully enclosed by the scalp compartment. Although this is only a rough approximation of the tissue structures surrounding the eyes, it was chosen because detailed information on compartment shapes around the eyes was, as mentioned above, not available and because this simplification facilitates calculations. The whole triangular mesh of the head is shown in one of the boxes of Figure 2.1. The next step adds electrode positions to this mesh. The positions, as specified in e.g. the 10-5 system [28], are based on relative distances between landmark points on the scalp (nasion and inion). To map the electrode positions we use a spherical template with nasion and inion on opposite sides and with a radius equal to the mean radius of the outer boundary of the head. According to the 10-5 system specifications we place one marker for each position on the spherical template.

Because the outer boundary of the head is not spherical, not all of the markers on the template are on the triangular mesh. The last step in defining the electrode positions is thus to project these "off mesh" markers onto the nearest triangle of the mesh.

The upper part of Figure 2.1 illustrates the simulation of electric dipoles inside the mesh. These dipoles simulate electric activity in the head. Each dipole has its own specific location, orientation and intensity. In this study the dipoles were of two types. The first type simulated the ocular activity. Each eye has a fixed location, so the dipole modeling this eye is also fixed. If illumination is constant, the potential difference between the front and the back of the eye is also constant [112]. Therefore the intensity of the dipole is also chosen constant. We use an eye tracker system to monitor eye movements and use the eye tracker data to model orientation of the ocular dipole. The use of eye tracker data for simulating dipole rotations ensures that the trajectory of the simulated eye movements is realistic. Even during fixation, the eyes may slightly move, and change the electrical potential at the electrode position. Moreover, during tracking of an object that moves at constant velocity, the eye may not always move equally smooth [113]. In the simulations one ocular dipole is used for each eye. The second type of dipole simulates the brain activity. Electrical brain activity originates from all synaptic connections between the neurons in the brain, approximately 10^{11}. Representing each neuron or each synaptic connection by a dipole is impossible, so we model large groups of neurons as one 'equivalent dipole'. One group would model approximately 10^{10} neurons. Because the EEG signal originates mainly from pyramidal neurons in the cortex, each equivalent dipole is randomly positioned in the outer 20% of the brain tissue. In this study the positions of these equivalent dipoles are fixed, but their orientations and intensities vary. Whereas one pyramidal cell has a fixed position and orientation, the combined average orientation and position of a group of pyramidal cells may vary, given that not all cells are innervated simultaneously. For simplicity, the model uses a varying orientation but a fixed position. The number of equivalent dipoles needed to simulate EEG recordings depends on the required simulation accuracy. In our simulations we want the average absolute potential to be equal for all electrode positions because this is also observed in EEG recordings. With a small number of dipoles (e.g. 2) the electrodes close to the source-dipoles record a much stronger EEG signal than other electrodes further away. Increasing the number of dipoles smoothes these differences. For this study 10 equivalent dipoles are used. The frequency spectrum of an EEG is not white, but consists of characteristic frequency bands containing most of the EEG power spectrum. These bands range from 0 to 30 Hz. The EEG spectrum is assumed to be unrelated to the direction of the ocular dipole [114]. For each participant we recorded the EEG at Cz position during a period of no eye

movement. This was verified in the simultaneously recorded EOG and eye tracker data. In this period 25 blocks of 512 samples are selected, Fourier transformed, and averaged. The resulting average spectrum of the EEG is stored and used in the model to simulate EEG signals for the specific participant.

The locations of the simulated brain dipoles are chosen randomly as described earlier in this section. The orientation and intensity of each dipole need to be chosen in a way that the resulting $c(t)^s$ resembles $c(t)$ in spectrum shape. The orientation of a single neuron in the brain does not change, nor does the direction of the electric current generated by the neuron. However, a large group of neurons, which we represent by one equivalent dipole, will have a mean current-direction that changes with time. Therefore the orientation of the simulated brain dipole should vary in time. To simulate this property the brain-dipole is split in three orthogonal vectors, each of them having a time-varying length. This varying length is simulated by passing a white noise through a filter with the spectral shape as in the stored spectrum for this participant. Combining the three vectors results in a brain dipole that has a time varying orientation and intensity. The simulated $c(t)^s$ resembles $c(t)$ in spectral shape at any electrode position.

An EEG electrode configuration is often selected based on the aim of the study and/or on the hardware available. The number of electrodes used in recordings has increased in the last decades, resulting in new standards for electrode positioning. The first real standard was introduced with the 10-20 system [26], later the 10-10 [27] and the 10-5 system filled the need for a standard that could be used with a larger number of electrodes. The performance of an artifact correction algorithm might depend on the EEG configuration. Therefore we determine the performance of correction algorithms for 5 different configurations, including the 10-20, 10-10, and 10-5 systems, as shown in Table 2.2.

Table 2.2: Electrode configurations

EEG configuration	EEG electrodes
1	Cz
2	Midline: Nz, Fpz, AFpz, AFz, AFFz, Fz, FFCz, FCz, FCCz, Cz, CCPz, CPz, CPPz, Pz, PPOz, POz, POOz, Oz, OIz, Iz.
3	10-20 system (21 electrodes)
4	10-10 system (85 electrodes)
5	10-5 system (340 electrodes)
EOG configuration	**EOG electrodes**
2	Outer canthi left (EO5) and right (EO6) eyes
4	Above (EO2) and below (EO4) the right eye, + EO5 + EO6
6	Above (EO1) and below (EO3) the left eye, + EO2 +EO4 + EO5 + EO6
8	Inner canthi left (EO7) and right (EO8) eyes +EO(1-6)

For each of the EEG configurations the number of EOG electrodes can be varied. Usually an even number of EOG electrodes is used and pairs of two electrodes are combined in horizontal- and vertical EOG (H-EOG, V-EOG). We combine 2, 4, 6 or 8 EOG electrodes with each of the EEG configurations. Which EOG electrodes are added is also shown in Table 2.2.

At every EOG electrode position, an EOG is recorded with respect to the same common reference as used for the EEG recordings. Such EOG recordings are commonly referred to as monopolar. For some algorithms, it is common to use bipolar EOG recordings measuring the difference between the two monopolar recordings known as the V-EOG or H-EOG. For the algorithms that require bipolar recordings V-EOG or H-EOG was calculated from the electrodes in that EOG configuration, e.g. V-EOG=EO1-EO3. Other algorithms do not have this convention and use monopolar recordings. Simulations only contain even numbers of EOG electrodes because of the bipolar measurement used in some algorithms.

To determine the intensities of the equivalent dipoles and the ocular dipoles, we use the ratio between $c(t)$ and $e(t)$ in experimental data. This ratio indicates how large the ocular artifact is with respect to the artifact-free EEG. The ratio, determined by dividing the mean of $c(t)$ over the mean of $e(t)$ for a fixed time period, is different for every electrode position because the amplitude of $e(t)$ decreases as the distance to the eyes increases. We determined the ratio at the Fpz position for all participants and use the average ratio of 1:3 in our simulations to scale the intensities of the dipoles in a way that the ratio between $c(t)^s$ and $e(t)^s$ is also 1:3 at Fpz. Finally, $r(t)^s$ should have the same maximum amplitude as $r(t)$ and therefore we scale all intensities in a way that the resulting $r(t)^s$ has a maximum amplitude of 150 μV at Fpz position. A small part of this 150 μV is due to $n(t)^s$ which is set to have a maximum amplitude of 1 μV.

2.4 Data acquisition

EEG, EOG and eye tracker measurements are gathered from 9 participants aged 19-21, 5 male and 4 female. The participants perform a task involving fast eye movements. During this task, a dot appears in the middle of the upper edge of a 19-inch monitor. After 1.33 s the dot disappears and immediately reappears in the middle of the next counterclockwise edge of the screen. The participant is asked to keep his eyes on the moving dot. An eye tracking system is positioned directly below the monitor and records the position of the participants left eye. It uses an infrared light and from the light reflected by the eye the position of the center of the pupil is determined. EEG measurements are performed with 21 EEG electrodes positioned according to the 10-20 system. Another 6 electrodes are used to record the EOG. They are positioned above and below both eyes, left of the left eye and right of the right eye. Recordings for all electrodes are offline referenced to averaged mastoids. EEG and EOG are recorded at 256 Hz using the BioSemi ActiveTwo system with sintered Ag/AgCl electrodes using a low pass filter of 67 Hz. Eye tracker data are recorded at 50 Hz using the SensoMotoric Instruments RED eye tracker with an angle resolution better than 0.1 degree. The eye tracker data are up-sampled from 50 to 256 Hz afterwards because the EEG is simulated at 256 Hz, illustrated by the upward arrow in Figure 2.1. During the task, the participant sits comfortably in front of a monitor at 0.8 m distance with the head supported and eyes in line with the center of the screen.

2.5 Validation of correction

With this model any artifact correction algorithm can be tested on the simulated data. In the lower half of Figure 2.2 the corrected EEG, $\hat{c}(t)^s$, can be compared to the $c(t)^s$ to validate the correction procedure.

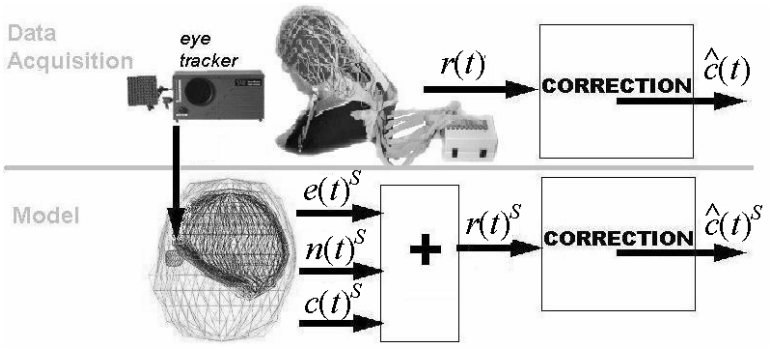

Figure 2.2: Diagram illustrating the nomenclature of different data types. Part of the figure is taken from www.biosemi.com, with permission of BioSemi.

Unfortunately this is not possible for the upper half of Figure 2.2 because there is no knowledge of $c(t)$. To quantify the resemblance between $\hat{c}(t)^s$ and $c(t)^s$ a correction performance measure is defined. Because we are looking for the overall correction, our performance measure treats all frequencies in the signal equal. Other performance measures, as in [16], can stress on specific properties of the EEG by emphasizing e.g. evoked potentials or alpha rhythms. This can be done by removing all frequencies not belonging to the alpha band for both $c(t)^s$ and $\hat{c}(t)^s$, and compare the resulting band-limited signals. There are important factors like the number of electrodes and the configuration of electrodes that can have a significant effect on an algorithms performance. In this study we determine which algorithm performs best for a specific electrode configuration.

For the performance measure we use the signal-to-noise ratio (SNR) of both $r(t)^s$ and $\hat{c}(t)^s$. Prior to SNR calculation the mean of $c(t)^s$ and $r(t)^s$ is subtracted, because in EEG recordings the DC component is also removed. We define SNR_r as:

$$SNR_r = \frac{\frac{1}{T}\sum_{t=1}^{T}\left(c(t)^S\right)^2}{\frac{1}{T}\sum_{t=1}^{T}\left(r(t)^S - c(t)^S\right)^2}. \qquad (2.1)$$

The noise in $r(t)^s$ is given by $r(t)^s - c(t)^s$ and thus contains both $e(t)^s$ and $n(t)^s$. For $\hat{c}(t)^s$ we also define SNR_c as:

$$SNR_c = \frac{\frac{1}{T}\sum_{t=1}^{T}\left(c(t)^S\right)^2}{\frac{1}{T}\sum_{t=1}^{T}\left(\hat{c}(t)^S - c(t)^S\right)^2}. \qquad (2.2)$$

We have to assume here that the signal part in the SNR does not change due to correction. After correction this numerator still has the same mean amplitude and shape as before and thus still is equal to $c(t)^s$. None of the correction algorithms that are used in this chapter (intentionally) change the amplitude of $c(t)^s$, therefore this assumption appears valid. An effective correction algorithm will reduce the noise and will have $SNR_c > SNR_r$ and have a high value for SNR_c. The gain in SNR, *g*, is a good indicator of the algorithm's performance,

$$g = \frac{SNR_c}{SNR_r}. \qquad (2.3)$$

This *g*-value can be calculated for each electrode. With *N* electrodes, this results in *N g*-values. SNR_c, SNR_r and *g* are not evenly distributed over the *N* electrode positions on the scalp. To obtain an overall score for each correction algorithm the γ-values are averaged and converted to a dB scale,

$$G = 20 * \log_{10}\left[\frac{1}{N}\sum_{n=1}^{N} g_n\right]. \qquad (2.4)$$

The resulting score *G* is an indicator for the performance of a correction algorithm. *G* (in dB) is positive if the SNR has improved. It has a negative value if the SNR has decreased and is zero only if the SNR has not changed. An alternative definition for *G* could use a weighting function to give more weight to those electrodes that contain the largest artifacts. In this alternative situation, electrodes with only small eye movement artifacts, e.g. the occipital electrodes, have only a very small contribution in determining *G*. This alternative has some advantages over the definition we use. The alternative *G* would enable us to determine a *G* that is mainly based on those electrodes where correction is most needed. The main disadvantage is that if a correction algorithm would increase SNR at frontal sites and decrease SNR at occipital sites this will stay unnoticed in the alternative *G* score, and the corrected EEG will contain artifacts introduced by the correction algorithm. This is the main reason why we did not use the alternative *G*.

2.6 Evaluated algorithms

In principle any correction algorithm can be evaluated by the score outlined in this chapter. Over the last decades many algorithms have been proposed. Independent Components Analysis (ICA) algorithms appear in recent articles on artifact rejection [16;73]. FastICA, [115], (FICA) is an efficient

implementation of ICA, Joint Approximate Diagonalization of Eigen matrices (JADE) [59] was among the first ICA algorithms to be developed. The main difference between EOG-based algorithms on the one hand, and PCA and ICA algorithms on the other is that the EOG-based methods do not use the data of EEG electrodes simultaneously but perform correction for 1 EEG electrode at a time, whereas the PCA and ICA methods use data from all EEG and EOG electrodes simultaneously to perform the correction. This might be an advantage of the PCA and ICA methods.

In this study a selection of six algorithms, shown in Table 2.3, is evaluated.

Table 2.3: The six algorithms evaluated in this chapter

Abbreviation	Description	Reference
MLR	Multiple Linear Regression	[116]
RARE	EOG-based algorithm using regression with an autoregressive structure to model the EEG	[46]
PCA	Principal Components Analysis	[117]
SOBI	Second Order Blind Identification, a components analysis technique that exploits autocorrelation the components.	[51]
JADE	Joint approximate decomposition of Eigen matrices. One of the first ICA algorithms.	[59]
FICA	FastICA, an efficient ICA algorithm.	[118]

Detection of ocular components for the PCA, SOBI, JADE and FICA algorithm is achieved based on cross correlation between components and EOG signals. If the cross correlation between an extracted component and one of the recorded EOG signals exceeds a threshold value, the component is marked as an ocular component and is removed. The threshold value was optimized in a pilot measurement and set to 0.7. The RARE and the SOBI algorithm require a choice of parameters. For RARE this is the order of the AR-model used to model the EEG, set to 4 following [46]. For the SOBI

algorithm a number of time lags need to be chosen. The components retrieved by the SOBI algorithm are not correlated with each other. The autocorrelation of each component is calculated at the time lags chosen, the SOBI algorithm maximizes the sum of these autocorrelations. In this study we use lags of 0, 1, 2, 3, 5, 10, and 20 samples at 256 Hz. These lags were found to yield good corrections in a pilot study. It should be noted that the components-based algorithms probably have a different performance when two EOG electrodes are used with one positioned above the eye and one beside the eye. In addition odd numbers of EOG electrodes could be used with the components-based algorithms.

ICA algorithms require more electrodes than there are expected sources (dipoles) and require roughly more time points than the square of the number of electrodes. In order to comply with the latter requirement, the time window of 10 s. used in this study is insufficient. Either this window should be increased, or the sample frequency of the EEG should be increased. This would lead to very large datasets containing over 10^5 samples for every EEG electrode and the use of such large sets is computationally undesirable for most of the algorithms. It should therefore be noted that for the dataset simulated in this study, with only 2560 time samples, the ICA algorithms do not perform optimally for the two largest EEG electrode configurations. Increasing the window size will probably increase their performance, but at the expense of larger computational effort. Even though the simulated dataset was too small for the ICA algorithms, they still succeeded in removing part of the artifact, resulting in a positive G. Therefore, the results of applying ICA for correction of the larger electrode configurations will still be mentioned in the results of this study.

2.7 Results

In Figure 2.3 an example of the measured $r(t)$ is shown. To illustrate that this data resembles simulated EEG data, $r(t)^s$, $c(t)^s$, and $e(t)^s$ are also displayed. The left column shows a 10 s window (window length = 2560 samples) of the data, the right column shows the amplitude spectrum after applying a Hanning window. The difference in variability between $r(t)$ and $r(t)^s$ is caused by the error in the ratio $c(t)^s / e(t)^s$. This ratio was set to 1:3 for the Fpz position, as discussed in Section 2.3. For other positions the simulated ratio can deviate from the ratio for experimental data because the simulation uses only a limited number of dipoles.

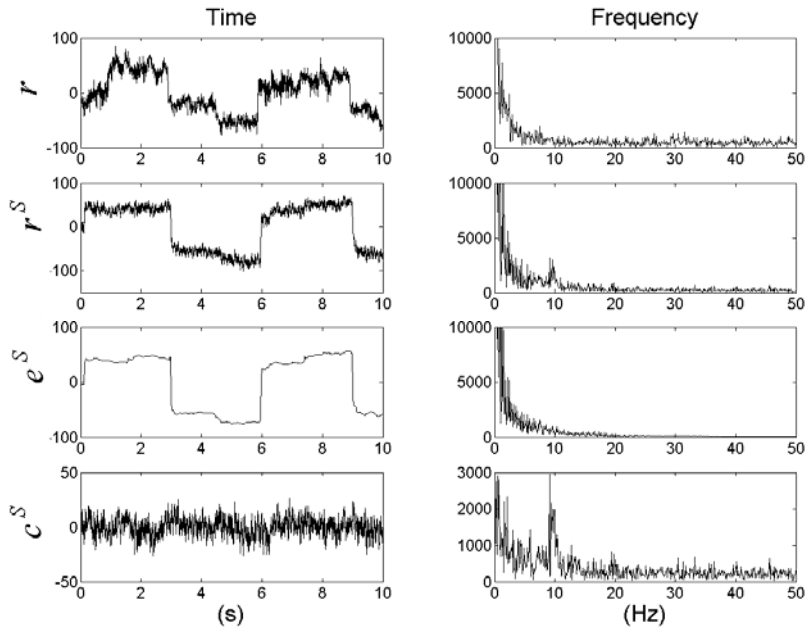

Figure 2.3: From top to bottom: measured EEG, simulated measured EEG, simulated artifact, and simulated true EEG for the F7 position. Left column shows 10 seconds of data (2560 samples) with y-axis in μV, right column shows the amplitude spectrum.

Data segments of 10 seconds (2560 samples) are corrected by all 6 methods and for all 5 electrode configurations. G scores are calculated for each participant for all EEG and EOG configurations and subsequently averaged over the 9 participants. The results are shown in Figure 2.4.

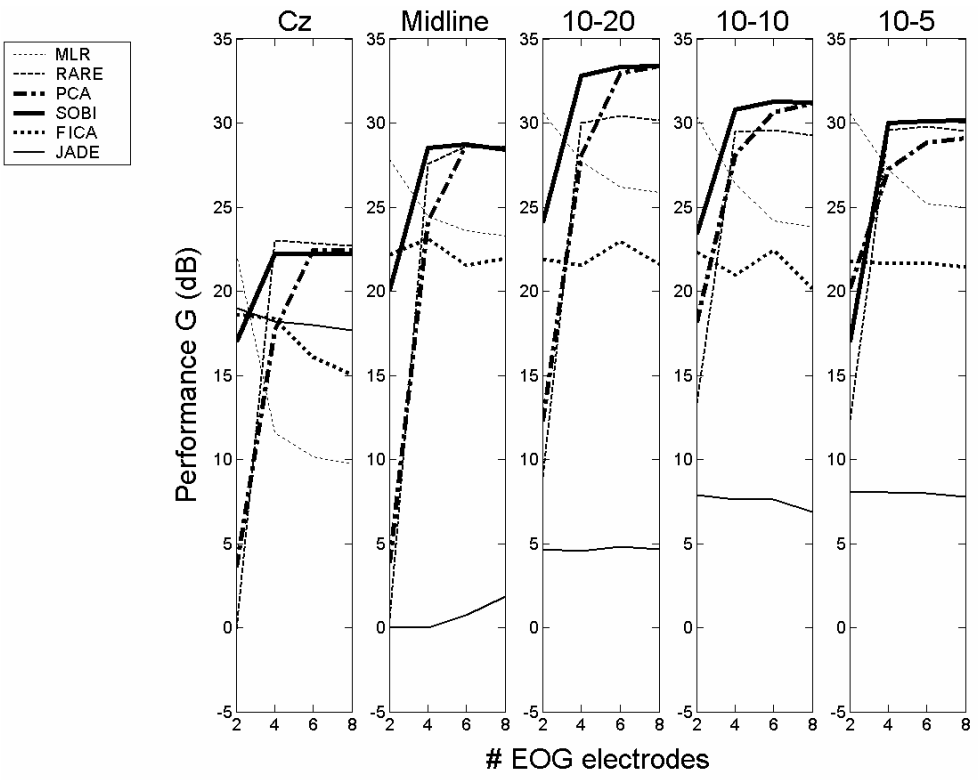

*Figure 2.4: Performances. The 5 graphs each show the score for one of the EEG configurations. The x-axis of these graphs indicates the number of EOG electrodes that was combined with the EEG configuration. For all 20 possible electrode configurations (5*4) the performance grade G in dB is plotted for the 6 algorithms.*

This figure shows the following results:

- All performance values are positive or 0. This implies that all correction algorithms improve the SNR for all configurations studied.
- The best performing algorithms increase the SNR by approximately 25 to 35 dB.
- The differences between the various algorithms are large. FICA and JADE deviate most from the other algorithms.
- When four EOG electrodes are applied, PCA and SOBI have much better correction performance than when using only two EOG electrodes.
- Adding more electrodes (EEG or EOG) in general improves the correction of the components-based algorithms.
- For increasing number of EOG electrodes, MLR has a decreasing performance, whereas the other algorithms have an increasing performance.

- For almost every EEG configuration the SOBI algorithm shows the best correction.
- The highest level of performance for 4 out of 5 EEG configurations is obtained by applying the SOBI algorithm using 6 EOG electrodes. Averaged over the 5 EEG configurations the SNR improvement is 29.0 dB, with a standard deviation of 4.3 dB.
- In most EEG configurations however, the results of applying MLR with only 2 EOG electrodes are close to SOBI's performance, with an average SNR improvement of 28.1 dB and with a standard deviation of 3.6 dB.

To illustrate the results, we also apply the correction algorithms to the EEG data that was recorded during an experiment. The corrected EEG is shown in Figure 2.5.

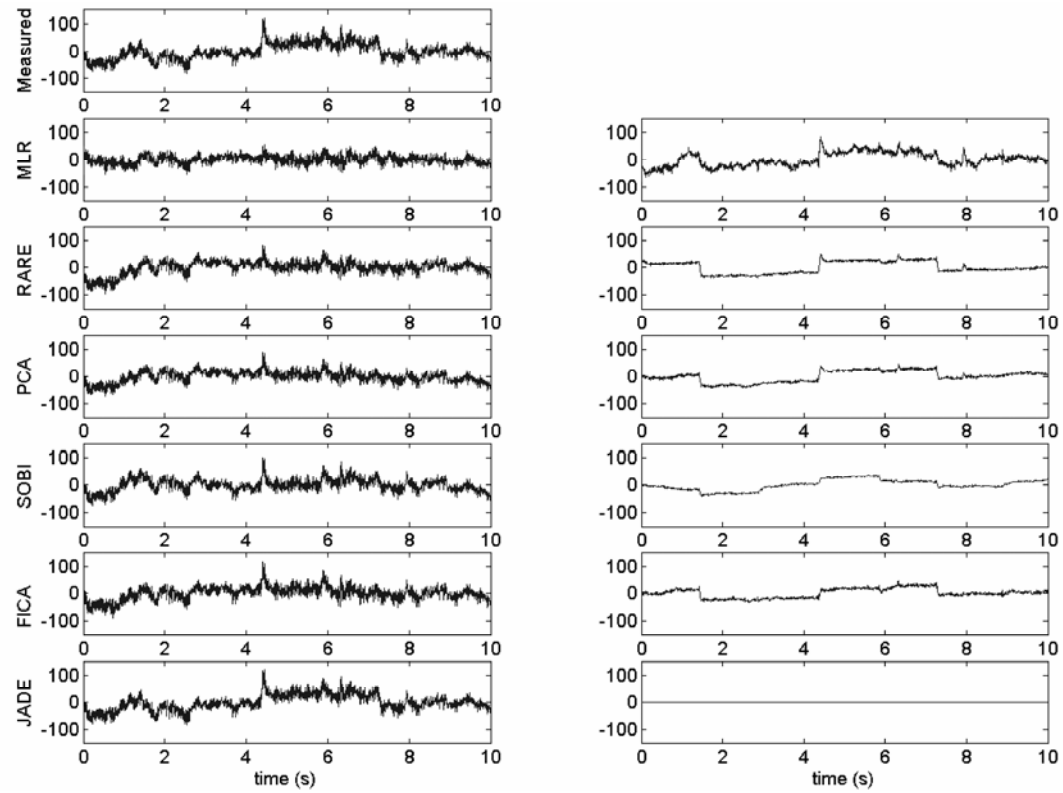

Figure 2.5: Results of the algorithms applied to experimental data of one participant. On the upper left is the measured EEG at Fp2 position. The other graphs in the left column show the EEG after applying the six correction algorithms. In the right column the rejected part of the EEG is shown for each corresponding method. All y-axes show potential (μV).

2.8 Discussion

First of all, it should be mentioned that the use of an eye tracker in this performance evaluation does not imply that all future EEG studies require eye tracker recordings. Once an algorithm is validated with the use of an eye tracker and appears to perform adequately, it can be applied to correct EEG data, without using eye tracker recordings. The recordings of the eye tracker were only used in this study to provide "clean" input data for the model simulations. Compared to other evaluations that use EOG or extracted components to model EOG artifacts, the eye tracker approach has the important advantage that there is no brain related disturbance in the simulated eye movement. Using the 'Boundary Element Method' we are able to simulate recordings for different EEG electrodes configurations that are often used.

The results for the ICA algorithms, JADE and FICA, are rather disappointing, which is in agreement with a recent study in which the FICA algorithm was used [16]. The most probable reason for this is that components were extracted that were not (entirely) of ocular origin. These components have a correlation of more than 0.7 with one of the EOG signals, but were very noisy. Removing them probably attenuates the EOG artifact, but introduces strong noise into $\hat{c}(t)^s$. A component selection by visual inspection, as in [16], did not yield better results. However, results might improve by using a larger window and thus more samples for correction. When performing an MLR, the first EOG signals will remove most of the eye movement artifact, which explains the good performance of the MLR algorithm with only two EOG electrodes. If more EOG signals are used in MLR, they will effectively start to remove actual EEG information. Remarkably, the performance for four EOG electrodes is worse than when using only two EOG electrodes. This is not intuitive since the first two EOG electrodes do not have information on vertical eye movements, present in $r(t)^s$. A possible explanation for this result is that the EOG electrodes in the model are not positioned exactly in line with the eyes. This might be due to the mesh used in this study. For the PCA and SOBI algorithms the increase in performance with increasing number of electrodes was expected because these algorithms make use of the information in all electrodes. Applying more than 6 EOG electrodes does not increase the performance any further. Our data acquisition is performed using the 10-20 system with 6 EOG electrodes, thus corresponding to the middle graph in Figure 2.4. In Figure 2.5 we can visually verify that the part of the signal removed by the SOBI algorithm shows most resemblance with the eye movement artifact in the experimental data. SOBI is the only algorithm that clearly removes a signal that changes every 1.33 s. This is the time the dot in our experiment stayed at the same position.

In Figure 2.5, JADE did not remove any artifact. However, this example of JADE correction is based only on results for one subject, and on real data. In Figure 2.4, results for nine simulated signals are averaged. In some of these nine signals JADE also did not remove any artifact, in others some artifact was removed. Averaged results are shown in Figure 2.4. The PCA, MLR, RARE, and FICA algorithms remove most of the artifact, but not as much as SOBI.

The results shown are limited to eye movements. For blinks, the model should be more detailed around the eyes. The movement of the eyelid could have a very large influence on the conductivity properties of the model near the eyes because tissues here have very different conductivities. Movement of the eyelid thus would not directly influence the eye-dipole itself but rather the model surrounding the dipole. Other studies [104] state that the location of the dipole causing the eye-blink artifacts is different from the location of the eye movement dipole. However since here a 3-shell head model was used, the exact tissue structure around the eyes was not modeled and no sliding eyelid could be simulated. The absence of these characteristics in the model might cause a shifted dipole location when performing source localization for eye blinks.

Some of the parameters that are described in Section 2.3, and that are used in the model to simulate the data, are obtained from experiments. These include the number of dipoles, the EEG spectrum shape, the amplitude ratio between $c(t)$ and $e(t)$ of 1:3, and the amplitude of the electrode-noise $n(t)$. Small fluctuations in the number of dipoles and the spectral shape will have almost no effect on the calculated SNR improvement. The potential distribution over the scalp was already smoothed, and adding more brain dipoles will not change this distribution significantly. The EEG spectrum shape is averaged over 25 measurements. However, the ratio between $c(t)$ and $e(t)$, and the amplitude of $n(t)$ can have impact on the calculated SNR improvement. Changing the ratio to 1:1 would reduce the need for a correction algorithm because it reduces the artifact. This implies that detecting the artifact is more difficult and the SNR improvement will probably decrease. On the other hand, changing the ratio to 1:5 will increase the need for a correction algorithm. Artifact detection will be easier now and the SNR improvement might be higher. But it is not likely that the SNR of the corrected signal is higher because that would imply that very strong artifacts would yield the cleanest results after correction. If there is more electrode-noise, $n(t)$, in the measurement, both the SNR prior to correction and after correction will decrease. The magnitude of $n(t)$ is determined by e.g. the placement of the electrode.

The score G, defined in Section 2.5, is used to determine which correction algorithm performs well. It does not indicate whether the correction algorithms perform well enough. The definition on what is well enough is very subjective and depends on the specific application of the EEG recording.

Moreover, G indicates an increase in SNR whereas the statement of what is well enough should be based on the SNR after correction. The SNR_c would be more suitable for this. The aim of this chapter is to evaluate and compare correction algorithms based on their ability to remove eye movement artifacts and not to determine the (subjective) threshold of what SNR_c is well enough. Therefore G is defined not only by the SNR_c after correction, but also by the SNR_r prior to correction.

Our simulations might be improved by using a more sophisticated BEM implementation to reduce simulation error and give a better resemblance between $r(t)$ and $r(t)^s$. Another improvement to the simulations might be the use of a more detailed mesh of the head, including e.g. details about the eye sockets in the skull [119]. Both improvements will increase complexity. Our main goal was to evaluate the algorithms, not to simulate EEGs as realistic as possible and therefore these improvements were not made. Without the improvements, the simulated EEG might deviate from raw EEG on some properties. However, the properties that are of most importance for our evaluation are simulated, like the instantaneous way in which the conduction through the head takes place and the different origin of ocular and cerebral signals.

2.9 Conclusion

We present a method to evaluate algorithms that correct eye movement artifacts in simulated EEG recordings. The method is based on eye movement data recorded by an eye tracker, ensuring that the eye movement recordings are uncontaminated by brain activity. The data for the evaluation are simulated using a realistic model of the head, based on the boundary element method. Correction results from six algorithms are evaluated. As a measure of performance, we compare the signal to noise ratio before and after applying each correction algorithm. All algorithms reduce the artifact for all electrode configurations. MLR performs best when only two EOG electrodes are used. We recommend using 6 EOG electrodes and performing a SOBI artifact correction. In practice however, calculations with the SOBI algorithm are computationally demanding, especially with the 10-5 system. If faster solutions are required, the use of the MLR algorithm with 1 H-EOG is recommended. Comparing our results with [16] we see that in both studies MLR and PCA perform better than FICA. However the SOBI method, not included in [16], performs even better. This indicates that PCA with autocorrelated components, as applied in SOBI, is also a good candidate for correction.

Other correction algorithms, not mentioned in this chapter, can also be evaluated by the method presented here. Given the assumptions stated in this

chapter, it is shown that the proposed method can be used to determine how well an algorithm performs and which correction algorithm can be used best for any specific EEG/EOG electrode configuration.

Chapter 3

Using an eye tracker for accurate eye movement artifact correction

3.1 Abstract

We present a new method to correct eye movement artifacts in EEG data. By using an eye tracker, whose data cannot be corrupted by any electrophysiological signals, an accurate method for correction is developed. The eye tracker data is used in a Kalman filter to estimate which part of the EEG is of ocular origin. The main assumptions for optimal correction are summed and their validity is proven. The eye tracker-based correction method is objectively evaluated on simulated data of four different types of eye movements and visually evaluated on experimental data. Results are compared to three established correction methods: Multiple Linear Regression, Principal Components Analysis and Second Order Blind Identification. A comparison of signal to noise ratio after correction by these methods is given in Table 3.2 and shows that our method is consistently superior to the other three methods, often by a large margin. The use of a reference signal without electrophysiological influences, as provided by an eye tracker, is essential to achieve optimal eye movement artifact removal.

3.2 Introduction

To correct the electroencephalogram (EEG) for eye movement and blink artifacts, many correction methods have been developed over the past years [8;38;98;106]. Especially in research areas where the EEG signals of interest have very low amplitudes and are of short duration, as for single trial experiments, it is important that the correction method removes as much of the artifact as possible. Often, like in habituation studies or in studies involving children or ADHD subjects, it is not possible or undesired to repeat the experiment numerous times if artifacts occur. Furthermore, the electrical activity of brain processes that mainly occur in the frontal lobe is difficult to

JJM Kierkels, Riani, JWM Bergmans, GJM v. Boxtel, TBME, 54(7), pp1256-1267, 2007

detect because frontal electrode positions can contain eye movement artifacts of large amplitude.

Both brain activity and eye movements cause electric currents through the brain. Therefore the raw EEG signal is a combination of ocular and brain related components. After a recorded signal is corrected for ocular artifacts it is difficult to judge if, and to what extent, correction was successful because the brain and ocular components are not separately known. For this reason, it is also not yet possible to objectively determine the quality of existing correction methods, and hence their adequacy for challenging applications like those mentioned above.

In order to develop a standard against which existing methods can be compared, it is necessary to have a method that, in principle, can achieve optimal correction. The goal of the study in this chapter is to develop such a method and use it to objectively determine the quality of correction of existing methods.

All existing correction methods are, to our knowledge, purely based on electrical potential recordings. If either the ocular or the brain component in the EEG can be reconstructed without the other, it is possible to extract both components from the mixture and objectively determine the quality and adequacy of correction methods. The ocular component is caused by a difference in potential between the front and the back of the eye, known as the corneo-retinal dipole [104]. Eye movements change the orientation of this dipole and thus, via volume conduction through the head, also change the magnitude of the ocular component. Eye blinks and smaller eyelid movements also cause changes in potential at the electrode positions, which can result in artifacts with amplitudes of up to 300 μV. The origin of the change in potential as caused by blinks is different from eye movement potential changes. Blinks briefly change the shape of the volume that surrounds the corneo-retinal dipole. As a result, the attenuation of blink artifacts from frontal to occipital electrodes is different from the attenuation of eye movement artifacts. Moreover, the specific influences of eye movements or eyelid movement on the EEG are difficult to discern. Many studies have demonstrated that there is an accompanying eye movement during a blink and, similarly, during most eye movements there is an accompanying eyelid movement [21;120;121]. Modeling these two artifacts requires two different approaches. In this chapter the focus is on both simulated and recorded eye movement artifacts. By omitting the effects of blinks and eyelid movement during eye movements in our simulations, a considerable simplification is made. A correction method that claims to correct for both blinks and for eye movements should however be able to correct the data presented here as well, because the eyelid position is fixed in our simulations.

We propose to record the orientation of the eye by an eye tracker in order to provide information on the ocular artifact that does not contain any cerebral component. As a measure that represents the orientation of the dipole, the eye tracker records the horizontal and vertical position of the pupil, denoted by $p_1(t)$ and $p_2(t)$ respectively. These positions, combined in a vector $\underline{p}(t) = [p_1(t), p_2(t)]^T$, are indicative of the ocular orientation.

In Figure 3.1 is illustrated that a raw EEG, $r(t)$, contains potentials of both cerebral, $c(t)$, and ocular $e(\underline{p}(t))$ origins, with e for eye. The potential $e(\underline{p}(t))$ is determined by the ocular orientation and by the conductive properties of the head and is assumed to be a function of $\underline{p}(t)$. The separation of the components in $r(t)$ is illustrated in the lower part of Figure 3.1.

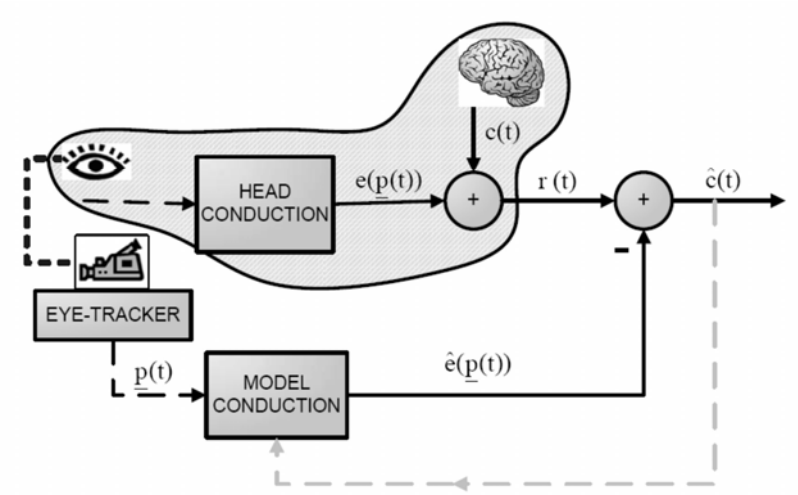

Figure 3.1: Use of an eye tracker as a basis for eye movement artifact correction. The enclosed shape in this figure represents the human part of the setup. Solid arrows indicate potentials.

Because changes in $\underline{p}(t)$ have instantaneous effects on electric potential, due to volume conduction through the head [105], vector $\underline{p}(t)$ can be converted to an estimate of $e(\underline{p}(t))$, denoted by $\hat{e}(\underline{p}(t))$. For this conversion it is necessary that the conductive properties of the head are parameterized in a way that allows for the calculation of $\hat{e}(\underline{p}(t))$ based on the vector $\underline{p}(t)$. By subtracting $\hat{e}(\underline{p}(t))$ from $r(t)$, an estimate for the cerebral component can also be obtained, denoted as $\hat{c}(t)$.

The relation between $\underline{p}(t)$ and $e(\underline{p}(t))$ is unknown and depends, among other things, on physical properties of the subject, like the diameter of the head and exact morphology of the skull, brain and other biological tissues. Obviously, the relation also depends on non-subject-related properties, like electrode placement and the luminance over the retina.

In this chapter it is assumed, and verified, that $e(\underline{p}(t))$ is a first or second order function of $\underline{p}(t)$. Other parameters that may affect $e(\underline{p}(t))$ are a priori unknown as they represent the physical- and non-subject-related properties discussed above, and must be estimated based on experimental data. For accurate artifact removal it is essential that this estimation is accurate. The motivation behind the use of (at most) second order parameterization is that $e(\underline{p}(t))$ is expected to have only one extremum. This extremum is expected to occur if the orientation of the ocular dipole is oriented towards the electrode, which corresponds to a specific value of $\underline{p}(t)$. Moving the dipole away from this orientation, and hence changing pupil position, is expected to results in a smooth change in potential.

Traditionally, as shown in (1.2), artifact correction also combines several unknown elements in one parameter or a vector $\underline{\alpha}(t)$ of parameters. The main difference with the current approach is that parameter estimation now focuses exclusively on the relation between pupil position and raw EEG.

The vector $\underline{\alpha}(t)$ is usually estimated non-adaptively, either during a calibration session, or directly on the data of interest, and leading to estimate vector $\underline{\hat{\alpha}}(t)$. Non-adaptive methods estimate a constant $\underline{\hat{\alpha}}$, over a period of time. Fluctuations of $\underline{\alpha}(t)$ in time will result in sub-optimal correction as a fluctuation of only one percent can cause new artifacts of several μV.

This can be overcome in two ways. Firstly, the length of the recording can be reduced to decrease fluctuations of $\underline{\alpha}(t)$ within this recording. Examples of such are recordings during which $\underline{\hat{\alpha}}$ is recalibrated at fixed times, or components analysis over an epoch of only a few seconds. The effects of a shorter epoch on accuracy of EOG-based and components-based methods is studied e.g. in [16]. In [16] it was found that small parameter fluctuations are less problematic for EOG-based methods. Furthermore correction over a 60 s epoch was significantly worse than correction over a 1 s epoch, which supports the idea that $\underline{\alpha}(t)$ does fluctuate. A difficulty with this approach is that after correction the epochs need to be concatenated and jumps may occur. Secondly, by using parameter adaptation to track $\underline{\alpha}(t)$, it is possible to adapt to parameter fluctuations and have an accurate $\underline{\hat{\alpha}}(t)$ throughout a recording of any duration. This results in a smooth corrected signal that does not suffer from re-attaching problems. Given these advantages, adaptive parameter estimation is used. The parameters that describe how $e(\underline{p}(t))$ depends on $\underline{p}(t)$ are thus obtained adaptively by a feedback-loop in which $\hat{c}(t)$ is used as a basis for adaptation. Adaptation is indicated in Figure 3.1 by the dashed gray arrow.

For the method to work, it is necessary that three requirements are met.

1. Changes in ocular orientation have instantaneous effects on electric potential.

2. Ocular orientation is statistically independent of brain activity, as reflected in the EEG.
3. The relation between $\underline{p}(t)$ and $e(\underline{p}(t))$ is adequately parameterized by 1st and 2nd order combinations of $\underline{p}(t)$, i.e. higher-order terms are negligible.

Assuming that these requirements are met, we will demonstrate that optimal correction can, in principle, be achieved, such that no ocular artifact remains. Requirement one, i.e. instantaneous conduction, has been analytically verified in literature [105]. Requirement two, statistical independency, is probably never completely true. However, in practice this dependence tends to be negligible, as demonstrated in [114]. Section 3.3 will introduce and validate the parameterization scheme, associated with the third requirement, in more detail.

In Section 3.4 a Kalman filter is tailored to our parameter estimation. The Kalman filter is designed to estimate changes in a system in which some prior knowledge on noise and system structure is available. Kalman filters are frequently embedded in control systems because they can be used for real-time operations and because it is essential that system parameters are estimated accurately in order to control the system. The filter minimizes the mean squared error of the parameters in a given system. Since the structure of the system is known, as explained in Section 3.3, such a Kalman filter will be used. Because filtering and parameter estimation is possible online as well as offline, making brain-computer interfaces and direct neurofeedback possible. The trade-off between speed of filter adaptation and estimation variance is explained. It is described how the basic Kalman filter can be tuned to the requirements of eye movement correction. A clear tutorial on Kalman filtering, including examples and program code is given by [122].

In Section 3.5 simulated data are used, in which $e(\underline{p}(t))$ and $c(t)$ are known and combined in order to simulate $r(t)$. By comparing these to $\hat{e}(\underline{p}(t))$ and $\hat{c}(t)$ it will be shown that the new method separates the components accurately. These comparisons are made for various types of eye movement to illustrate that the method still performs very well, even in EEG signals with large eye movement artifacts. An important question to be answered is how these results compare to results of existing techniques. Results will be compared objectively to the Multiple Linear Regression (MLR), Second Order Blind Identification (SOBI) and Principal Components Analysis (PCA) methods. As a yardstick, a signal to noise ratio, SNR, is defined.

Next in Section 3.6, the eye tracker method is applied to experimental data. The estimated potential $\hat{c}(t)$ is displayed for different types of eye movement. As there is no reference on the exact ocular artifact in this case, a qualitative discussion on these results is provided, in lieu of an objective evaluation.

3.3 Second order structure

The correction method is based on the three key requirements listed in the introduction. The third assumption, on the relation between $\underline{p}(t)$ and $e(\underline{p}(t))$, will be investigated here in more detail.

An experiment is performed in which $\underline{p}(t)$ is changed in a regulated way. A participant is seated in front of a monitor, at a distance of 65 cm, the eyes horizontally aligned with the center of the monitor screen. The participant is asked to track a moving dot with his eyes, and instructed not to move his head. The dot appears for 0.5 seconds on 225 (15 x 15) different positions on the monitor, starting at the upper left position, going stepwise towards the upper right, then dropping one line and going stepwise back to the left side. This pattern continues until the bottom right corner is reached. EEG is recorded at 512 Hz. Electrodes are placed according to the 10/20 system [26]. A similar test is performed in a simulated environment, using a model of the head as described in Chapter 2. In this simulated environment, there are no cerebral potentials and the exact relation between $\underline{p}(t)$ and $e(\underline{p}(t))$ can be computed. For the experimental data, all samples recorded while the dot was at one position are averaged for each dot position.

Results for both the experimental and the simulated situation are shown in Figure 3.2. Because ocular artifacts are most profound frontally, the displayed results belong to Fz and Fp1 electrode positions. One of these, Fz, is on the midline, showing symmetry between left-right ocular orientations. For each electrode position, three plots are shown. The left one illustrates $e(\underline{p}(t))$, and the two right ones show cross-sections of this plot where either the horizontal or the vertical pupil position is fixed, resulting in $e(p_1 | p_2)$ and $e(p_2 | p_1)$.

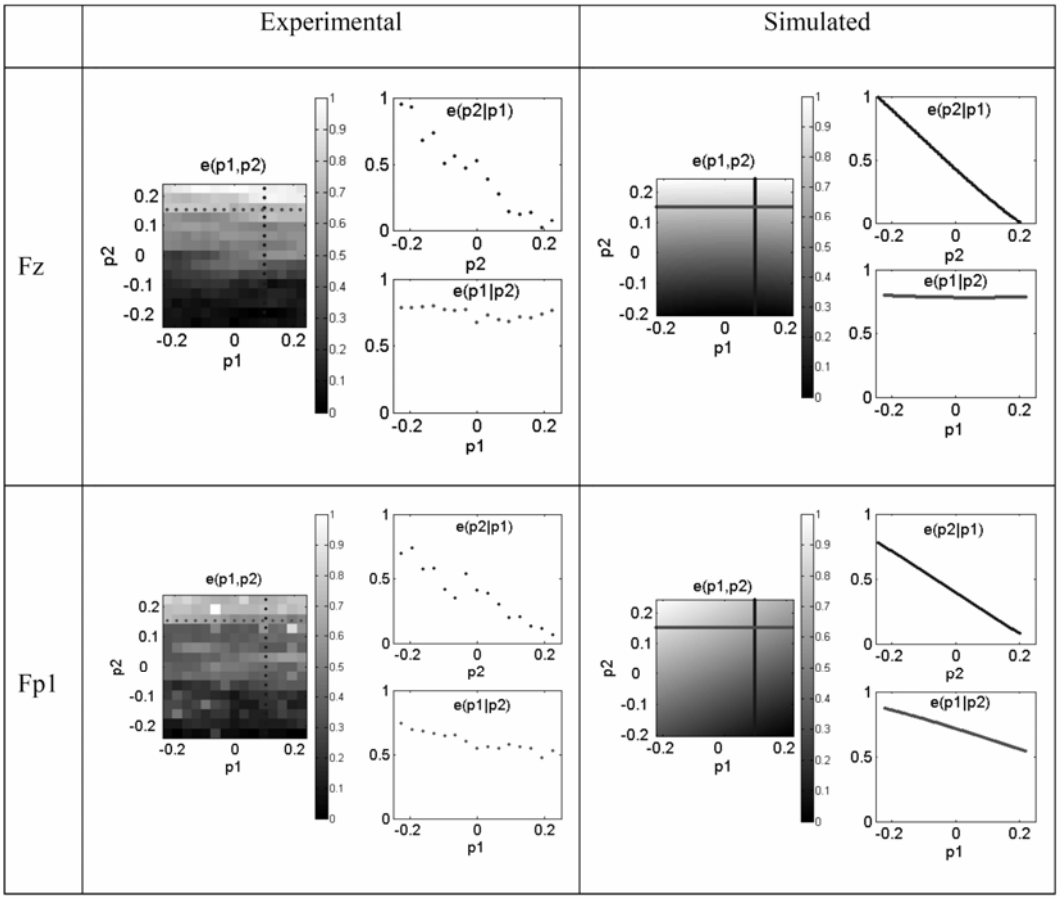

Figure 3.2: Potentials $e(p_1, p_2)$, $e(p_1|p_2)$, and $e(p_2|p_1)$ for experimental and simulated data. For each combination of p_1 and p_2, the potential $e(p_1, p_2)$ is determined and displayed in the image on the left of each of the four subplots. In each plot of $e(p_1, p_2)$, the values for p_1 and p_2 where the cross-sections $e(p_1|p_2)$, and $e(p_2|p_1)$ are made are indicated.

Note in Figure 3.2 that $e(\underline{p}(t))$ is arbitrarily scaled. Also note that p_1 and p_2 range from -0.22 to 0.22. This actually represents the position of a dot on the monitor screen, with $p_1 = p_2 = 0$ at the center of the screen. To convert this position on the screen to $\underline{p}(t)$ would require a minor extra transformation. However, proving that the relation between orientation and potential can be estimated from the data is identical to proving that this holds for the position of the dot. Furthermore, for small angles, the relation between position on the screen and $\underline{p}(t)$ can be assumed to be linear [14].

Clearly visible in Figure 3.2 is the well organized structure of $e(p_1, p_2)$. Vertical movements have a greater impact on the value of $e(\underline{p}(t))$ than horizontal movements for these electrode positions. Most cross-sections show a 1st order dependence. Obviously the plots for simulated data show less variance than plots for experimental data because the simulated ones do not contain any

cerebral component. In the experimental data $e(p_2|p_1)$, has greater variance than $e(p_1|p_2)$. This is due to the time between consecutive samples. The way the experiment is set up, $e(p_1|p_2)$ is recorded within 15*0.5 seconds, whereas $e(p_2|p_1)$ is recorded in $(15)^2$*0.5 seconds. As the recording takes more time, it is more difficult not to move the head and thus the variance of the recording will increase. Another important explanation for this variance is baseline fluctuation during the recording, e.g. due to electrode drifts. These fluctuations are typically of low frequency and are hard to distinguish from changes in $p_2(t)$, which occur once every 7.5 seconds in this experiment. In recordings with high amplitude drifts $e(p_2|p_1)$ can be completely obscured by these drifts, and even $e(p_1|p_2)$ can be affected. The results shown in Figure 3.2 are based on data in which baseline fluctuations were visually not detectable.

The only cross-section showing a 2nd order dependence is $e(p_1|p_2)$ for the Fz position. As this position is on the midline, the distances to both the eyes are equal. Therefore the effects of negative or positive deflection of $p_1(t)$ are identical, causing an optimum at p_1=0.

For other electrode positions, not shown in Figure 3.2, $e(p_1|p_2)$ and $e(p_2|p_1)$ also appear to be (at most) quadratic functions. We infer that $e(\underline{p}(t))$ may be approximated by a 2nd order function. The structure of such a function is given by[3]

$$\begin{aligned} e(\underline{p}(t)) = \phi_1(t) + \phi_2(t) * p_1(t) + \phi_3(t) * p_2(t) + \ldots \\ \ldots \phi_4(t) * p_1(t)p_2(t) + \phi_5(t) * p_1(t)^2 + \phi_6(t) * p_2(t)^2, \end{aligned} \tag{3.1}$$

or, more compactly, by

$$e(\underline{p}(t)) = \underline{\Psi}(\underline{p}(t))^T \cdot \underline{\phi}(t), \tag{3.2}$$

with $\underline{\Psi}(\underline{p}(t)) = [1, p_1(t), p_2(t), \ldots, p_2(t)^2]^T$ and $\underline{\phi}(t) = [\phi_1(t), \phi_2(t), \ldots, \phi_6(t)]^T$.

The six parameters $\phi_1(t)$, $\phi_2(t)$,.... $\phi_6(t)$ in (3.1) together determine the 'MODEL CONDUCTION' block in Figure 3.1. A procedure to estimate these six parameters is described in the following section.

In (3.1) it can be seen that the impact of $\phi_1(t)$ does not depend on $\underline{p}(t)$, making it strange that this parameter is involved in estimating an ocular artifact. Parameter $\phi_1(t)$ however is important in removing baseline fluctuations from $r(t)$. These fluctuations may change $r(t)$ and are independent of $\underline{p}(t)$. By including this parameter $\phi_1(t)$ in vector $\underline{\phi}(t)$, $e(\underline{p}(t))$ can be estimated while

[3] The compact notation $e(\underline{p}(t))$ is used throughout this thesis. This notation can be replaced by $e(\underline{p}(t), t)$ to stress time-dependency of $\underline{\phi}(t)$ in adaptive parameter estimation.

correcting for baseline fluctuations. The impact of $\phi_1(t)$ can be compared to that of a high pass filter. Section 3.4.3 will explain how $\phi_1(t)$ is tuned to track these fluctuations.

3.4 Implementing a Kalman filter

A Kalman filter is capable of estimating the state of a system, even when the exact structure of the modeled system is unknown. The relation between $\underline{p}(t)$ and $e(\underline{p}(t))$ may be considered as such a system because the structure for this relation is known from Section 3.3 while the influence of physical parameters on the system, as given in vector $\underline{\phi}(t)$, is unknown.

3.4.1 Basics of the Kalman filter

A Kalman filter estimates $\underline{\phi}(t)$ in a system that can be described by

$$\underline{\phi}(t) = \underline{\underline{\Phi}} \cdot \underline{\phi}(t-1) + \underline{w}(t), \qquad (3.3)$$

with matrix $\underline{\underline{\Phi}}$ representing the expected changes in $\underline{\phi}(t)$ over time and $\underline{w}(t)$ representing fluctuations in $\underline{\phi}(t)$ that are white, with normal distribution, and independent of $c(t)$. The notation $\underline{\phi}(t-1)$ is used to indicate the value of $\underline{\phi}(t)$ at the previous sample.

Vector $\underline{\phi}(t)$ represents the state of all unknown parameters that influence the relation between $\underline{p}(t)$ and $e(\underline{p}(t))$. As in most applications of the Kalman filter, $\underline{\phi}(t)$ cannot be measured and therefore can only be obtained indirectly by recording $r(t)$, as seen in

$$r(t) = c(t) + e(\underline{p}(t)) = c(t) + \underline{\Psi}(\underline{p}(t))^T \cdot \underline{\phi}(t). \qquad (3.4)$$

Because $\underline{\phi}(t)$ is unknown, it can only be approximated by an estimate $\hat{\underline{\phi}}(t)$. The Kalman filter in effect is a set of equations that iteratively minimizes $\underline{\underline{\Pi}}(t)$, defined as the a posteriori estimate error covariance.

$$\underline{\underline{\Pi}}(t) = E\left[\left(\underline{\phi}(t) - \hat{\underline{\phi}}(t)\right)\left(\underline{\phi}(t) - \hat{\underline{\phi}}(t)\right)^T\right] \qquad (3.5)$$

By minimizing $\underline{\underline{\Pi}}(t)$ a statistically optimal $\hat{\underline{\phi}}(t)$, with respect to any quadratic function of estimation error, is obtained. At each moment in time, the filter thus estimates a new optimal value $\hat{\underline{\phi}}(t)$ based on $\hat{\underline{\phi}}(t-1)$ and $r(t)$. With this estimate $\hat{\underline{\phi}}(t)$, the ocular component can be removed from $r(t)$.

In a system in which the exact system structure is known, in which all noise characteristics are known, and in which an infinitely long adaptation period is allowed, the Kalman filter will achieve perfect separation between artifact and signal. In practice the allowed adaptation time is limited and the noise characteristics are often not known exactly known. How this influences the

filter properties is explained in Section 3.4.2. In this chapter, the system is influenced by a noisy signal $c(t)$. Given only a limited amount of data, the Kalman filter returns the best possible estimate for $\underline{\hat{\phi}}(t)$.

The full Kalman filter equations are listed in equations (3.6)-(3.10).

$$\underline{\underline{\Pi}}^{-}(t) = \underline{\underline{\Phi}} \cdot \underline{\underline{\Pi}}(t-1) \cdot \underline{\underline{\Phi}}^{T} + \underline{\underline{Q}} \tag{3.6}$$

$$\underline{\hat{\phi}}^{-}(t) = \underline{\underline{\Phi}} \cdot \underline{\hat{\phi}}(t-1) \tag{3.7}$$

$$\underline{\kappa}(t) = \underline{\underline{\Pi}}^{-}(t) \cdot \underline{\Psi} \cdot (\underline{\Psi}^{T} \cdot \underline{\underline{\Pi}}^{-}(t) \cdot \underline{\Psi} + R)^{-1} \tag{3.8}$$

$$\underline{\hat{\phi}}(t) = \underline{\hat{\phi}}^{-}(t) + \underline{\kappa}(t) \cdot \left(r(t) - \underline{\Psi}^{T} \cdot \underline{\hat{\phi}}^{-}(t)\right) \tag{3.9}$$

$$\underline{\underline{\Pi}}(t) = \left(\underline{\underline{I}} - \underline{\kappa}(t) \cdot \underline{\Psi}^{T}\right) \cdot \underline{\underline{\Pi}}^{-}(t), \tag{3.10}$$

with $\underline{\kappa}(t)$ being the Kalman gain, $\underline{\underline{\Pi}}^{-}(t)$ the a priori estimate error covariance, $\underline{\underline{I}}$ the identity matrix, $\underline{\underline{Q}}$ the assumed covariances of $\underline{w}(t)$, and R the assumed variance of $c(t)$. Given the assumed values for $\underline{\underline{\Phi}}$, $\underline{\underline{Q}}$, R and the estimate $\underline{\hat{\phi}}(t-1)$, equations (3.6)-(3.10) can be used to estimate $\underline{\hat{\phi}}(t)$. More details and a derivation of these equations are given in [123].

3.4.2 Adaptation time versus estimation accuracy

The matrix $\underline{\underline{Q}}$ and scalar R are not defined by the Kalman equations, but by the dynamic properties of the system that is being modeled. They may be set based on prior knowledge on the dynamics or based on specific desires for the filter performance as will be explained in this section. In a Kalman filter, the time required for stabilization of $\underline{\hat{\phi}}(t)$ is influenced by both the choice of $\underline{\underline{Q}}$ and the choice of R. In (3.8) it can be seen that decreasing R, indicating the assumption of lower amplitude background EEG, increases the value of the elements in gain $\underline{\kappa}(t)$. Substitution of (3.6) in (3.8) reveals that a decrease in the values of the $\underline{\underline{Q}}$ has the opposite effect and decreases the value of the elements in gain $\underline{\kappa}(t)$. The gain $\underline{\kappa}(t)$ is, according to (3.9), related to the magnitude of changes in $\underline{\hat{\phi}}(t)$. It is therefore clear that changes in gain $\underline{\kappa}(t)$ affect the time required for parameter stabilization and parameter adaptation.

After sufficient iterations, $\underline{\hat{\phi}}(t)$ will stabilize. The Kalman gain $\underline{\kappa}(t)$ will still depend on R and therefore the fluctuations of $\underline{\hat{\phi}}(t)$ after stabilization also depend on R. These fluctuations influence the variance in $\hat{e}(\underline{p}(t))$. A similar reasoning applies for $\underline{\underline{Q}}$. The choices of $\underline{\underline{Q}}$ and R are always the result of a trade-off between adaptation time and estimation accuracy.

It is important that $\hat{e}(\underline{p}(t))$- $e(\underline{p}(t))$ is small compared to the signal of interest, $s(t)$. Because $\hat{e}(\underline{p}(t))$- $e(\underline{p}(t))$ represents the part of $r(t)$ that is not of cerebral origin, it will be referred to as noise This noise should not be confused with

what is known as 'electrode noise', an extra additive component to signal $r(t)$ that is caused by the recording equipment. What $s(t)$ is, depends on the specific EEG study that is being performed. Clearly, when the signal of interest is $c(t)$, more noise can be tolerated than when the signal of interest is only a small component of $c(t)$ as is the case in e.g. evoked potential, EP, studies. By using a signal to noise ratio defined as

$$\mathrm{SNR} = \frac{\frac{1}{T}\int_{t=t_1}^{t_1+T} s(t)^2\,dt}{\frac{1}{T}\int_{t=t_1}^{t_1+T} \left(\hat{e}(\underline{p}(t)) - e(\underline{p}(t))\right)^2 dt}, \qquad (3.11)$$

the performance of the correction can be objectively determined. In (3.11) t_1 represents the start of the period over which SNR is calculated and T represents the duration of this period. For ongoing EEG studies t_1 will be the start of the measurement and T the length of the measurement. For EP studies, SNR can be determined for each separate stimulus, with t_1 the stimulus time and T the (expected) duration of the stimulus response. For (3.11) it is required that $e(\underline{p}(t))$ and $s(t)$ are known. Therefore SNR can only be determined for simulated data. As $\hat{e}(\underline{p}(t))$ depends on the choices for $\underline{\underline{Q}}$ and R, it is clear that SNR also depends on these choices.

An optimal correction can be achieved after an infinitely long adaptation, assuming that the vector $\underline{\phi}(t)$ stays constant and that the spectrum of $c(t)$ is white. However in practice, the level of correction is restricted by the duration of the measurement, the frequency content of the EEG, and by the requirement that small changes in $\underline{\phi}(t)$ should be tracked. The physical processes that change $\underline{\phi}(t)$ are slowly varying and can be considered constant for several minutes, e.g. temperature and sweating. Changes in vector $\underline{\phi}(t)$ can also be due to e.g. electrode movement or small head movements. These will cause faster and greater changes in $\underline{\phi}(t)$. By instructing the participant not to move during the recording, these changes can be decreased. It will however still be necessary to track the remaining changes like baseline fluctuations. Typically these only contain very low frequencies, below 0.1 Hz. In the recordings that are used in this chapter, baseline fluctuation is detected visually. The maximum fluctuation frequency is app. 0.03 Hz. Therefore, in this study, it is required that changes in $\underline{\phi}(t)$ can be tracked within 30 seconds. This value is fast enough to track changes in $\underline{\phi}(t)$. A calibration period of 30 seconds should precede each experiment. Note that changes due to fast head movements cannot be tracked in this manner.

3.4.3 Tuning the Kalman filter

In (3.3), $\underline{\underline{\Phi}}$ reflects how $\underline{\phi}(t)$ may change. Such a change can for instance be caused by to changes in the amount of light at the retina, by sweating, or by electrode movements and drifts. Since there is no prior knowledge on what changes to expect, $\underline{\underline{\Phi}}$ is set to the identity matrix $\underline{\underline{I}}$. Alternatively, setting $\underline{\underline{\Phi}}$ equal to $0.99*\underline{\underline{I}}$ can be used to keep $\hat{\underline{\phi}}(t)$ from unbounded growth, although no extreme values were seen with $\underline{\underline{\Phi}}=\underline{\underline{I}}$. The expected variance of $c(t)$ is given in R. The basic Kalman filter assumes $c(t)$ to be white whereas in reality, $c(t)$ is known to be colored as the frequency content of the EEG is generally below 50 Hz. For now we will assume $c(t)$ to be white and use the basic Kalman filter. As the average variance of an EEG recorded with eyes open is approximately 144 μV^2, as determined experimentally, R is set to this value. It is known that choosing $\underline{\underline{Q}}$ is generally more difficult. As we typically do not have the ability to observe $\underline{\phi}(t)$ directly, it is also difficult to estimate the variances of these parameters. Because of this difficulty, the structure of $\underline{\underline{Q}}$ is simplified by assuming that the fluctuations in the parameters in $\underline{\phi}(t)$ are not correlated with each other. This implies that all off-diagonal entries in $\underline{\underline{Q}}$ are zero. The diagonal entries of $\underline{\underline{Q}}$ indicate the variances of the six parameters in $\underline{\phi}(t)$. They are set to track changes in a limited amount of time. As changes that influence conductance are expected to affect all parameters simultaneously, all diagonal entries should be set to obtain a similar tracking time of 30 seconds for the corresponding parameter. If the data is not rich enough it is not possible to estimate and thus track some of the parameters. If for instance there are no eye movements, only $\phi_1(t)$ can be estimated. For the Kalman filter the tracking time is determined by $\underline{\Psi}(\underline{p}(t))$, R and $\underline{\underline{Q}}$. The first two are fixed, and thus tracking time is set to 30 seconds by setting $\underline{\underline{Q}}$. In Figure 3.3 it is illustrated how the tracking time for $\phi_3(t)$ depends on the third diagonal element of $\underline{\underline{Q}}$, denoted as σ_{X3}^2.

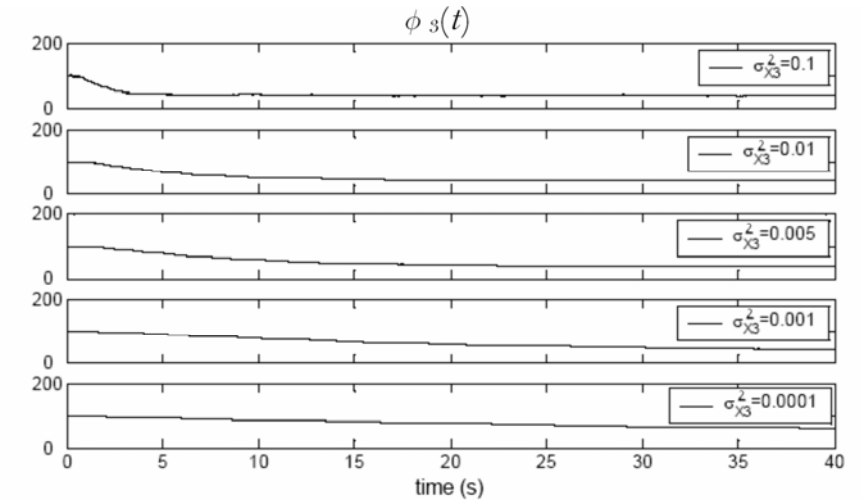

Figure 3.3: Influence of $\sigma_{X3}{}^2$ on tracking time. Each subplot is initialized at 100 ($\mu V/m$). Results are obtained using simulated data with random eye movements.

Because larger values for $\sigma_{X3}{}^2$ result in larger estimation variance, $\sigma_{X3}{}^2$ is set to the smallest possible value that stabilizes $\underline{\phi}(t)$ within 30 seconds; $\sigma_{X3}{}^2 = 0.005$. This is repeated for all six diagonal entries of $\underline{\underline{Q}}$, resulting in $\mathrm{diag}(\underline{\underline{Q}}) = [0.001, 0.005, 0.005, 0.6, 0.6, 0.6]^T$. Stabilization of $\underline{\phi}(t)$ is typically determined by the slowest tracking parameter in $\underline{\phi}(t)$. Setting $\sigma_{\underline{X}}{}^2$ for each element separately will lead to equal stabilization within 30 seconds and will result in minimal estimation variance for a given tracking speed. The risk of adaptive parameter estimation is that brain activity that correlates in time with eye movements is being removed as well. Although it is impossible to eliminate this risk completely, we note that such brain activities are usually reflected in brief evoked potentials, whereas the change in ocular orientation as caused by eye movements lasts much longer. The parameter tracking, with an adaptation speed of 30 s will hardly be modified by the correlation between brain activity and the change in $\underline{p}(t)$. In [114] the influence of ocular orientation on brain activity is found to be negligible.

3.5 Simulated data, accuracy of the new method compared to existing methods

The most important feature for any ocular artifact removal method is its performance on experimental data. Objective classification of removal performance based on this type of data is however very difficult or even impossible. A way to estimate this performance is to use simulated data. In order to obtain meaningful results it is important that the simulation model is a good representation of reality.

3.5.1 Simulated data

We simulate EEG data using a Boundary-Element-Method, BEM, based model of the human head. Brain activity is simulated in this model by rotating a fixed number of brain-dipoles with fixed dipole strength, and fixed position. This results in $c(t)$ with most of its signal power below 30 Hz, and having an exponential decay of power with increasing frequency. The exact properties of these dipoles, the model of the head, and properties of the dipoles used to simulate eye movements and EEG are described in detail in Chapter 2. The main advantages of this model lie in the ability to simulate separately, but realistically, the sources that are generating $e(\underline{p}(t))$ and $c(t)$ using dipole modeling. A minor drawback is the inaccuracy in the modeling of the skull. Whereas a skull has holes behind the eyes, the model only simulates a closed-surface skull. This may lead to an inaccurate representation of scalp topography of the ocular artifact. However, the topography of the ocular artifact is not used (explicitly) in the correction method presented here. Recall that spatial information on the topography of ocular artifacts is not used as only a single EEG recording is required. Inaccuracies in ocular artifact topography are therefore expected not to influence ocular artifact removal for the correction method that we propose. EEG is simulated at all positions of the 10-20 system. Because the properties that determine conduction remain constant during the whole simulation, $\underline{\phi}(t)$ is constant.

Next to the brain activity and eye movement artifact, electrode noise is also simulated, as described in Section 2.3. Each electrode has some intrinsic noise which we simulated to be normally distributed, with zero mean and a standard deviation of 1 μV. This is similar to electrode noise levels as determined for the active electrodes we used in our experiments. Since this electrode noise is small compared to the simulated brain activity, small changes in standard deviation are not expected to result in significant changes in correction performance.

Additional to EEG data, eye tracker data $\underline{p}(t)$ also needs to be simulated. Clearly $\underline{p}(t)$ will depend on the eye movement that is simulated. To simulate eye movements, the ocular dipoles, implemented in the BEM model, are oriented towards a dot that moves over a screen positioned 0.8 meters in front of the simulated head. As the dot moves, the ocular dipoles rotate, and an eye movement is simulated. The center of the screen is horizontally aligned with the eyes and is $45 \cdot 45\,\text{cm}^2$. An eye tracker positioned near the screen and directed to the head records $\underline{p}(t)$. The vector $\underline{p}(t)$ will resemble the data on the movement of the dot. Therefore, the moving dot data are converted to simulate $\underline{p}(t)$. For the conversion, the 2D position in cm is converted linearly to $\underline{p}(t)$.

In this chapter, four different types of data sets are simulated. Each of these sets can be characterized by a specific sort of eye movement. This is done

because any information on $\underline{\phi}(t)$ needs to be derived from the data. If the data for instance only contains one steady ocular orientation, it is not possible to accurately estimate all parameters in $\underline{\phi}(t)$. By using different sets, we can evaluate how well the correction methods perform for these situations.

The types of eye movement that are simulated in the different data sets are listed in Table 3.1. These types are chosen because they represent relevant eye movements that can occur during experiments.

Table 3.1: Simulated eye movements types and their descriptions

Type	Name	Constraints
1	Random eye movement	$p_1(t) \in \mathcal{N}(0,\sigma=d_m/4)$, $p_2(t) \in \mathcal{N}(0,\sigma = d_m/4)$
2	No eye movement	$p_1(t) = p_2(t) = 0$
3	Deterministic eye movement	$p_1(t) = d_m * \sin(\omega * t)$, $p_2(t) = d_m * \cos(\omega * t)$
4	Saccade eye movement	$p_1(t) \in \{-d_m, 0, d_m\}$, $p_2(t) \in \{-d_m, 0, d_m\}$

For random eye movements, the eyes are on average directed towards the center of the screen. Because the frequency of eye movements is physically limited, e.g. it is only possible to focus on approximately three different spots within one second, positions $p_1(t)$ and $p_2(t)$ are simulated by applying a low pass filter, with a cut off frequency at 3 Hz, to a random, white noise signal. The second type is less realistic, but illustrates what happens if there is no eye movement at all. In this case, an ocular artifact correction method should only remove a DC offset. The third type simulates a dot-tracking task where the dot makes a smooth circular movement over the screen. The fourth type simulates a dot-tracking task where the dot jumps once every two seconds from one point of the screen to another.

In Table 3.1, d_m is the maximum amplitude of vector $\underline{p}(t)$ with respect to the center of the monitor screen ($d_m = 0.225$ meter), ω represents the angular frequency of the deterministic eye movement in rad/s, and $\mathcal{N}(0,\sigma= d_m/4)$ indicates a normal-distribution around zero with a standard deviation of $d_m/4$. Note that the samples did not exceed d_m in our simulations. Samples for type the saccade movement are drawn from $\{-d_m, 0, d_m\}$, with equal probability for the three entries.

The amplitudes of $c(t)$ and $e(\underline{p}(t))$ can be scaled in the simulation by increasing the strength of the sources. This way both potentials are scaled to realistic values. For each electrode position, the amplitude of $e(\underline{p}(t))$ is scaled to an

experimentally determined appropriate value for the amplitude of ocular artifacts. Note that the value for $\underline{\underline{Q}}$, which was set in Section 3.4.3, was already based on these realistic values.

For each type, 40 seconds of data are simulated at a rate of 256 Hz. The first 30 seconds are used for parameter initialization. The last 10 seconds are used to evaluate the correction method.

The signal of interest in this case is $c(t)$. The SNR provides a good indication of how well the correction method succeeds in removing the ocular artifact. In the following sections, results are shown for the Fp1 position. This position is very close to the eyes and therefore contains the largest ocular artifact. Thus results for this position can be considered as 'worst case' results.

3.5.2 Comparison with other methods

It is important to see how these results relate to those of existing techniques because this can verify whether the extra effort of including an eye tracker in an experimental setup does improve ocular artifact removal. Three existing ocular artifact removal methods will be discussed.

MLR: Multiple Linear Regression [116]:

Bipolar recordings of the electro-oculogram (EOG) are scaled and subtracted from the EEG. The number of EOG channels that results in the best correction is still under debate. In the evaluation of correction methods, the best result of using either two, four, six or eight EOG electrodes, and hence one, two, three, or four bipolar EOG recordings, is displayed. Bipolar EOG recordings have the advantage that brain activity that is recorded by both electrodes is greatly reduced in the EOG and the bipolar EOG is thus relatively clean when compared to a common reference EOG. However, brain activity originating close to the eyes will still be visible in a bipolar EOG. Often a calibration period precedes the data that should be corrected. The MLR parameters are calculated over this period and subsequently fixed and used to correct the data of interest. Here, in all but one of the simulated eye movement types, the eye movements cover a wide range, similar to a range that would have been used during calibration. Adding a calibration period would therefore not enhance performance. The results shown here may be viewed as correcting calibration data with coefficients found on the same calibration data. Because many eye movements are made during each type, the coefficients will be accurate. Only the type 1 movement is likely to improve significantly when a calibration trial is added.

PCA: Principal Components Analysis [117]:

All raw EEG, and EOG, channels are projected onto a new set of orthogonal base vectors in an attempt to decorrelate brain and ocular activity. The vectors

that resemble the EOG channels are removed and the remaining vectors are used to construct a cleaned EEG.

SOBI: Second Order Blind Identification [51]:

Components analysis technique similar to PCA, but with the ability to exploit autocorrelation in brain activity and autocorrelation in ocular activity. In [100;124] it is shown that SOBI can be tuned very accurately for the purpose of extracting small components arising from the primary somatosensory cortex. Next to this, SOBI is capable of removing ocular artifacts and other artifacts, making it an easy to use and versatile algorithm. For the SOBI method a number of time lags need to be chosen. The components retrieved by SOBI are uncorrelated with each other. The correlations between all components are calculated at these specific time lags. The SOBI algorithm minimizes the sum of all calculated correlations, excluding all autocorrelations. Unfortunately the study as to which lags should be used to optimize SOBI performance is currently limited to extracting primary somatosensory cortex signals [124]. The optimal setting of lags depends on spectral properties of the signals that need to be separated and is therefore likely to be different here. In this chapter, the lags of 1, 2, 3, 5, 10, and 20 samples at 256 Hz are used. These lags are equal to those used in Chapter 1, where SOBI was found to be the best performing correction algorithm. The SOBI method may however improve if the optimization of the selected lags for ocular artifacts is studied in more detail.

These three methods are selected because Chapter 2, as well as other studies [16], has demonstrated these methods' adequacy for ocular artifact correction.

In order to make a fair comparison between the methods, it is important that the effective amount of data available to all methods is equal. The eye tracker method requires a 30 second parameter tracking period prior to the 10 s we use for evaluation. Even though this is merely a parameter initialization comparable to calibrating EOG-based approaches, this period provides the eye tracker method with extra information that should also be available to the other methods. In order to make a fair comparison, the other methods should thus estimate $\hat{e}(\underline{p}(t))$ based on a similar amount of data. The eye tracker method uses an adaptive filter. In principle, the data of the past 30 seconds is weighted exponentially, with the highest wait to the most recent sample, when estimating $\hat{\underline{\phi}}(t)$.

Because the other algorithms use datasets of fixed length and apply the same weight to each sample, the length of these datasets, T_w, should be matched to the amount of data in the exponentially weighted 30 seconds. This relation is given by

$$\int_{0}^{30}\left(1 - e^{\frac{-t}{\tau_w}}\right)dt = T_w. \qquad (3.12)$$

Stabilization of $\hat{\underline{\phi}}(t)$ occurs within three times the decay constant, τ_w, of this equation. Since this corresponds to 30 seconds, $\tau_w = 10$ seconds, and from (3.12) $T_w = 20.5$ seconds.

For a 40 second data-segment this means that in order to have matching amounts of data, the eye tracker method starts calibrating at the start of the segment whereas the other methods should operate on the last 20.5 seconds of the segment. Finally, the last 10 seconds are used to evaluate the correction methods.

As discussed in the introduction, most correction methods assume a stationary relation between eye movement and recorded artifact as well as a stationary relation between cerebral activity and raw EEG. In order to comply with this assumption, epochs of short duration are often used. Increasing the epoch duration for such methods, to compensate for the parameter tracking period, might actually be a disadvantage. Because in the simulated data all parameters in $\underline{\phi}$ are constant the assumption of stationarity is not violated, so there is no need to use shorter epoch duration and (additional) difficulties when re-attaching different epochs are avoided.

3.5.3 Results

All four data-types were corrected by the eye tracker-based method and also by the three other ocular artifact removal methods, the SNR calculated for all methods are shown in Table 3.2. The results are averaged over 20 simulations to decrease the influence of the randomness of $c(t)$ on the results.

Table 3.2: Performances of different ocular artifact removal methods for different types of simulated eye movements. Performance calculated over 10 seconds is expressed as SNR. Results are averaged over 18 simulated sets

		Eye tracker	**MLR**	**PCA**	**SOBI**
Type		SNR (dB)	SNR (dB)	SNR (dB)	SNR (dB)
1	Random	15.5	3.1	2.5	7.9
2	None	21.1	0.1	2.5	18.3
3	Deterministic	17.3	5.5	0.8	15.6
4	Saccade	10.3	5.4	1.2	9.9

3.5.4 Discussion

The eye tracker method consistently outperforms the three other methods, often by a large margin. In any of the four types of eye movement, the eye tracker method results in an average SNR of over 10 dB. This indicates that power of the remaining artifact after correction is approximately 10 times smaller than the power of the estimated $\hat{c}(t)$. The best SNR is obtained for type 2. For this type the optimal correction would be to remove only DC because the eyes did not move during simulation. However, prior to applying any correction method, the DC is already removed by subtracting the mean of the signal because this is common procedure with most EEG recordings. Therefore type 2 illustrates how the correction methods affect SNR if no correction is needed. Without correction the SNR in this case is infinitely large since there is no noise. All correction methods slightly distort $\hat{c}(t)$ because all SNR values in Table 3.2 are finite. The other three methods result in a lower SNR than the proposed eye tracker method. For the MLR method this is probably caused by the presence of a small cerebral component in the recorded EOG, due to volume conduction. For all eye movement types, the optimal MLR correction was achieved when two bipolar EOG recordings, and hence four EOG electrodes were used. The PCA and SOBI identify several different components the data of type 2 movement, but they lack the clean reference signal of an eye tracker. Therefore the EOG channels are used to determine which of the components are ocular and these channels will not show the eye movement as clear as $\underline{p}(t)$. For type 3 and 4 the SNR of the SOBI method is close to the SNR of the eye tracker method. The SOBI method exploits deterministic time structures that are hidden in the data, and it is therefore not surprising that under these circumstances SOBI achieves an SNR of 15.6 dB and 9.9 dB respectively. The use of $\underline{p}(t)$ in the eye tracker method does however perform slightly better. Indicating that the extra data that is available due to the use of the eye tracker, provides important extra knowledge on the ocular artifact. The PCA and the MLR methods are consistently outperformed by the SOBI and by the eye tracker methods. For PCA this is probably because PCA does not use the temporal information of $r(t)$, whereas SOBI does [51]. MLR has the risk of overcorrecting and removing brain activity from the EEG. As discussed, EEG registrations often contain baseline fluctuations due to e.g. electrode drifts. The eye tracker method is tuned to track these fluctuations. Even though in this simulated data there are no fluctuations in parameters, the performance of the eye tracker method is still better than the other methods. If the data would have contained baseline fluctuations, the eye tracker method would have removed them with essentially no impact on SNR. Because these fluctuations are mostly not correlated for different electrodes, both SOBI and PCA would not remove them and therefore the SNR shown for these methods

in Table 3.2 would decrease. The results in Table 3.2 are based on 20 simulated datasets. The deviation of single experiment results around this average are small and thus indicate reliable correction. For the type 1 movement e.g., only one simulation deviated by 1.8 dB (having an SNR of 13.7 dB), all other simulations deviated by less than 1.1 dB.

For the eye tracker method a one channel EEG recording is sufficient to obtain the results that are shown in this chapter. The extra requirement for this method is that an eye tracker is added to the experimental setup. For the SOBI and PCA method, no eye tracker is required, but EOG electrodes need to be included in the measurement as well as a larger number (21) of EEG channels to obtain the results presented here.

3.6 Experimental data, using the new method for correction.

EEG, EOG and eye tracker measurements are collected from 9 participants aged 19-21, 5 male and 4 female. The participants performed a task involving eye movements. During this task, a (moving) dot appears on a 19-inch monitor. Like with the simulated data, there are different types of eye movements, corresponding to types 2-4 from Table 3.1. The participant is asked to keep his eyes on the moving dot. An eye tracking system is positioned directly below the monitor and records the position of the participants left eye. It uses an infrared light and from the light reflected by the eye, the position of the center of the pupil is determined. EEG measurements are performed with 21 EEG electrodes positioned according to the 10-20 system. Another 6 electrodes are used to record the EOG. They are positioned above and below both eyes, left of the left eye and right of the right eye. Recordings for all electrodes are offline referenced to averaged mastoids. EEG and EOG are recorded at 256 Hz using the BioSemi ActiveTwo system with sintered Ag/AgCl electrodes using a lowpass filter with a cut-off of 67 Hz. Eye tracker data are recorded at 50 Hz using the SensoMotoric Instruments RED eye tracker with an angle resolution better than 0.1 degree. The eye tracker data are up-sampled from 50 to 256 Hz afterwards and synchronized with the EEG recording. During the task, the participant sits comfortably in front of a monitor at 0.8 m distance with the head supported and eyes are horizontally aligned with the center of the screen.

3.6.1 Results

With experimental data it is not possible to calculate the SNR because $c(t)$ is unknown. For this reason, the estimated EEG, $\hat{c}(t)$, is presented as a result of correction. The segment that is shown corresponds to the 10 seconds immediately after the 30 second initialization period. Because SNR cannot be

determined, it is not possible to objectively prove the accuracy of these corrections. Results, again shown for the Fp1 position, are illustrated in Figure 3.4 for the eye tracker and the SOBI method as these performed best on simulated data.

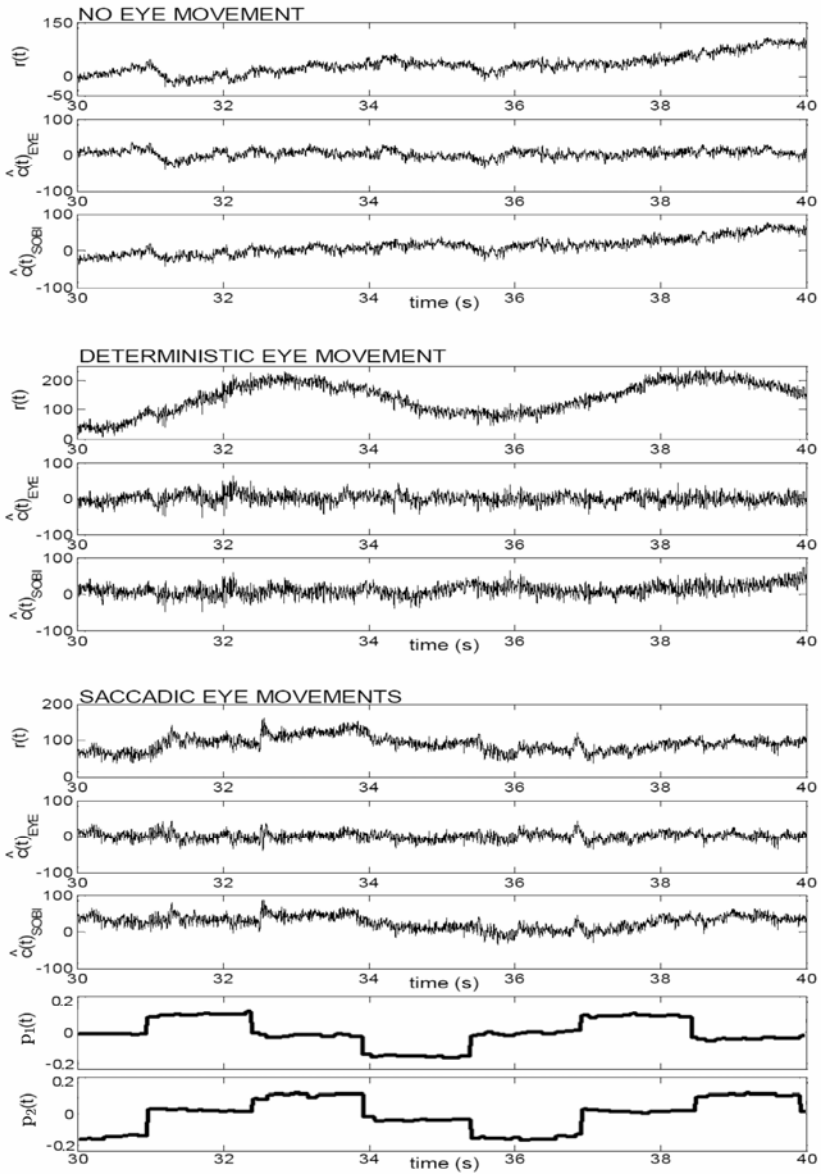

Figure 3.4: Experimental data for three different types of eye movement in the first row of each subfigure, recorded at Fp1. The estimated $\hat{c}(t)$ corrected by the eye tracker method and the SOBI method are in respectively the second and third row of each subfigure. For saccadic eye movements, $\underline{p}(t)$ is also displayed. Note the different scales of the y-axis (μV), which are used to show the full range of $r(t)$ while also showing some detail in the corrected data.

The matrix $\underline{\underline{Q}}$ is set to make sure that all parameters in $\underline{\phi}(t)$ stabilize within 30 seconds.

3.6.2 Discussion

When $\hat{c}(t)$ is observed for these three situations using the eye tracker method, the only remarkable disturbance that is still clearly visible in $\hat{c}(t)$ is in the saccade data. Here there remain some small disturbances directly after the onset of each saccade. The disturbance is also visible after SOBI correction, and therefore it is unlikely that this disturbance is caused by the correction method itself. The disturbances are probably caused by what is known as the rider-artifact [22]. This artifact is often seen with saccadic eye movements and is caused by slight changes in the positions of the eyelid that occur when saccadic eye movements are made. Because the eye tracker did not monitor eyelid movement, this type of artifact could not be removed by the eye tracker method. The artifact is mostly seen with vertical eye movements. When the SOBI results are compared to the eye tracker results it appears that the eye tracker method is better in removing the baseline drifts from the data. These drifts can be uncorrelated between electrodes, and because SOBI relies on inter-electrode correlations to detect artifacts, the SOBI method will not correct them as well as the eye tracker method. It should be noted that for consistency with the simulated data, the MLR method uses only two bipolar EOG recordings. This corresponds to the optimal setting found on simulated data. On experimental data it can be argued that a third recording is required to compensate for blinks and small eyelid movements. However, adding a third EOG recording increases the risk of overcorrection and removing brain related activity from the EEG.

3.7 Discussion & conclusions

As eye movement artifacts are often seen in EEG recordings, correction for these artifacts is frequently needed to get a clear indication of the electrical activity of the brain. For the purpose of correction, it is desirable to have an indicator of which eye movements were made during the recording. Often the EOG is used for this purpose, however in this chapter we introduce the use of an eye tracker to monitor eye movements. This has the advantage that the data recorded by the eye tracker cannot be corrupted by any electrophysiological signals. Using the eye tracker data as a reference for correction thus is potentially very powerful. Nevertheless two issues related to the eye tracker should be addressed. Firstly, the eye tracker used in the experiments, is not able to distinguish between small head movements and eye movements. It only represents the position of the pupil in a fixed frame. Although this implied for

our experiments that the participants had to be specifically instructed not to move their head, in the future the use of a head mounted eye tracker can avoid this constraint. During the experiments the position of the head was continuously observed and no large movements were seen. Secondly, the eye tracker is not capable of detecting pupil position while the eyes are closed during blinks or during periods of prolonged eye closure. For prolonged closure periods, like during sleep, this implies that the eye tracker-based method cannot be used. For blinks it implies that the pupil position information will be briefly interrupted causing a gap in the pupil information. Although in the current study such gaps were not present by selecting segments without blinks, in most data they will occur. For such a brief period it seems fair to halt adaptation, and continue once the pupil position can be recorded again. The properties that determine the parameters in $\underline{\phi}(t)$ are expected not to change significantly in these brief periods.

By using both simulated and experimental data, it is determined how the orientation of the eye, $\underline{p}(t)$ recorded by the eye tracker, influences the EEG signal, $r(t)$, that is recorded at an electrode. This relation, described in (3.1), is at most of second-order.

Knowing the order of the relation between $\underline{p}(t)$ and $r(t)$, a Kalman filter is used for obtaining the parameters that specify the exact relation for each electrode position. The Kalman filter is an adaptive filter that can estimate these parameters and track their changes in a limited period of time. In Section 3.4.3 a tracking time of 30 seconds was selected, after which the estimated parameters should have stabilized.

To gain insight in how well this new correction method performs, it is applied to both simulated and experimental data. The same data are also corrected by three established correction methods, which have been previously reported to result in accurate ocular artifact removal. Different types of eye movements are analyzed because the morphology of $\underline{p}(t)$ is likely to influence the performance of some correction methods.

On simulated data, the eye tracker method performs very well. When the method is tuned optimally for this data, the SNR after correction is over 10 dB for all types of eye movements. When compared to the other three methods, only the SOBI method shows similar results for one eye movement type.

It should be noted that low frequency components in $c(t)$ also cause slow changes in $r(t)$. These will affect $\phi_1(t)$ and therefore influence $\hat{e}(\underline{p}(t))$. This has a negative effect on the correction. The estimate $\hat{e}(\underline{p}(t))$ is correlated to $c(t)$, while $e(\underline{p}(t))$ is independent of $c(t)$. After stabilization, the difference $u(t) = c(t) - \hat{c}(t)$ is not white noise but $u(t)$ may display considerable fluctuations. These fluctuations are proportional to fluctuations in $c(t)$ because of the small

cerebral influence on $\hat{e}(\underline{p}(t))$. The amplitude of these fluctuations depends on the first diagonal element of matrix $\underline{\underline{Q}}$, denoted as ${\sigma_{X1}}^2$. Larger ${\sigma_{X1}}^2$ will lead to higher amplitude fluctuations in $u(t)$. For the tracking time used in this study the amplitude of these fluctuations is found to be negligible. When the new method is applied e.g. to data containing a lot of blinks, it is desirable to have a much shorter tracking time after each blink. If a shorter tracking time is required, the fluctuations in $u(t)$ need to be considered. For now, a Kalman filter that assumes that $c(t)$ is of white spectrum already outperforms the other methods, even though in simulations and reality this spectrum is not white. The assumption of matrix $\underline{\underline{Q}}$ being diagonal is, as mentioned in Section 3.4.3 a simplification of reality. This assumption is necessary because the true interactions between parameters are very difficult, if not impossible, to assess. Therefore a choice needs to be made on how to implement matrix $\underline{\underline{Q}}$. By using the simplest scenario, of $\underline{\underline{Q}}$ being a diagonal matrix, adequate correction is already achieved, although there is still room for improvement.

On experimental data results for the different correction methods also look convincing. When inspected visually, the $\hat{c}(t)$ that is estimated by the eye tracker method appears to be a clean EEG signal that does not show obvious ocular influences any more. The only exception to this is a small change in potential that is seen for saccadic eye movements. This change is probably caused by a rider-artifact that starts simultaneously with the start of some saccades. As this artifact is known to be caused by movement of the eyelid, it cannot be removed by the new correction method. The results for the SOBI method appear to contain small baseline fluctuations that are not corrected for. It should be noted here that components-based methods are often praised for 1: their ease of use, 2: their ability to remove eye movement artifacts as well as blink artifacts and 3: their ability to extract small specific brain activities, like EPs, in trial-based studies accurately. In this chapter, the two components-based methods are outperformed by the eye tracker-based method. Nevertheless, this chapter does not distinct in any way on how well any correction method will be successful in extracting small EP signals. The vector $\underline{\phi}(t)$ can be affected by properties, like retinal luminance, that influence the relation between the corneo-retinal dipole and recorded signal. Some of these properties will not affect the relation between a brain activity dipole and the recorded signal, and hence the fluctuations in these relations parameters will be different. Deciding which method is best at detecting EPs requires a different study, and could be combined with an ocular artifact removal method.

For the eye tracker method a one channel EEG recording is sufficient to obtain the results that are shown. The extra requirement for this method is that an eye tracker is added to the experimental setup. For the SOBI method, no eye

tracker is required, but EOG electrodes need to be included in the measurement as well as a larger number of EEG channels to obtain the results presented here.

Currently the applications for which this method can be used are greatly limited by the inability to correct blink artifacts. In order to increase the variety of applications the new method can be used for, a more advanced eye tracker which also monitors movement of the eyelid can be used. Such an eye tracker may also be used for the removal of blink artifacts. The use of a head-mounted eye tracker can eliminate the strict need to avoid any head movements during the recording. Some head-mounted eye trackers can be worn like glasses and do not interfere with electrode caps. An extra problem that will arise concerns pupil position detection during a blink and during periods of prolonged eyelid closure. The SOBI method and the PCA method are based on correlation between different electrode positions. Because these two methods do succeed in removing part of the ocular artifact, this correlation does contain information that is relevant for determining which part of $r(t)$ is caused by eye movement. The eye tracker method is not yet able to use this extra information because it is based on a one channel recording. The method can, however, be extended and improved to deal with multiple electrodes and the covariances between the different $r(t)$ for these electrodes. In summary, if eye movement artifacts need to be accurately removed from EEG signals, especially for demanding applications such as single trial-based experiments, the use of an eye tracker during experiments is essential.

Chapter 4

The use of an eye tracker with EEG allows for improved ocular artifact removal

4.1 Abstract

An electro-encephalogram, EEG, often contains artifacts that should be removed prior to interpreting the EEG. Ocular artifact correction methods use multi-electrode recordings to determine which part of the experimental data is relevant and which part is artifactuous. In this chapter we show that by monitoring ocular movements with an eye tracker, an extra source of potentially useful information is available that can be exploited to get a more accurate ocular artifact correction. This does require the use of extra equipment, but can by-pass known difficulties such as the forward/backward propagation issue because an eye tracker cannot pick up cerebral activity. By recording horizontal pupil position, vertical pupil position, and eyelid position, an eye tracker provides all information that is relevant for ocular artifact correction. With a Kalman filter, this information is converted to an estimate of the ocular artifacts in the EEG. To evaluate the accuracy of this estimate, both simulated and experimental data are used and the new method is compared against six well known correction methods. The new correction method is found to be highly robust over a wide range of simulated ocular artifacts, including both blinking and eye movement. The simulations show that it consistently outperforms the other correction methods. For this comparison two objective signal-to-noise based performance standards are defined and used. On experimental data the new method also appears to be superior to the other methods.

4.2 Introduction

The focus of this work is on correcting ocular artifacts from the electro-encephalogram (EEG). The EEG is important for the field of cognitive neuroscience, in clinical practice as well as in experimental work. Even with the important developments in brain scanning techniques of the last decade, EEG recordings can be expected to remain important for a good number of years to come. A strong advantage for many applications is its excellent

temporal resolution (milliseconds). EEG recordings are easy to use, and can be employed in the clinic as well as in non-medical laboratories. Researchers may focus on different aspects of EEG recordings; the continuous background EEG can be analyzed, for instance into frequency components for sleep recordings, but analyses may also proceed event-based, so that brain potential components related to cognitive events can be extracted. In addition, analyses are possible online as well as offline, making brain-computer interfaces and neurofeedback possible.

Artifacts in the EEG may arise, for instance, from body movements or laboratory equipment, and can usually be avoided by restricting freedom of movement during the measurement, and by electrical shielding, respectively. Other artifacts may have a biological origin. For instance, the electrical activity of muscles from the neck or face may be picked up by electrodes placed on the head. Jaw muscle activity frequently picked up by EEG electrodes placed over the temporal bone is notorious in this respect. The most obvious example of such activity for anyone who has ever witnessed an EEG recording is undoubtedly the electrical activity of the eyes, which is volume-conducted to nearly the whole scalp, grossly distorting the recording.

The question of how to handle ocular artifacts in EEG recordings depends largely on the application under study, and the methods of analyses that are going to be employed. In clinical screening for epilepsy, for example, simple rejection of epochs containing artifacts may suffice; there is enough remaining data available that can be analyzed. For most experimental work focused on cognition, however, rejection of epochs with artifacts is not appropriate for several reasons. First, rejection may lead to a selection bias because of a correlation between eye movements and cognition. Furthermore, rejection leads to loss of data. Researchers often try to compensate for this by instructing participants to keep their eyes still, thus introducing a secondary task that may interfere with the task under study. Finally, in rejection procedures there is a risk that artifacts with low amplitude relative to the background EEG are not removed. In sum, rejection of ocular artifacts is troublesome in many cases, and some correction of the artifacts might be more appropriate. Unfortunately, there does not seem to be much agreement in the field on which correction method to use, and under which circumstances or for which application a certain correction method is deemed to perform sufficiently. This becomes apparent from the relatively high number of reviews on ocular artifact correction methods that have appeared in the literature over the years, each stressing that no general consensus has been reached, e.g.,[8;38;39;49;85].

Early correction methods, inspired by [125], worked by estimating the ocular artifact from the electro-oculogram (EOG), and then somehow subtracting the

artifact from the EEG recording. We shall refer to these methods as EOG-based correction methods. Justification of the EOG-based methods is based on the biophysical properties of the ocular artifacts, which arise from the potential difference between the back (retina) and front (cornea) of the eye, which can be modeled by a rotating dipole of fixed strength [40]. Recording some extra EOG electrodes (recommendations on the optimal number differed somewhat) used to be a problem, but does not require much extra effort anymore and can be realized easily nowadays. The EOG-based methods often use regression techniques to estimate the ocular artifact based on the correlation between the EOG and the EEG, and then subtract that estimate from the EEG, electrode by electrode. The methods mainly differ in how the estimate is obtained. Some methods used a straightforward regression procedure [126;127], others incorporated autocorrelation in the estimate [46], and still others treated saccades and blinks separately [35;128]. The latter procedure was justified because the eye movement artifact and the blink artifact have a different biophysical origin, that is, rotation of the eyeball and closure of the eyelid, respectively. The need for separate scaling factors (regression weights) for saccades and blinks has also been debated though [43;106].

The advantages of EOG-based regressive procedures for ocular artifact correction are their ease of use, the possibility that they could be applied in real-time as well as offline, and on event-based as well as continuous data. EOG-based procedures have a serious drawback, however, which is known as the forward propagation problem. Not only does the electrical ocular activity propagate backward to the scalp where it is picked up by the EEG electrodes, but the reverse is also true; brain activity propagates forward and is picked up by the EOG electrodes. Because the very same EOG is used for computing the scaling factors (regression weights) for the correction, there is a risk that brain activity might be unjustly removed from the EEG. Especially, the removal of a part of the task-related EEG is undesirable for task-related brain-activity as observed in event-based experiments because such task-related brain-activity typically has very low amplitude. The importance of this problem likely depends on the brain regions from which this activity originates, and could be significant for tasks activating frontal brain regions, where the ocular artifacts are greatest, and relatively minor for perceptual tasks involving primarily posterior brain areas. In [44], the negative effects of this problem to artifact correction were studied. When assuming that all brain activity at the moment the ocular artifact occurs is localized in a single location in the brain, [44] finds the effects caused by the EOG-based correction to be detectable but nevertheless preferable to any of the available alternatives. However, because it is not known in advance which brain areas are active in a given task – these brain areas are the very object of the research – EOG-based methods suffer from a possibly serious flaw in this respect. Just how serious this flaw is,

especially when tasks elicits task-related brain-activity in multiple brain regions simultaneously, is unknown.

Two solutions have been proposed to deal with this problem. First, separate 'calibration' measurements have been proposed to avoid contamination of the EOG by task-related brain activity, e.g., [46]. Before the start of each experiment or task block, the participants are asked to produce eye movements, and these separate measurements are used to calculate the scaling factors. Although this effectively avoids task-related activity when calculating the scaling factors, it is also uncertain to what extent the ocular artifacts in the calibration measurement are identical to those in the actual recording. Another procedure was proposed for event-based experiments, in which selected segments of data around the event of interest are usually averaged together. [35] proposed to subtract the event-related average from each single-event epoch prior to calculating the scaling factors. This also effectively removes the (average) task-related activity, but has two disadvantages; it is only useful for event-based experiments, and it can only be used after the full experiment has been completed. It is thus unsuitable for real-time work such as brain-computer interfaces, and for much clinical work, such as sleep recordings, which are not event-based.

An entirely different solution to the problem of correcting ocular artifacts is provided by the components-based methods. These multivariate methods take advantage of the fact that the ocular artifact does not affect all brain regions equally. They use the recordings at multiple electrodes to identify 'components' that represent brain activity on the one hand, and artifacts (ocular or otherwise) on the other. In the field of ocular artifact correction, these methods separate brain and ocular components that are either uncorrelated, as in Principal Components Analysis (PCA, e.g., [129]), or independent, as in Independent Components Analysis (ICA, e.g., [130]). Physiological as opposed to statistical approaches have also been proposed [87]. Components-based methods do not suffer from the forward propagation issue that plagues EOG-based procedures, and can even be used without recording the EOG. They therefore do not require separate calibration measurements. However, they do suffer from two important disadvantages. First, they require a full segment of data for analysis, making real-time application in brain/computer interface or neurofeedback difficult if not impossible. Secondly, although they do not suffer from the forward propagation problem, they have still been found to be susceptible to overcorrection, in which part of the relevant signal is removed together with the artifact [16].

It thus seems that there remain a number of important problems to overcome. In Chapter 3 we attempted to launch an entirely new point of view to this discussion by proposing a tracker-based method. We reasoned that, contrary to

EOG electrodes used in the EOG-based methods, an eye tracker can provide information on ocular artifacts that is unaffected by brain activity, thus avoiding the forward propagation problem. Recall that the main disadvantage of the EOG-based methods was the forward propagation problem and the resulting overcorrection of the brain activity, but otherwise EOG-based methods have the advantage, compared to components-based methods, that they can be applied in real time, and on continuous as well as event-based data. We reasoned that by using an eye tracker we could keep these advantages while getting rid of the major disadvantage. In [131], it was shown that an eye movement video tracking system provides an estimate of eyeball rotations and hence of eye movements that is more accurate than the estimate provided by EOG.

The approach of using an eye tracker to estimate eye movements by means of a Kalman filter in Chapter 3 was shown to permit accurate removal of eye movement artifacts, yet retains the advantages of the EOG-based methods.

The main deficiency of the tracker-based method in Chapter 3 is that it will only correct for eye movements, and not for blinks. This deficiency comes from the fact that an eye tracker records the horizontal and vertical position of the eye by focusing on the pupil. This way, an eye tracker monitors eye movements but not blinks. We expect, however, that this problem can be overcome by future technological advances. Eye trackers may evolve to easy-to-use and easy-to-wear devices that are integrated with a pair of glasses, which do not limit the freedom of the participant's or patient's movement and are capable of monitoring both pupil- and eyelid- movements. Easy-to-wear devices have already been used successfully for detecting, separately, movements of the eye [131] and of the eyelid [132], so our expectations in this regard are not unrealistic.

The purpose of the present study is

1. to extend the functionality of the tracker-based method , and
2. to obtain an objective quantification of the success of the tracker-based method on simulated data, and verify this on experimental data.

To address the first point, we take from literature the relation between eyelid position and blink artifact and incorporate this in the relation that was used by the existing tracker-based method. Because our eye tracker cannot detect eyelid position, we suggest an alternative approach to estimating eyelid position based on a single EOG recording and a blink-template. To address the second point, we constructed simulated data based on realistic models, broadly covering common EEG measurements. We also included simulations with very high numbers of blinks and eye movements, representing the most challenging situations. These data sets were subjected to the tracker-based method, and compared to six commonly used correction methods. We defined and used two

separable objective performance measures, based on signal-to-noise ratio, and will show that the tracker-based method outperforms the other methods used in this study, often by a large margin. During a blink, the eyelid covers the pupil, and pupil position information becomes temporarily unavailable. It is known that during these brief periods small eye movements occur, which cause artifacts in the EEG. In our simulations, the eyes are therefore allowed to move while a blink occurs. For our tracker-based correction method we do not have information regarding eye movements during a blink and we therefore have to impose the assumption that the eye does not move during these periods. One of the defined performance measures focuses specifically on these brief periods and can indicate the impact of this lack of information.

In order to exclude the possibility that these conclusions were reached based on peculiarities of our simulated data, or of our performance measures, we also applied all methods to three experimental data sets. Of course, objective quantitative comparisons are not possible in that case, but visual inspection of recorded waveforms before and after correction, confirmed the robustness of the tracker-based method.

4.3 Methods

Previously, in Chapter 3, we specifically selected periods of the EEG in which no blink artifacts occurred. During these periods, an eye tracker recorded the horizontal and vertical position of the pupil, respectively denoted as $p_1(t)$ and $p_2(t)$, and these recordings were used to correct the raw EEG for eye movement artifacts. In this study it is proposed to detect eyelid position, $p_3(t)$, in combination with $p_1(t)$ and $p_2(t)$. Because movements of the eyelid are the main cause of blinking artifacts, as was suggested in [120], it is expected that incorporating knowledge on eyelid position in an artifact correction method will improve the accuracy of correction significantly.

We propose using the position vector $\underline{p}(t)=[p_1(t),p_2(t),p_3(t)]^{\mathrm{T}}$ as a basis for estimating the ocular artifacts that are seen in the raw EEG. This EEG, $r(t)$, contains a cerebral component, $c(t)$, and an eye related component, $e(\underline{p}(t))$. Both components are related to changes in electric fields inside the head and because electric fields are additive,

$$r(t)=c(t)+e(\underline{p}(t)). \tag{4.1}$$

As demonstrated in Chapter 3, during periods without blinks the relation between $e(p_1,p_2)$ and $p_1(t)$ and $p_2(t)$ may be approximated by

$$\begin{aligned} e(p_1,p_2)=&\phi_1(t)+\phi_2(t)p_1(t)+\phi_3(t)p_2(t)+\phi_4(t)p_1(t)p_2(t)+\ldots \\ &\phi_5(t)p_1(t)^2+\phi_6(t)p_2(t)^2. \end{aligned} \tag{4.2}$$

The parameters ϕ_1, ϕ_2, .. are unknown and depend, among other things, on physical properties of the subject like the diameter of the head and exact morphology of the skull, brain and other biological tissues. Obviously, parameters ϕ_1, ϕ_2, ... also depend on non-subject-related properties, like electrode placement. Because of slow variations in some of these properties, the parameters ϕ_1, ϕ_2, ... are slowly time-varying. The estimates of these parameters are denoted by $\hat{\phi}_1, \hat{\phi}_2, \ldots$

In this study we define both $p_1(t)$ and $p_2(t)$ in a way that they are zero if the eye is oriented towards the center of a screen placed in front of the subject. Furthermore $p_1(t)$ and $p_2(t)$ are expressed in m and reflect the change in orientation point on this screen. For eyelid position, we will use $p_3(t)=1$ if the eyelid is fully opened and $p_3(t)=0$ if fully closed, with a linear scale in between.

4.3.1 Modeling and detecting blink artifacts in the EEG

The eyelid position $p_3(t)$ is of no influence in (4.2) because there, $p_3(t)$ is assumed constant. When $p_3(t)$ does vary, and a blink artifact is detected, equation (4.2) should be extended. If $p_3(t)$ is measured simultaneously with $r(t)$, as in [21] and [20], it is found that $p_3(t)$ and $r(t)$ are highly correlated and that there appears to be a linear relation. Therefore, in (4.3) an extra term is added to (4.2) in order to include the blink artifacts in the modeled relation.

$$\begin{aligned}\hat{e}(\underline{p}(t)) = \hat{\phi}_1(t) + \hat{\phi}_2(t)p_1(t) + \hat{\phi}_3(t)p_2(t) + \hat{\phi}_4(t)p_1(t)p_2(t) + \ldots \\ \hat{\phi}_5(t)p_1(t)^2 + \hat{\phi}_6(t)p_2(t)^2 + \hat{\phi}_7(t)p_3(t),\end{aligned} \tag{4.3}$$

with $\hat{e}(\underline{p}(t))$ an estimate for $e(\underline{p}(t))$. Equivalently

$$\hat{e}(\underline{p}(t)) = \underline{\Psi}(\underline{p}(t))^{\mathrm{T}} \cdot \underline{\hat{\phi}}(t), \tag{4.4}$$

with $\underline{\Psi}(\underline{p}(t)) = [1, p_1(t), p_2(t), \ldots, p_3(t)]^T$ and $\underline{\hat{\phi}}(t) = [\hat{\phi}_1(t),\ \hat{\phi}_2(t), \ldots \hat{\phi}_7(t)]^{\mathrm{T}}$.

Given the relation in (4.4) it is possible to determine $\hat{e}(\underline{p}(t))$, given $\underline{p}(t)$. The effects of other eyelid related terms, like $p_1(t)p_3(t)$, are briefly mentioned in [21] where eye movements were performed either with opened eyelids or with closed eyelids. No significant differences in eye movement artifacts were found related to the eyelids being opened or closed and therefore the terms $p_1(t)p_3(t)$ and $p_2(t)p_3(t)$ are not used in (4.3).

In the Appendix in Section 4.6, we briefly discuss whether $\underline{p}(t)$ can be seen as an accurate estimate of the gaze direction and eyelid position.

Unfortunately, eye trackers are commonly designed to track the eye pupil and not to track the eyelid, even though this is not difficult in principle. Determining $p_3(t)$ is not possible in most eye trackers, including the one at our disposal.

For this reason, we now revert to an alternative way to detect eyelid position, based on an electro-oculogram (EOG). Future advances in the versatility of eye trackers may, however, turn this alternative obsolete.

4.3.1.1 Estimating eyelid position from the electro-oculogram

The linear relation between $e(\underline{p}(t))$ and $p_3(t)$, suggested in [21], implies that instead of using the eye tracker, eyelid position may also be estimated from the electro-oculogram (EOG). This provides a practical alternative for altering the eye tracker software, or for purchasing a different eye tracker. Although currently such an alternative way to detect eyelid position is very useful, the use of an EOG for estimation of eyelid position has two disadvantages compared to the use of an eye tracker for the same purpose, as will be described below.

1. Eye movements are (nearly) always accompanied by small eyelid movements [22]. For the artifact correction method that we propose in Section 4.3.1, a separate detection of eye movements and of eyelid movements is required. With an eye tracker, detecting both these movements separately yet simultaneously is, in principle, not difficult. Making this distinction based on an EOG is less straightforward because only the combined effects of the eye- and eyelid-movement are reflected in the EOG. For this reason, we have to define in our method that the EOG-based estimate of eyelid position only changes during the brief periods that blinking occurs. By doing this, we choose to ignore the smaller eyelid movements that occur during eye movements.
2. EOG electrodes record some cerebral activity together with the ocular activity. Especially for situations with little or no eye movements, this results in a correlation between $c(t)$ and the EOG recordings. This correlation can lead to overcorrection, causing part of the cerebral activity to be removed from $r(t)$.

It will be shown that despite these disadvantages, the proposed method still is superior to the other methods that are evaluated in this study.

By placing the EOG electrode directly above the eyebrow, the change in potential due to the eyelid movement is picked up. Because the EOG electrode is close to the eye compared to EEG electrodes and is further from the cerebral cortex, it records blink artifacts and eye movement artifacts with high amplitude and with less influences of cerebral activity.

Because of the difference in shape and often also amplitude between blink artifacts and eye movement artifacts, it is not difficult to detect each separate blink artifact. The number of blinks, *B*, in a recording is obtained by applying a threshold value to the potential as recorded by the EOG electrode. The number of times this threshold is crossed is divided by two to obtain *B*. Changes in

eyelid position are smooth and consist of an upward and a downward movement during each blink. In order to estimate the eyelid position from the EOG recording, we propose to approximate each blink artifact as an asymmetric peak which resembles the typical shape of a blink artifact. Note that we assume that the recorded blink artifact in the EOG and the estimate for eyelid position are of similar morphology, this assumption follows from [21] and [20].

On experimental data, the correction accuracy will be affected by our choice for the asymmetric peak function. For this reason a function was chosen that resembles the basic shape of an averaged blink artifact, yet retains the flexibility to be tuned to a single blink artifact using a limited number of parameters. A suitable asymmetric peak is given by

$$\hat{\Gamma}_b(t) = \xi^1{}_b \quad \frac{e^{\frac{\xi^4{}_b - t}{\xi^2{}_b}}}{\left(1 + e^{\frac{\xi^4{}_b - t}{\xi^3{}_b}}\right)^2}, \tag{4.5}$$

an example of such an asymmetric peak is illustrated in Figure 4.1.

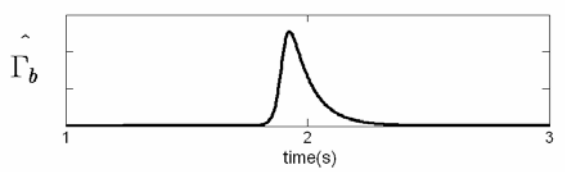

Figure 4.1: Illustration of an asymmetric peak function (with $\xi^1{}_b = 4$, $\xi^2{}_b = 0.09$, $\xi^3{}_b = 0.03$, *and* $\xi^4{}_b = 1.9$*).*

Parameter b is the specific index of each blink, assuming a total of B blinks in the entire recording, $\hat{\Gamma}_b(t)$ represents the estimated part of $e(\underline{p}(t))$, and thus of $r(t)$, that is caused exclusively by the b^{th} blink artifact. Parameter $\xi^1{}_b$ represents the estimated amplitude of the blink artifact, $\xi^4{}_b$ the estimated time of maximum blink artifact amplitude, and $\xi^2{}_b$ and $\xi^3{}_b$ together estimate the duration of the blink and the differences in speed between upward and downward movement of the eyelid. For each blink artifact these four parameters may be determined by minimizing the squared difference between $r(t)$ and $\hat{\Gamma}_b(t)$ throughout the duration of the blink artifact.

By assuming (4.5) for each blink artifact, the EOG-based eyelid position is approximated by

$$\hat{p}_3(t) = \sum_{b=1}^{B} \hat{\Gamma}_b(t). \tag{4.6}$$

The corresponding estimate for the position vector will be denoted as $\underline{\hat{p}}(t) = [p_1(t), p_2(t), \hat{p}_3(t)]^{\mathrm{T}}$. By using an asymmetric peak template for each blink artifact, as given in (4.5), we reduce the possibility of cerebral activity in $\hat{p}_3(t)$ influencing correction.

Related to the first disadvantage of using an EOG, as discussed at the beginning of this section, it is worth mentioning that even though small eyelid movements are ignored in our EOG-based estimate of eyelid position, it is possible that these movements are automatically compensated during artifact correction by adaptation of the parameters in $\underline{\hat{\phi}}(t)$ that relate to the pupil position. Such automatic compensation may occur if the small eyelid movement is typical for the specific eye movement that occurs simultaneous to it. Whether or not such an adjustment occurs, should become apparent when the correction method is applied to real data, where the eyelids do move during eye movement [22]. Failure to compensate would inevitably lead to artifacts remaining after correction.

On simulated data, introduced further on in Section 4.4.1, the choice for the asymmetric peak function to estimate eyelid position becomes arbitrary because the same asymmetric peak function is used to simulate the eyelid movements and therefore to simulate the blink artifacts. Many other functions could have been used for the simulated data, provided that estimated eyelid position and simulated artifact share similar morphology as is suggested in [21] and [20].

Again, the use of an eye tracker with embedded tracking of eyelid position would totally overcome the difficulties that are addressed in this subsection.

4.3.2 Parameter estimation and correction performance

By using a Kalman filter [123], an estimate $\underline{\hat{\phi}}(t)$ is obtained.

4.3.2.1 Parameter estimation using a Kalman filter

Vector $\underline{\phi}(t)$ may change over time as described by

$$\underline{\phi}(t) = \underline{\underline{\Phi}} \cdot \underline{\phi}(t - 1) + \underline{w}(t), \tag{4.7}$$

with matrix $\underline{\underline{\Phi}}$ representing the expected changes in $\underline{\phi}(t)$ over time and $\underline{w}(t)$ representing fluctuations in $\underline{\phi}(t)$ that are assumed to be white and of normal distribution, independent of $c(t)$. The notation $\underline{\phi}(t - 1)$ is used to indicate the value of $\underline{\phi}(t)$ at the previous sampling instant. In this study $\underline{\phi}(t)$ represents the state of all parameters that influence the relation between $\underline{p}(t)$ and $e(\underline{p}(t))$. Unfortunately, $\underline{\phi}(t)$ cannot be measured and therefore can only be obtained indirectly by recording $r(t)$, as seen by combining (4.1) and (4.4) to

$$r(t) = c(t) + e(\underline{p}(t)) = c(t) + \underline{\Psi}(\underline{p}(t))^{\mathrm{T}} \cdot \underline{\phi}(t). \tag{4.8}$$

Because of this, $\underline{\phi}(t)$ can only be approximated by an estimate $\underline{\hat{\phi}}(t)$. The Kalman filter provides such an approximation by minimizing $\left(\underline{\phi}(t) - \underline{\hat{\phi}}(t)\right)^2$. Details on the derivation of the Kalman filter can be found in [123]. Here it suffices to point out that minimization requires prior knowledge on the variances of $c(t)$ and $\underline{\phi}(t)$.

In the filter it is required to estimate a priori the variances of $c(t)$ and $\underline{\phi}(t)$ in order to determine which one of them is more likely to cause changes to $r(t)$. Based on these a priori estimates, $\underline{\hat{\phi}}(t)$ is estimated. The variance of $c(t)$ is determined by selecting a segment of $r(t)$ in which careful visual inspection reveals no ocular artifacts. For such a segment the variance, indicated as *R*, is determined. The vector $\underline{\phi}(t)$ is related to numerous processes and physical properties, and therefore its variances, indicated as $\underline{\underline{\sigma}}_{\underline{X}}^2$, cannot be estimated as easily as *R*. For now it is assumed that all parameters in $\underline{\phi}(t)$ are mutually uncorrelated and slowly time-varying. These slow variations could e.g. be due to temperature changes. Matrix $\underline{\underline{\sigma}}_{\underline{X}}^2$ is therefore a diagonal matrix with the variances of the parameters in $\underline{\phi}(t)$, indicated as $\sigma_{X_1}^2, \sigma_{X_2}^2, \ldots$, on its diagonal.

The matrix $\underline{\underline{\sigma}}_{\underline{X}}^2$ influences two properties of the Kalman filter. Firstly, a Kalman filter automatically changes the rate at which the parameters in $\underline{\hat{\phi}}(t)$ are adapted based on the variance in the data. Thus, the adaptation speed depends on the variances defined in $\underline{\underline{\sigma}}_{\underline{X}}^2$ and *R*. Secondly, if there is much variance in $\underline{\phi}(t)$, the estimate $\underline{\hat{\phi}}(t)$ will be allowed to vary accordingly, resulting in less accurate estimation. These two properties are related in a way that if accuracy increases, the adaptation speed decreases and vice versa. This implies that finding the optimal filter settings requires making a trade off between adaptation speed and estimation accuracy. The primary goal of ocular artifact removal is to remove the ocular artifact as accurately as possible, and this would require slow adaptation. Because the processes that cause changes in $\underline{\phi}(t)$ are slowly varying, the adaptation-speed should be high enough to still track these variations.

Typically temperature may be assumed constant for several minutes. But since not all processes that influence $\underline{\phi}(t)$ are specified, and some of these may change somewhat faster, it is assumed that $\underline{\phi}(t)$ is constant over a period of 30 seconds. Variations in the strength of the ocular dipole e.g., due to changing illumination of the retina, can cause such more rapid changes in $\underline{\phi}(t)$. This implies that if $\underline{\hat{\phi}}(t)$ can track changes in $\underline{\phi}(t)$ within 30 seconds, a sufficiently fast and maximally accurate parameter tracking is achieved. This tracking time of 30 s is used for all parameters in $\underline{\hat{\phi}}(t)$. Note however that $\hat{\phi}_7(t)$ will only

adapt during a blink. The effective tracking time during this 30 second period is thus smaller for $\hat{\phi}_7(t)$. With an average blink duration of approximately 270 ms [133], and an average blink frequency, F_b, of 15 blinks/min the effective tracking time for $\hat{\phi}_7(t)$ is only 2.03 s. The value for $\sigma_{X_7}{}^2$ is set, based on this average blink frequency, in the way that $\hat{\phi}_7(t)$ tracks changes in 30 s.

4.3.2.2 Performance measures

In order to have an objective evaluation as to how clean the corrected signal $\hat{c}(t)$ is, two signal to noise ratio measures are defined that compare $\hat{c}(t)$ to $c(t)$, or equivalently $\hat{e}(t)$ to $e(t)$. For periods without blink artifacts, the first measure, SNR_1, is defined according to Chapter 3 as

$$SNR_1 = \frac{\frac{1}{T}\int_{t=t_1}^{t_1+T} s(t)^2 \,\mathrm{d}t}{\frac{1}{T}\int_{t=t_1}^{t_1+T} \left(\hat{e}(\underline{\hat{p}}(t)) - e(\underline{p}(t))\right)^2 \mathrm{d}t}, \tag{4.9}$$

with T the duration of the recording, and t_1 the start of the recording. The signal of interest is denoted $s(t)$. What $s(t)$ is, depends on the application. Clearly, when the signal of interest is $c(t)$, more estimation noise can be tolerated than when the signal of interest is a small component of $c(t)$ as is the case in e.g. event-related potential (ERP) studies. In this study, performance measure SNR_1 is used to evaluate the correction, regardless of whether or not the data set contains blink artifacts.

Because blink artifacts can occur in the data, and are corrected with a relatively short adaptation time, special attention is paid to evaluation of the accuracy of removing blink artifacts. Therefore a second measure, SNR_2, is based only on periods where $p_3(t)$ is close to zero. Because the onsets and the endings of blink artifacts in an EOG recording are not strictly defined both in reality and in equation (4.5), we define a subset S_{BA} as containing only those time instants with $\hat{p}_3(t) > B_T$, $S_{BA} = \{t | \hat{p}_3(t) > B_T\}$. Parameter B_T is a threshold value that is set at 0.5 % of the maximum blink amplitude. In effect this implies that we ignore blink effects that are smaller than 2 μV in the EOG channel. For SNR_2 we define

$$SNR_2 = \frac{\int_{S_{BA}} s(t)^2 \,\mathrm{d}t}{\int_{S_{BA}} \left(\hat{e}(\underline{\hat{p}}(t)) - e(\underline{p}(t))\right)^2 \mathrm{d}t}. \tag{4.10}$$

The measure SNR_2 hence only reflects periods that are relatively hard to correct. These periods contain blink artifacts and may contain eye movement artifacts as well. The sequence of samples that contribute to SNR_2 is not

necessarily continuous because the samples may be interrupted by blink artifact free periods. Moreover, blink artifacts in general have durations of less than a second.

The periods with blink artifact influence both SNR_1 and SNR_2, and therefore there is some interaction between SNR_1 and SNR_2. A possible way to reduce this interaction would be to exclude periods with blink artifact from (4.9). This would reduce interaction but not eliminate it, because blink artifacts will influence the length of the periods that contribute to SNR_1. Moreover, after a period with a blink artifact, $\left(\hat{e}(\underline{\hat{p}}(t)) - e(\underline{p}(t))\right)^2$ is expected to have increased slightly because of the relatively short effective tracking time of $\hat{\phi}_7(t)$. Therefore it seems appropriate to have one overall measure SNR_1 and one specifically aiming at quantifying blink artifact suppression.

As an illustration of SNR_1 values that are required in practice, we will briefly consider an ERP potential called the mismatch negativity, MMN, which provides a physiological measure of sensory information being processed by the brain [134]. The MMN is the electrical response of the brain, as measured on the scalp, which is related to a stimulus that is deviant from other stimuli. Although MMN can be determined for different types of deviations, e.g., stimulus duration or frequency, in general the MMN potential starts 100 ms after the stimulus and lasts 150 ms. During this brief period, it has a maximum amplitude of approximately only 2 μV. Adequate ocular artifact removal is essential during these periods, since the presence of normal cerebral activity already makes MMN detection a challenging task. Additional artifacts should therefore be eliminated. For simplicity we assume a constant MMN potential of 0.5 μV and of 150 ms duration. To adequately detect this MMN, the remaining ocular artifacts during this period should be several times smaller in amplitude, which would require an SNR_1 of approximately 10 dB.

4.3.3 Existing correction methods

Most of the early correction methods are EOG-based [38]. They use one or more EOG recordings as a reference on what part of $r(t)$ to remove. Later, components-based correction methods like Principal Components Analysis (PCA) and Independent Components Analysis (ICA) have been suggested [98]. These methods decompose a multivariate signal into underlying components which are assumed to have some statistical property. This statistical property is usually either mutual independence, or mutual uncorrelatedness. By selecting the components that resemble ocular artifacts and eliminating these in the process of reconstructing the multivariate signal out of the components, artifacts are removed.

Since [38], several EOG-based methods have been newly introduced or revised. The main reasons for these changes related to the questions of whether

or not blink artifacts and eye movement artifacts need to be corrected with different regression coefficients, whether or not forward propagation, i.e. the presence of cerebral potentials in the EOG, is indeed an important issue with related to these correction methods, and which and how many EOG recordings should be used in the process of correction. From the fact that some of the latest of these correction methods still differ in their answers to these questions, we can conclude that consensus has still not been reached. For example, the RAAA method [42], stresses that the blink artifact for most electrode positions requires a different way of correction compared to the eye movement artifact. To this end, three bipolar, orthogonal, EOGs are used. Furthermore, RAAA assumes that consequences of forward propagation are marginal [44]. By contrast, the correction that is suggested in [128] uses the same propagation factor for blink artifacts and eye movement artifacts, and it avoids using a third EOG in order to reduce the possible negative effects due to forward propagation.

Comparisons between EOG-based methods and the components-based methods are scarce. Components-based methods are versatile and can correct simultaneously for a variety of artifact types, not exclusively ocular artifacts like the EOG-based methods.

As mentioned in [128], it still is unclear whether or not (parts of) cerebral signals are unjustly removed when using the components-based correction methods. Some studies, e.g., [82], suggest that the underlying components which these methods extract can contain fluctuations related to cerebral activity. As a result, their performance could deteriorate significantly.

The eye tracker method presented in this chapter has the advantage that its reference signal on ocular artifacts is not influenced by any other biological signals, in particular by cerebral activity. The direct reference measurement is expected to be better than the use of 'underlying components', because it is obtained directly from the eye, while components are obtained indirectly through a possibly inaccurate mathematical recipe.

To gain insight in the performance of the eye tracker-based method compared to some of the existing methods, this study will have multiple correction methods correct the same data sets. For comparison, six methods are selected either because they performed well in other comparisons, including [16;48] and Chapter 3, or because they are frequently used today. These methods are listed in Table 4.1 together with some of their characteristics.

Table 4.1: Overview of evaluated methods and some of their properties

Full name	Abbr.	Reference	Component- / EOG-based	Minimal number of electrodes (EEG/EOG)
Eye tracker-based correction	EYE			1/0#
Multiple Linear Regression	MLR	[116]	EOG	1/1°
Regression with AutoRegressive Error	RARE	[46]	EOG	1/1°
Principal Components Analysis	PCA	[117]	Component	1/0*
Second Order Blind Identification	SOBI	[51]	Component	1/0*
Fast ICA	FICA	[115]	Component	1/0*
Joint Approximate Diagonalization of Eigen values	JADE	[59]	Component	1/0*

#: The current implementation requires 1 EOG electrode, this can be reduced by using an eye tracker that detects eyelid movements.

°: 1 EOG electrodes assumes a monopolar reference but often, as in this study, a bipolar reference with at least 2 EOG electrodes is used.

*: Minimal requirement is 2 electrodes, EEG, EOG or mixed. However, for accurate results these methods require more electrodes.

The MLR correction method can be implemented using either a single EOG, using two EOGs which makes the method identical to the correction method of [127] as used in [50], or with three EOGs. In our results, all three implementations are considered and the highest SNR using either one, two or three EOGs is automatically selected and used for comparison against other correction methods.

For the components-based algorithms it is not a priori known which underlying components will be detected. If detected, components that are related to ocular artifacts should be removed. This can be done either manually or automatically. For an objective evaluation of these methods, an automatic detection is preferred. In this study, if the normalized cross-correlation between a component and one of the recorded EOG signals exceeds a threshold value, the component is marked as ocular and is removed. The threshold value was optimized and set to 0.5. The RARE and SOBI algorithms require a choice of parameters. For RARE this is the order of the AR-model used to model the EEG, set to 4 following [46]. For the SOBI algorithm a number of time lags needs to be chosen. The correlation of each component with respect to all other components and to the component itself is calculated at the specified time lags. The SOBI algorithm minimizes the sum of these correlations for different components. In this study we use lags of 1, 2, 3, 5, 10, and 20 samples at 256 Hz. These lags were found to yield good corrections in a pilot study, as well as in Chapter 3. An optimal selection of these lags requires a separate detailed study as was done for the extraction of primary somatosensory cortex signals [52]. Such an extensive extra study is, however, beyond the scope of this chapter, and therefore it cannot be concluded that the number of lags and the choice of lags we use is optimal.

Considering the large number of existing correction methods, it is obvious that not all correction methods can be included in our evaluation. We will briefly discuss what we consider to be the two most significant omitted methods.

The Gratton method [35] is frequently used for correction of ocular artifacts in event-based experiments. It can however not be used for the correction of continuous EEG recordings as are considered in this study. The RAAA method [42] was indicated as the most accurate correction method in a recent comparison between four methods on event-based experiments [50], including the aforementioned Gratton method. This RAAA method requires the careful alignment of artifacts in a set of calibration trials to estimate propagation factors for three EOG recordings. The experimental data that is used in our study (discussed in one of the following sections) has been recorded prior to the publication of the methods comparison in [50]. We therefore did not include such calibration sessions in our experimental protocol, and hence we are not able to show the correction results of the RAAA method on the experimentally recorded data of this study. Because a method should ultimately be validated on experimental data rather than simulated data, we feel that quantitative comparisons between the performances of different methods on simulated data always need to be supplemented and backed by correction results on experimental data. The inability to provide such backing for the RAAA method is the key reason why we chose to exclude this method from the simulated data section as well.

4.4 Evaluation

The performance measures defined by (4.9) and (4.10) can only be calculated if $e(t)$ and $s(t)$ are known. In practice these signals are never known, because that would eliminate the need for artifact removal. The objective evaluation of the different methods can thus only be performed for simulated data sets in which $e(t)$ and $s(t)$ are known.

An argument against the use of simulated data was given in [50]. Because any model that simulates EEG data and artifacts is based on certain assumptions, it was claimed that poor correction results on simulated data can be attributed either to bad correction methods or to erroneous assumptions in data modeling.

In principle this argument is correct. Nevertheless, it does not disqualify the use of modeled data. It merely calls for an adequate and detailed description of the assumptions underlying the modeled data. By providing this, the validity of the assumptions can be addressed and, if necessary, debated. Because the possibility that certain assumptions in modeled data are erroneous, or simplified too much, always exists, we feel that comparisons on simulated data should always be interpreted in combination with correction results on experimental data. The correction results on experimental data provide a 'sanity check' that can guard, and warn, for erroneous modeling assumptions.

The important advantage of using simulated data clearly is the fact that both $s(t)$ and $e(t)$ are exactly known, and that an objective, quantitative evaluation of the corrected data is possible. For experimental data, it remains impossible to exactly quantify how well the EEG is preserved during the removal of ocular artifacts. Existing correction validation measures for experimental data, such as those suggested in [50], focus on features within the EEG that are related to the eye movement. They are not (negatively) affected by correction methods which corrupt the background EEG, which is a considerable disadvantage because many correction methods are at risk of removing part of the background EEG in the process of removing artifacts.

4.4.1 Simulations

We simulate EEG, EOG and eye tracker data using a Boundary-Element-Method, BEM, based model of the human head. The exact model is described in more detail in Chapter 2 and 3, and defines the simulation of $c(t)$ and eye movement artifacts. This model simulates separately, but realistically, the sources that generate $e(\underline{p}(t))$ and $c(t)$ and reflects the main biophysical properties of EEG generation and conductance. The EEG is simulated at all positions of the 10-20 system. Because properties that determine conduction remain constant during the simulation, the simulated vector $\underline{\phi}(t)$ is constant.

4.4.1.1 Simulating the eye movement artifact

The eye movement artifact is simulated by rotating two of the dipoles in the head model, as described in Chapter 2. Several types of eye movement are simulated ranging from no eye movement to very fast and unpredictable eye movement. In Table 4.2 the different eye movement artifacts are listed and described.

Table 4.2: Simulated eye movements types and their descriptions

Type	Name	Constraints
Random	Random eye movement	$p_1(t) \in \mathcal{N}(0,\sigma = d_m/4)$, $p_2(t) \in \mathcal{N}(0,\sigma = d_m/4)$
No	No eye movement	$p_1(t) = p_2(t) = 0$
Deterministic	Deterministic eye movement	$p_1(t) = d_m * \sin(\omega * t)$, $p_2(t) = d_m * \cos(\omega * t)$
Saccadic	Saccade eye movement	$p_1(t) \in \{-d_m, 0, d_m\}$, $p_2(t) \in \{-d_m, 0, d_m\}$

In Table 4.2, d_m is the maximum amplitude of $p_1(t)$ and $p_2(t)$ with respect to the center of the monitor screen (d_m =0.225 m), ω represents the angular frequency of the deterministic eye movement in rad/s, and $\mathcal{N}(0,\sigma = d_m/4)$ indicates a normal distribution around zero with a standard deviation of $d_m/4$. None of the samples drawn from this distribution exceeded d_m in our simulations. Samples for saccadic eye movements are drawn from $\{-d_m, 0, d_m\}$, with equal probability for the three entries.

For random eye movements, the eyes are on average directed towards the center of the screen. Because the frequency of eye movements is physically limited, e.g. it is only possible to focus on approximately three different spots within one second, positions $p_1(t)$ and $p_2(t)$ are simulated by applying a low pass filter, with a cut off frequency at 3 Hz, to a random, white noise signal. In the simulations without eye movement artifact, correction should only remove a DC offset. The deterministic eye movement simulates a dot-tracking task where the dot makes a smooth circular movement over the screen. The saccadic eye movement simulates a dot-tracking task where the dot jumps once every two seconds from one point of the screen to another. For the variance of $c(t)$, as described in Section 4.3.2.1, we find R to be 144 μV^2, averaged over nine subjects.

The amplitudes of $c(t)$ and $e(\underline{p}(t))$ can be scaled in the simulation by increasing the strength of the neural sources in the model. This way potential is scaled to realistic values, with the amplitude of the eye movement artifact scaled to experimentally determined values for each specific electrode position.

4.4.1.2 Simulating the blink artifact

The scalp topography of the blink artifact may be different from the scalp topography of the eye movement artifact. The eye movement artifact is caused by a rotation of an electrical source in a steady volume conductor, whereas the blink artifact is caused by a slight change in conductive properties of the volume because of the eyelid movement. Implementing a volume conductor of time varying shape in the BEM is complicated, and therefore the blink artifact is simulated in a different way. To obtain the scalp topography of blink artifacts, an experiment is performed in which the EEG is recorded at several electrode positions, referenced to averaged ears. During this experiment the participant performs no task. After two minutes, the recording is stopped and all blinks in the recording are detected from the EOG electrode above the right eye. For all detected blinks, the time of maximum blink amplitude is selected. The simultaneously recorded amplitudes at all other electrodes at these times are selected and averaged. In Figure 4.2 these averages and their standard deviations are shown together with the averaged amplitude of 24 samples drawn randomly from the same data set. Note that the blink-locked average is consistently higher than the random average. This indicates that the blinks can be seen at all electrode positions with the same polarity. The only exceptions to this are two EOG electrodes placed below the eyes, indicated by $_{D}$ (down). The two EOG electrodes above the eyes, indicated by $_{U}$ (up), record the largest amplitudes. The $_{L}$ and $_{R}$ symbols indicate left and right respectively.

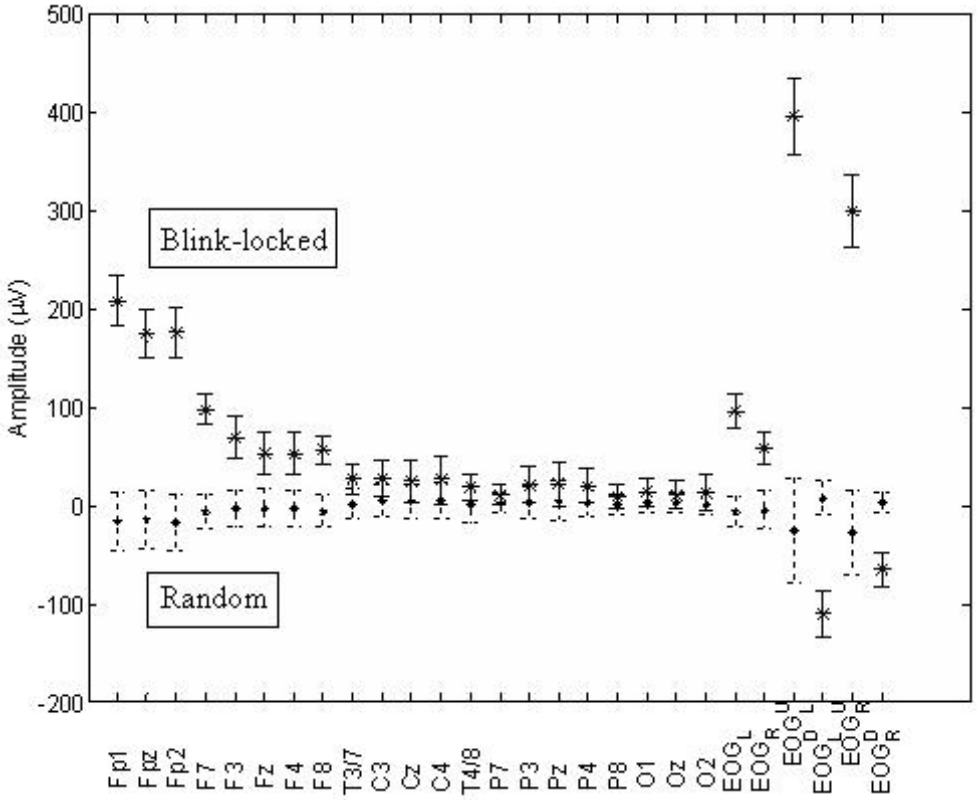

Figure 4.2: Amplitude at the time of maximum blink amplitude (solid) and at randomly selected times (dashed) for several electrode positions, averaged over 24 blinks.

Each simulated data set should represent a different subject with different blink properties. Therefore equation (4.5) is fitted on the blinks recorded from 9 different participants. For all of these participants, the mean parameter values ξ^1,ξ^2,ξ^3,ξ^4 describing the blink artifact, and their standard deviation, are derived. Note that these parameters represent the blink artifact at the EOG_L^U electrode. For every simulated data set, the mean values for ξ^1,ξ^2,ξ^3,ξ^4 and their standard deviations, belonging to a randomly selected participant, are used to simulate blink artifacts of varying shape duration and amplitude. The blink frequency F_b at which blinks occur is typically around 0.25 blinks/s for humans. In this study F_b will be set to 0.1, 0.25, 0.5, and 1 blinks/s to evaluate also low and high frequent blink data. By using the differences in blink amplitude for different electrode positions, as illustrated in Figure 4.2, the blink artifact sequence is scaled and simulated at all desired electrode positions. This way, no explicit assumption on differences between blink artifact scalp topography and eye movement artifact scalp topography is made, as both are based on experimental data. Note that from experimental data it is known that voluntary blinks can have a different duration and shape compared to

involuntary blinks [133]. This is not simulated in this study. All blinks made in our experimental datasets are voluntary.

4.4.2 Combining Simulations

For each type of eye movement artifact of Table 4.2, 60 seconds of data are simulated at a rate of 256 Hz. The first 30 seconds are used for parameter initialization. The last 30 seconds are used to evaluate the correction method. The blink artifact is also simulated for 60 seconds and added to the simulated eye movement artifact data. The scalp topography of the blink artifact is different from the topography of the eye movement artifact.

Note that especially for low F_b values, it is possible that there are fewer than two blinks in the first 30 seconds of simulated data, and parameter $\hat{\phi}_7(t)$ will not have converged once performance evaluation starts. In practice, this will not cause any problems, because the participant can be instructed to blink. For the simulated data, this problem will be overcome by adding an extra 60 s of simulated data to the 30 s of initial parameter stabilization time. This does not influence performance since the tracking time remains 30 s, but it does greatly reduce the chance of non-converged $\hat{\phi}_7(t)$ during the performance evaluation.

The measure SNR_1 is calculated over the last 30 s of the measurement, and SNR_2 is calculated over those periods during the last 30 s where a blink artifact occurs. The signal of interest in this case is $c(t)$. In the following section, results are shown for the Fp1 position. This position is close to the eyes and the EEGs recorded here contain large ocular artifacts. The results for this position can be considered as 'worst case' results.

4.5 Results, discussion & conclusions

4.5.1 simulated data

Figure 4.3 shows respectively the mean SNR_1 and SNR_2 values for the different sorts of simulated eye movement and blink frequencies. The results shown in this figure are averaged each over 20 simulated data sets. In all our performance evaluations the desired signal component $s(t)$ is equal to $c(t)$ because we want to remove ocular activity from $r(t)$ and detect all cerebral activity.

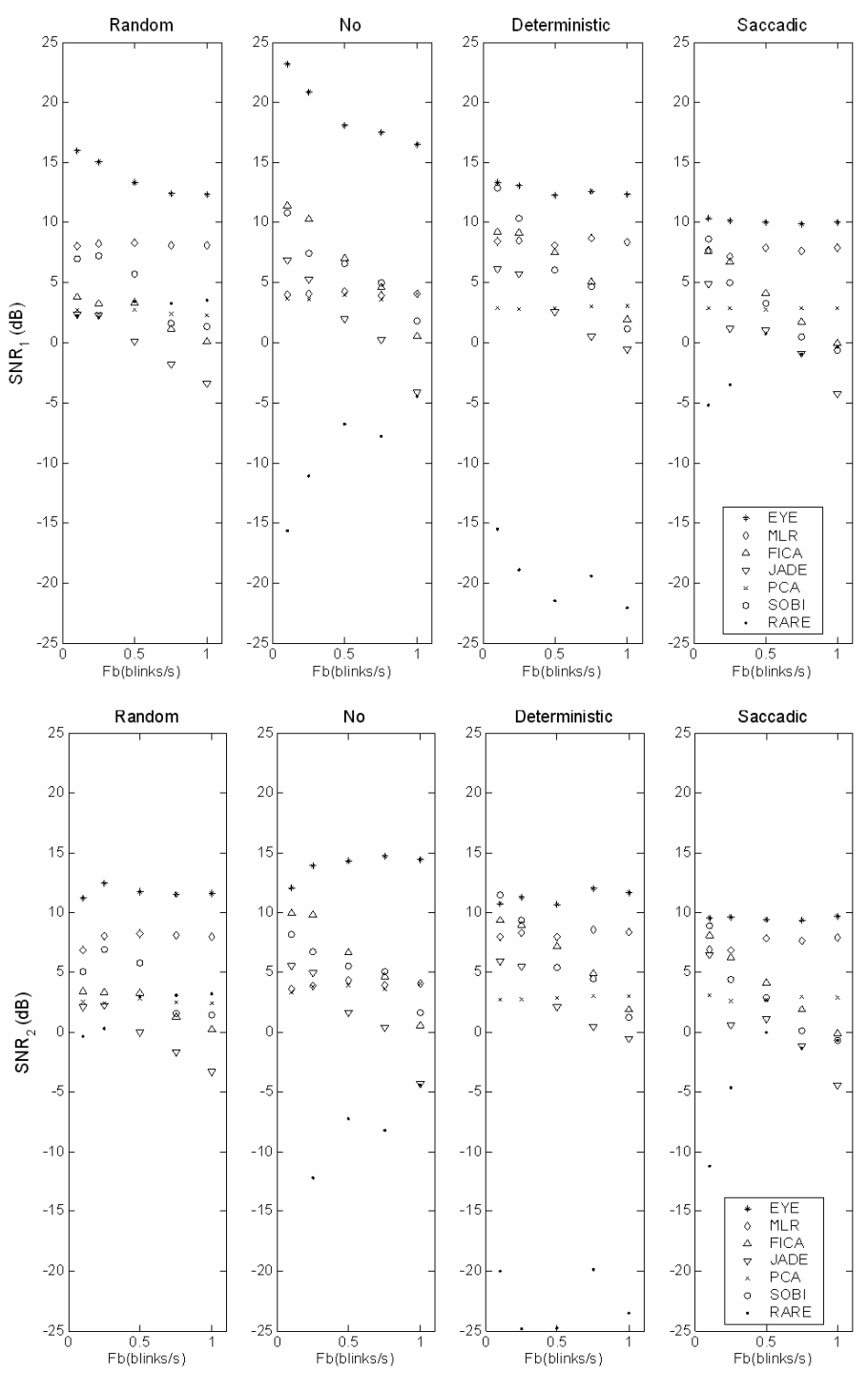

Figure 4.3: Performances SNR_1 and SNR_2 for simulated data sets, calculated at Fp1. Each of the four different eye movement artifact types, as described in Table 4.2, is a subfigure. On the x-axis the blinking frequency is indicated.

Note that the amount of data from which we determine the average SNR_1 and SNR_2 values are different. For F_b=0.1, measure SNR_2 is calculated using approximately only 3 % of the data that is used for SNR_1. We validated that

this amount of data is sufficient for getting an adequate estimate by comparing results to a value of SNR_2 calculated for simulations over a prolonged period (only for the deterministic eye movement artifact at F_b=0.1, the resulting simulated dataset was 900 s).

In Figure 4.3 it can be seen that:

- SNR_1 decreases when F_b increases. This is true for almost every sort of simulated eye movement artifact and correction method and shows that an increasing number of ocular artifacts decreases the quality of correction. If a correction is not perfect, each blink can leave a small residual artifact after correction. Higher F_b indicates more blinks and thus lower SNR_1.
- SNR_1 is higher than SNR_2, which was expected because SNR_2 in general represents the most challenging data with both blink artifact and eye movement artifact.
- SNR_1 and SNR_2 are highest when no eye movement artifact was simulated. In this situation it was only necessary to remove blink artifact and thus, similar to the first remark, a decreasing number of ocular artifacts increases the quality of correction.
- Most of the SNR_1 and SNR_2 values are above 0 dB, indicating that the power of the signal is greater than the power of the remaining noise.
- For all simulated data sets the EYE method has the highest SNR_1 of all evaluated correction methods, indicating that the EYE method is very robust and consistently superior compared to the other methods in this study. Also for the more challenging data considered for SNR_2, the EYE method is superior to all other evaluated methods. Only once, for a deterministic eye movement artifact with an F_b of 0.1 blinks/s, is the SNR_2 of the EYE method slightly exceeded by the SNR_2 of the SOBI method.
- With the EYE method, a SNR_1 value of at least 10 dB is achieved, regardless of the type of eye movement and the blink frequency. This implies that if this method is applied after (or during) EEG experiments, the power of the remaining signal will be at least 10 times higher than the power of the remaining noise.
- In a standard situation, with the random eye movement artifact and an F_b of 0.25, the EYE method has the highest SNR_1 and SNR_2. For that situation the MLR method performs second best.
- The MLR method is the only method that performs worse when there is no eye movement artifact, which is in accordance with Chapter 3. This is probably caused by an overcorrection. Cerebral signals of low amplitude, as can be present in EOG electrodes, are subtracted from the EEG electrode that is being corrected.

- The SOBI method has comparatively low SNR_1 and SNR_2 values for the higher values of F_b. For low values of F_b, the *SNR* values increase and are close to MLR and EYE values. In a previous study with $F_b = 0$, in Chapter 3, it was found that SOBI correction results in *SNR* values that are close to results for EYE correction. This is also to be expected when extrapolating the results shown in Figure 4.3.
- The RARE method has surprisingly low *SNR* values. The reason for this is a combination of blinks, DC adjustment and non-adaptive correction. When blinks occur as 'spikes' in the data set and the mean of the data is set to zero, the resulting data will not have an average of zero during non-blinking periods. This average value will be different for all electrodes, including the EOG electrodes. When parameter calibration is performed, the parameters will not converge to a value that represents ocular artifact in the EEG, but to a value that corrects this offset. Therefore the RARE method should not be used for correcting data that contains blinks or the RARE method should be altered to estimate different parameters for blinking and non-blinking periods.

For these simulated data sets, the EYE method is concluded to be highly robust and the best choice for correction. Results for other electrode positions also showed a similar ranking between the different methods, with the EYE method again performing best.

4.5.2 Experimental data

EEG, EOG and eye tracker measurements are collected from 9 participants aged 19-21, 5 male and 4 female. The participants perform different tasks involving eye movements. These tasks correspond to eye the random, the deterministic and the saccadic eye movement artifacts of Table 4.2. The participant is asked to keep his eyes on a dot that appears on a 19-inch monitor. An eye tracking system is positioned directly below the monitor and records the position of the pupil of the participants left eye. It uses infrared light and from the light reflected by the eye, the position of the center of the pupil is determined. EEG measurements are performed with 21 EEG electrodes positioned according to the 10-20 system. In lieu of the possibility to detect eyelid position with the eye tracker, another 6 electrodes are used to record the EOG. These are positioned above and below both eyes, left of the left eye and right of the right eye. Recordings for all electrodes are referenced offline to averaged mastoids. The EEG and the EOG are recorded at 256 Hz using the BioSemi ActiveTwo system with sintered Ag/AgCl electrodes using a lowpass filter with a cut-off frequency of 67 Hz. Eye tracker data are recorded at 50 Hz using the SensoMotoric Instruments RED eye tracker with an angle resolution better than 0.1 degree. The eye tracker data are up-sampled from 50 to 256 Hz afterwards and synchronized with the EEG recording. We chose to up-sample

the eye-tracker data, as would be possible with a more advanced eye tracker, rather than down-sample the EEG because down-sampling would remove part of the important EEG frequency spectrum. The latest eye trackers are already capable of sampling at rates of over 1 kHz. Up-sampling is obviously inferior to using a higher sampling rate; up-sampling does not restore the missing part of the eye movements' frequency spectrum. Especially for saccadic eye movements, this can cause inaccuracies because the high frequencies that are associated with the saccades are overlooked [131]. Note however that this should be considered merely as a practical limitation, and not a fundamental limitation. During the task, the participant sits comfortably in front of a monitor at 0.8 m distance with the head supported and eyes horizontally aligned with the center of the screen. The subject is instructed to avoid blinking if possible because experimental data was intended primarily for use in Chapter 2. Despite the instruction, there are still several blinks in all recordings. For experimental data, (4.9) and (4.10) cannot be determined. Therefore Figure 4.4 shows the signals $r(t)$, $\hat{e}(\underline{\hat{p}}(t))$ and $\hat{c}(t)$ for different correction methods and eye movement artifacts.

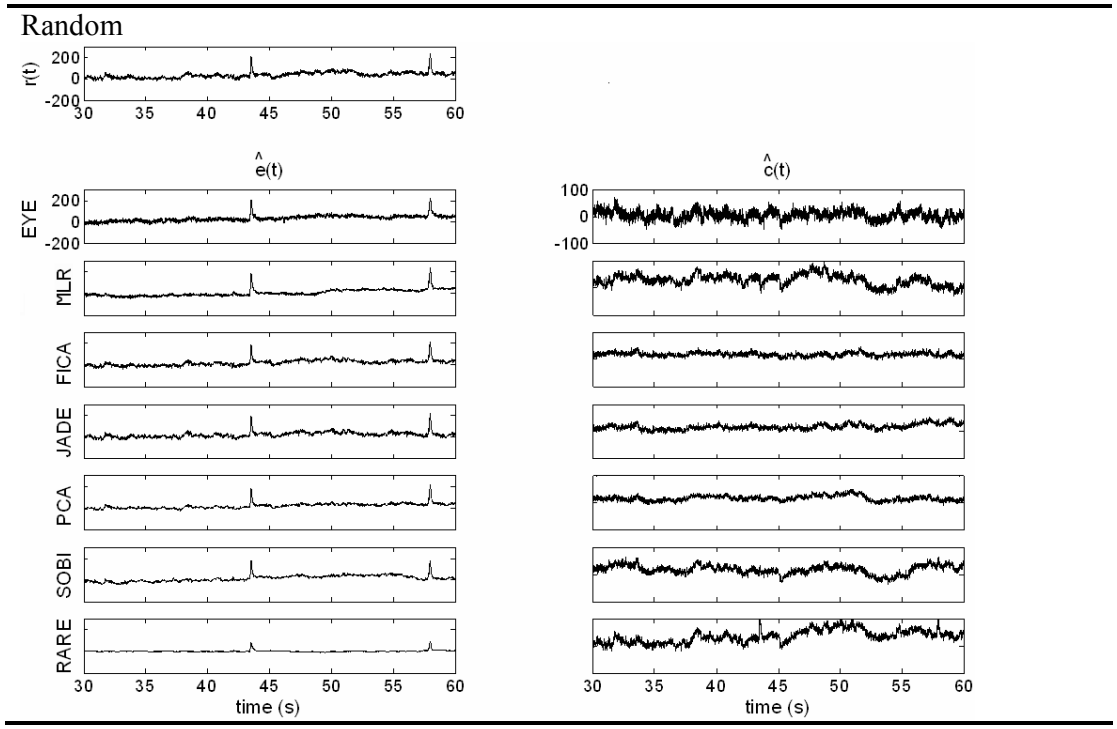

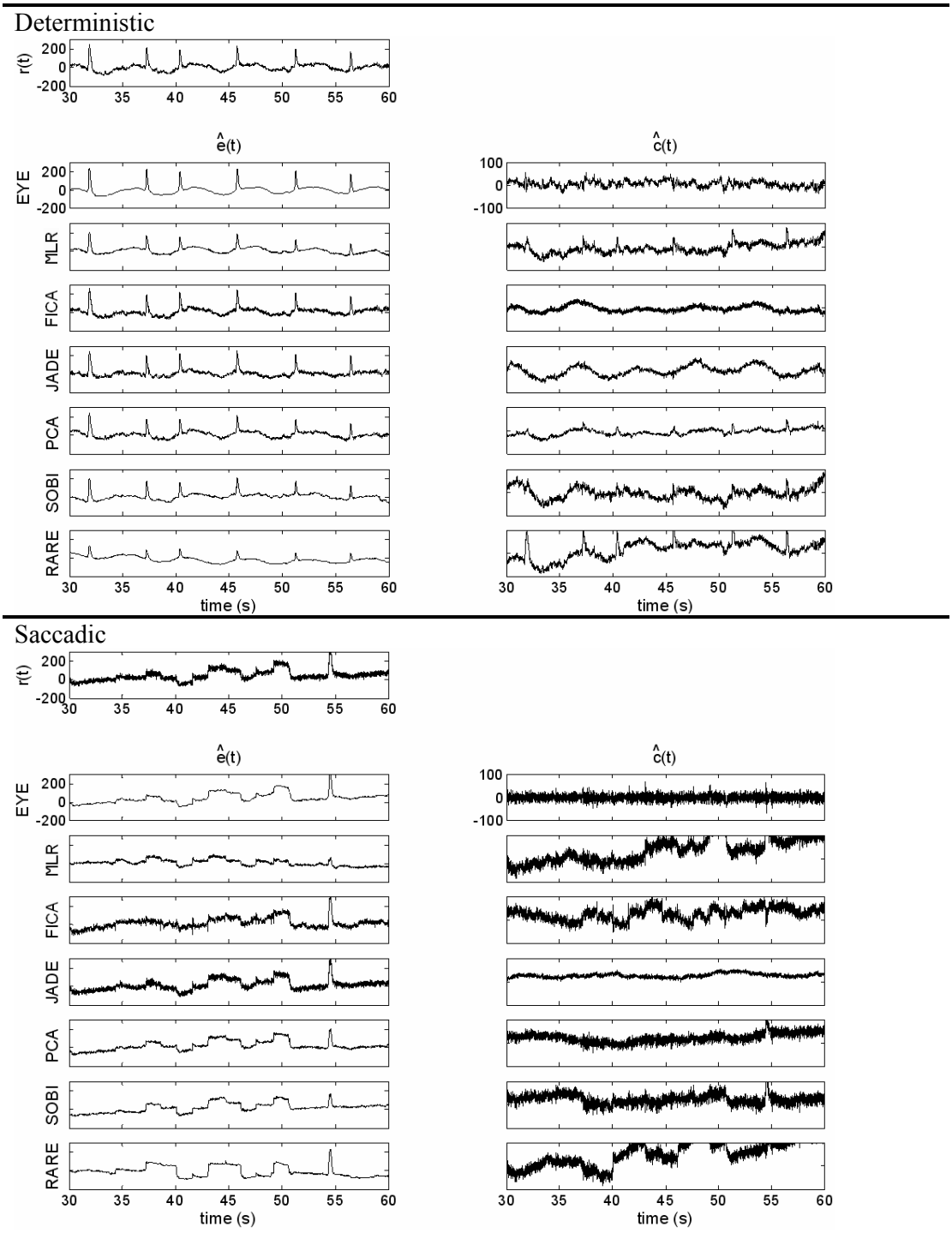

Figure 4.4: Experimental data for three different types of eye movement artifact, recorded at Fp1. In the first row of each subfigure, the EEG $r(t)$ is shown. The estimated components $\hat{c}(t)$ and $\hat{e}(\underline{\hat{p}}(t))$ are in respectively the first and second column of the other rows. Scalings of both axes are identical for each subfigure in a column. The y-axis indicates voltage (μV).

In Figure 4.4, a basic visual inspection does not detect ocular artifacts, after correction by the EYE method. For some of the other correction methods, there clearly remains some ocular artifact after correction, whereas for other ones the ocular artifact also appears to be removed completely.
From the remaining estimate for the cerebral electrical activity, $\hat{c}(t)$, the distinction between the performances of the methods that do appear to remove the ocular artifact completely cannot be made. Strikingly, some of the correction methods appear to remove not only the ocular artifact, but also part of $c(t)$. Especially the components-based methods appear to have a much smaller signal $\hat{c}(t)$ after correction. Purely based on the experimental data it is not possible to verify whether the components-based methods remove too much, or whether the EYE method removes too little of the ocular artifact. However, for ICA-based methods it is demonstrated in [16], that correction can result in a spectral distortion of the estimated cerebral electrical activity which will remove part of the cerebral electrical activity. In Chapter 2, it was also demonstrated that ICA-based correction methods can remove part of the cerebral electrical activity. This is obviously unacceptable, because it eliminates the possibility of recording the full electrical activity of the brain and possibly important information might be deleted. The MLR method does not appear to correct well for the saccadic eye movement artifact. This data showed a considerable electrode drift in the Fp1 recording, which cannot be compensated for by the EOG reference. A possible solution to this is high pass filtering of $r(t)$, but for a fair comparison between different methods such filtering should either be applied to all correction methods, or to none.
It should be noted here that the displayed results are on data without periods of prolonged eyelid closure. For these periods the method using an EOG electrode is not capable of detecting a clear $p_3(t)$ because (4.5) is not valid for prolonged closure periods. When $p_3(t)$, determined by an eye tracker, is used instead of $\hat{p}_3(t)$, estimating the blink artifact using (4.5) is no longer required, and periods of prolonged eyelid closure can be corrected. Furthermore, for the saccadic eye movement artifact data, both horizontal and vertical eye movements are included. The method is shown in Figure 4.4 to remove the eye movement artifact accurately.
This result on saccadic data suggests that the consequences of the up-sampling of eye tracker data from 50 Hz to 256 Hz are only minor, even for the saccadic data. For some vertical eye movement artifacts however, there is a small remaining artifact at the moment of each the saccadic movement. Although this could be caused by the insufficiently high sampling rate of the eye tracker, there is a also a second explanation for this artifact, known as the rider artifact [22]. Rider artifacts occur during vertical eye movements and are caused by small coinciding movements of the eyelid. This small eyelid movement is not present in $\hat{p}_3(t)$ because $\hat{p}_3(t)$ is based only on blinking periods, as shown in

(4.6), and therefore cannot be corrected based on the $\hat{p}_3(t)$ reference. Because we only detect the artifact for vertical saccades, the rider artifact appears to be a more plausible cause of the artifact than the sampling issue. Recording $p_1(t)$ and $p_2(t)$ at higher sampling rates can clarify this issue.

Although with the current implementation the prolonged eyelid closure periods and the rider artifacts thus cannot be corrected, this is merely a matter of implementation. If a future eye tracker is capable of detecting $p_3(t)$, these two issues will be resolved.

One remaining drawback of using an eye tracker, even if all suggestions regarding the use of different equipment are implemented, would be that the eye tracker cannot detect the pupil position while the eyelid is down. For the brief period that pupil position is 'missing' during a blink, the consequence of this is probably not too large because accompanying eye movements and their effects are in general small. More seriously, this disqualifies the use of an eye-tracker for EEG recordings that are taken while the eyes remain closed. An alternative could be the use of magnetic coils for the detection of eye movements and eyelid movements as discussed in [131], but this would require very different equipment.

4.5.3 Conclusions

In Section 4.3 a new eye tracker-based method for the correction of ocular artifacts in EEG recordings is introduced. This method uses a Kalman filter for the estimation of the ocular artifact. The method is evaluated on simulated data and is shown to improve simulated ocular artifact correction when compared to six well known existing methods.

In order to quantify the performance of different correction methods and compare them, two different SNR-based measures are defined in (4.9) and (4.10). The first, SNR_1, quantifies the correction of the entire simulated data set and the second, SNR_2 , focuses on those segments containing simulated blink artifacts. The current implementation is shown to result in an average SNR_1 and SNR_2 of at least 9 dB. This implies that the power of the corrected signal is at least eight times the power of the remaining noise. The simulated data sets contain a wide range of eye movements and blink frequencies. For almost all of these data sets, 16 out of 20, the correction results for the new method are better than any of the other evaluated algorithms. The only method that has a higher SNR_2 value for one of the simulated data sets is the SOBI method. The SNR values for the EYE method in this data set, are just slightly lower.

The standard Kalman filter used here is based on the assumption that component $c(t)$ is white. In reality, $c(t)$ represents the cerebral component of $r(t)$. The spectrum of $c(t)$ hence has a band pass nature with frequencies between approximately 0.5 and 30 Hz. Accordingly, the noise is not white and

the Kalman filter considered here is not optimal. Implementing whitening filters prior to the Kalman filter can in the future improve correction results even further.

By using an advanced eye tracker for the detection of eyelid position, as discussed earlier, a signal that is clean of all brain-, or muscle-, electrical activity can be recorded. Using such a signal instead of the EOG electrode that is used in this study is likely to further improve correction performance. Also, this will have the advantage that some minor artifacts, like the rider artifact that is mentioned in Section 4.5.2, can be corrected.

On experimental data, the correction method appears to adequately remove the ocular artifact. Considering the simplicity of the MLR method, this method performs remarkably well, which might explain why basic regression is still often used for correction.

4.6 Appendix

In Section 4.3.1 we proposed to use an eye tracker to record the position of the pupil and the eyelid. In the subsequently following sections, it was assumed that the recorded positions are accurate registrations of the true positions. This assumption overlooks possible inaccuracies of eye-tracker recordings.

- Random Disturbances. Noise in the video image of the eye tracker may affect the recorded position.
- Systematic Disturbances. By assuming that the positions as detected by the eye tracker are accurate measures of gaze direction and eyelid position, a systematic error is made. The assumption ignores that an eye is (approximately) spherical and the eye tracker only detects a two dimensional projection of this.
- Quantization Disturbances. All recorded positions are quantized because the eye tracker has a limited spatial resolution.
- Head movements. Movements of the head can be compensated by the Kalman filter which will adjust vector $\hat{\underline{\phi}}(t)$. During the period that vector $\hat{\underline{\phi}}(t)$ is adapted, correction errors may occur.

The random noise mainly concerns image quality in the eye tracker recording. Each pixel in this image may record some noise. In the process of determining the pupil position from a video image, a threshold is set manually in order to separate pixels that belong to the pupil from other pixels. After this, all pupil pixels are weighted equally when determining the pupil position. Because the distinction between pupil pixels and other pixels is generally very clear, effects of image noise are probably negligible.

When the eye is looking directly towards the eye tracker, a change in gaze direction will yield the largest change in pupil position. If the eye looks away from the eye tracker, an equally large change in gaze direction will cause (slightly) smaller changes in pupil position, as is illustrated in Figure 4.5.

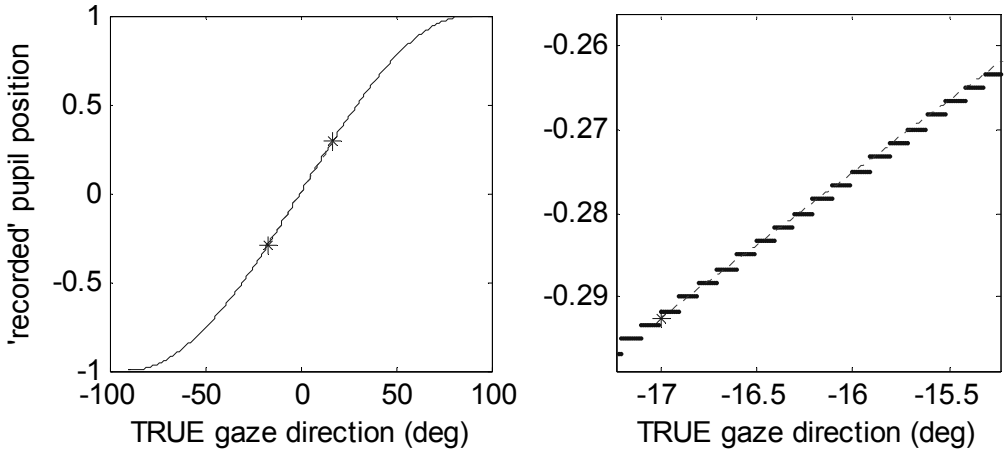

Figure 4.5: Illustration of eye tracker recording inaccuracies. Our method assumes a linear relation between recorded pupil position and gaze direction. The left plot illustrates that within a limited range of gaze directions (asterisks), this assumption holds. Additional errors due to quantization of the pupil position within this range are small, as illustrated in the right plot.

Pupil position alone is thus not optimal for determining the gaze direction of the eye. In [135], it is demonstrated how additional light sources and reflections of these sources on the cornea can be used for a more accurate detection of gaze direction. When the range of eye movements is restricted, as it is in our experiments and simulations, the range of possible gaze directions is limited, as indicated by the asterisks in Figure 4.5. The relation between pupil position and gaze direction is approximately linear over this range.

Quantization noise is inevitable when pupil position is digitally recorded because pupil position accuracy is limited by eye tracker resolution and by the distance between eye tracker and eye. As a result of this, only a fixed number of possible values for pupil position and eyelid position exist, as illustrated in Figure 4.5. Taking into account that the eye tracker we used is claimed to have a spatial resolution $<0.1^{o}$ for tracking, the error due to quantization is very small, as can be seen in Figure 4.5.

Because the participant's chin and forehead were supported during the measurements, effects due to head movements are probably negligible. Although head movements were not monitored during our study, literature [136] suggests that head movements under similar circumstances are smaller than 80 μm when measured over a one minute period.

Chapter 5

Evaluating correction methods on challenging experimental data

5.1 Abstract

Numerous ocular artifact correction methods exist. They aim to remove the electrical activity associated with eye- and eyelid movement from the electro-encephalogram. A previous comparison of such methods, based on simulated datasets, ranked a selection of these methods in terms of their correction accuracy. As simulated data is limited by model restrictions, this chapter aims to use experimentally recorded data and determine an accuracy ranking based on real data. An experiment is set up that is expected to generate low-amplitude ERPs, located mostly at frontal electrode positions. For this type of data, it is essential that ocular artifacts are adequately removed. Next the recorded ERPs are categorized based on whether or not they contain ocular artifacts, and the stimulus related activity is removed. A yardstick for the accuracy of the correction methods is derived based on the power of background EEG as recorded during each trial. Accuracy, as estimated by this yardstick, complies very well with the accuracy as found on the simulated data.

5.2 Introduction

The electro-encephalogram (EEG) is a valuable tool for analyzing cerebral activity and for studying the brain's response to stimuli. An important problem in the analysis of the EEG is the presence of ocular artifacts, caused by eye movement and blinking [8;16;38].

In Chapter 3 and Chapter 4, we introduced a correction method, dubbed EYE, which uses an eye tracker to monitor features that are closely linked to the timing and amplitude of ocular artifacts. EYE uses gaze direction and eyelid position, estimated from eye tracker recordings or alternatively from the electro-oculogram (EOG), to obtain an estimate of the ocular artifact and to correct the EEG. On simulated data, we showed objectively that EYE leads to

improved ocular artifact correction when compared to other commonly used correction methods.

The purpose of the present chapter is to evaluate the success of the EYE method on real experimental data. Evaluating the performance of methods solely with simulated data is insufficient for full, comprehensive testing of these methods [50]. Aspects that are not simulated, because a study might erroneously assume that they are merely of minor impact, could be overlooked and lead to a false evaluation of the methods. Although some of this criticism against simulated data can, to some extent, be put aside by continuously improving the models that simulate the data, the obvious challenge is to evaluate EYE's correction accuracy on experimental data.

Two issues are important in evaluating artifact correction methods in experimental data: the choice of the experimental task, and the choice of the measure for evaluating the performance of the correction method.

As to the first issue, we used the stop-signal task [137] for experimental manipulation. In this task, participants are focused on task execution. They are not instructed to produce artifacts intentionally. This is an important point in that it has been shown that properties of ocular artifacts can depend on whether or not artifacts occur intentionally or unintentionally [21]. For instance, the shape of a blinking artifact as seen during a series of intentional blinks differs from the shape of an unintentional blinking artifact. Furthermore, the stop-signal task has a high need for accurate correction because the cerebral activity of interest is mainly detectable on frontal electrodes, where the ocular artifact is also relatively large [138]. In addition, the effects observed in this task are usually of small amplitude, making the need for accurate correction even higher. In summary, using the stop-signal task for evaluating the correction methods provides us with a strong test of these methods.

With respect to the second issue, it should be noted that evaluation of correction methods on experimental data is often limited to a visual check of the corrected EEG, e.g. as is done in chapters 3 and 4, as well as in [74]. To reduce subjectivity of evaluations, we want to use a more objective and quantitative measure. Selecting this measure is difficult because the reference one would like to use, e.g., comparing the corrected EEG to the real artifact-free EEG, is impossible.

One way to obtain such a measure is to compare the power of corrected EEG to the power of an artifact-free EEG segment [13]. Because ocular artifacts increase the power of raw EEGs, high power, with respect to the power of artifact-free EEG, thus indicates that ocular artifacts occur. This assumes that the power of artifact-free EEG does not change significantly during a measurement.

A power-based measure of correction accuracy does not require intentional eye movements and blinks, and thus can easily be applied to data obtained with the stop-signal task. In addition it can, to some extent, indicate how well the EEG is preserved during correction. In this chapter, the power of 2 s segments of EEG will be compared to the power of 2 s segments of artifact-free EEG. A 2 s segment will be referred to as a trial.

All trials are categorized according to the amount of ocular artifact they contain. We use both the EOG and an eye tracker for categorization. A trial is categorized as OA^0 when both EOG and eye tracker indicate that a trial of EEG is without significant ocular artifacts. When a trial contains at least one blink according to both the EOG and the eye tracker, it is categorized as OA^+. All other trials, containing significant eye movements but no blinks, are categorized as OA^-.

The stop-signal task results in experimental data that contain event-related potentials (ERPs). These ERPs reflect the brain's response to the stimuli. ERPs may vary in amplitude, latency and waveform [139], even when they are elicited by identical stimuli. To ensure a fair comparison of the power in segments, these ERPs will be estimated and removed prior to calculating power spectra of the background EEG. After ERP removal, we determine the power of all trials in each category prior to and following ocular artifact correction. Of special interest are the OA^0 trials which, after ERP removal but prior to correction, should only contain background EEG. This makes the power of these OA^0 trials a suitable estimate for the power of artifact-free EEG.

After correction, all three categories of trials should only contain background EEG. It is therefore expected that a successful ocular artifact correction method will reduce the power of all corrected trials to the level of the uncorrected OA^0 trials. By comparing the power of all corrected trials to uncorrected OA^0 trials, combining the results for the three trial categories, and averaging over multiple subjects to reduce the influence of inter-subject variability, one overall yardstick for the accuracy of correction is obtained. The details on this yardstick are given in Section 5.4.

In Section 5.5 the EYE correction as well as several other frequently used ocular artifact correction methods will correct the same raw EEG. These other methods include both components-based methods and EOG-based methods. Illustrations, highlighting raw and corrected EEG, of data with ocular artifacts will be shown and discussed. By determining correction accuracies for all these methods, and comparing these against each other, a comparison of correction accuracy on experimental data is obtained. It is expected that, in line with results on simulated data, the new EYE method will outperform existing correction methods because this method is the only method that makes use of

the extra eye tracker information. Section 5.6 briefly summarizes and presents a general conclusion.

5.3 Stop-signal tasks & ocular artifact correction methods

5.3.1 Stop-signal tasks

A choice-reaction task is frequently used as a basis for a stop-signal task. In a choice-reaction task, a subject receives one of two possible GO-stimuli and has to respond by pressing one of two corresponding buttons on a keyboard. Typically, the time between stimulus and response in such tasks is around 300 ms. In stop-signal tasks, a STOP-stimulus is occasionally presented to the subject in between GO-stimulus and response. In our experiments, 30 % of all GO-stimuli were followed by a STOP-stimulus. If a STOP-stimulus occurs, the subject should try to inhibit responding. In general, inhibition is fairly easy if the STOP-stimulus is presented briefly after the GO-stimulus, and as a result no button will be pressed. When the STOP-stimulus is delayed more with respect to the GO-stimulus and occurs close to the response, inhibition fails. For stop-signal tasks a theoretical model was proposed in 1984 [140]. This model assumes that the GO-stimulus and the STOP-stimulus initiate two independent processes. The first process to be completed determines whether or not a response occurs.

EEG recordings during stop-signal tasks focus on two scalp regions [141]. Firstly, recordings at C3 and C4 position, according to the 10/20 system, are used to detect motor preparation. The C3 and C4 positions are located directly above the left and right motor cortices of the brain. Secondly, recordings at Fz, F3 and F4 position can show a negative peak known as N200 that is believed to be associated with the inhibition of the response. These frontal electrodes are close to the cortex area where the STOP-stimulus is believed to be processed. Further interpretation of the physical background of this signal is beyond the scope of this study. It is the signal recorded at Fz, F3 and F4 that this chapter will focus on. Typical N200 amplitudes are very low and ocular artifacts are very prominent here because the frontal electrode positions are close to the eyes. Removal of ocular artifacts prior to other signal processing is thus essential.

In our experiments, nine healthy participants, aging from 24 to 37 (average 28.2, SD. 3.7), with normal or corrected to normal vision participated.

During the experiment, stimuli appear at the center of a 17 inch computer display for 1000 ms. The GO-stimulus is a green arrow that appears at the center of a monitor screen and points either to the left or to the right, with

equal probability. The respond buttons for left and right are 'z' and '/' respectively on a standard QWERTY keyboard. For 30 % of the GO-stimuli, the arrow turns red shortly after appearing. This is the STOP-stimulus that triggers the inhibition of the response. The occurrence of a STOP-stimulus is randomized, and the timing of the STOP-stimulus with respect to the GO-stimulus is controlled stepwise to achieve an inhibition rate of 50 %. The stop stimulus delay, SSD, represents the time interval between the appearance of the GO-stimulus and the STOP-stimulus. Initially, the SSD is set to 200 ms but after each correct inhibition 50 ms is added to this, whereas after each unsuccessful inhibition 50 ms is subtracted. An inter-stimulus interval, varying randomly from 1500 to 2000 ms, separates consecutive GO-stimuli. During this interval, a fixation marker appears at the center of the screen.

A total of 1210 GO-stimuli are presented to each participant, 395 of which are followed by a STOP-stimulus. By using a variable SSD as described above, 50% of these 395 stimuli should be inhibited successfully. Participants are asked to react as fast as possible and thus not to anticipate on a STOP-stimulus that might appear. They are told that their primary focus should be on reacting fast and that, as a result of this, not all inhibitions will be successful.

During the task, the participant sits comfortably in front of a monitor at 0.8 m distance with the head supported and eyes horizontally aligned with the center of the screen. EEG recordings are performed with 21 EEG electrodes positioned according to the 10-20 system [26]. Another 6 electrodes are used to record the EOG. These are positioned above and below both eyes, left of the left eye and right of the right eye. Recordings for all electrodes are referenced to the right mastoid. EEG and EOG are recorded at 256 Hz. An eye tracking system is positioned directly below the monitor to record the gaze direction of the participants left eye. The eye tracker uses an infrared light and from the light reflected by the eye, the position of the center of the pupil is determined and tracked throughout the experiment. Eye tracker data are recorded at 50 Hz using the SensoMotoric Instruments RED eye tracker. After the experiment, the eye tracker data are up-sampled from 50 to 256 Hz and synchronized to the EEG recording.

5.3.2 Ocular artifact correction methods

Over the past decades many ocular artifact correction methods for electro-encephalography have been developed, and several excellent overviews have been published, e.g. [8;38;43;85;94]. Next to this, considerable effort was spent on getting to understand the biophysical cause of the ocular artifact [21;40]. Currently, the ocular artifacts are believed to be caused by the corneo-retinal dipole which represents a steady difference in electrical potential when measured over the eye. Eye movements rotate this dipole, whereas blinks move

the eyelid over the cornea and affect the shape of the electric field that surrounds the dipole.

In Chapter 3 and Chapter 4 it is shown for simulated data that accurate ocular artifact correction can be achieved by exploiting useful information on eyelid position and ocular movements, as obtained by an eye tracker. This information has the advantage that, as opposed to using EOG electrodes to monitor eye movements, it cannot be corrupted by cerebral activity. Therefore EYE does not have to consider the traditionally difficult issue of propagation of cerebral activity into the EOG. This new correction method will be tested and evaluated on the EEG as recorded during the stop-signal task.

The same raw data will also be corrected by seven other methods. None of these other methods use additional eye-tracker recordings, which is both an advantage, as less hardware is required, and a disadvantage, as potentially valuable information is ignored. The added value of using an eye-tracker should therefore be derived from improved correction accuracy, to warrant the use of extra hardware in experiments where accuracy is essential. We will not go into details about the seven correction methods and restrict to mentioning the main assumptions that underlie each method. Details can be found in the references given with each method.

FastICA [64], FICA, is an Independent Components Analysis, ICA, based correction method that assumes that the recorded signal is composed of underlying components which are mutually independent. FICA defines independence based on fourth order cumulants, and is perhaps most widely used of all current ICA implementations.

Gratton [35], GRAT, is an EOG-based correction method that corrects for blinking and eye movements separately and that is frequently used in EEG research. The method differs from most EOG-based methods in that it uses multiple, aligned, trials in the process of estimating eye movement artifacts in EEG recordings. Prior to this, GRAT detects and removes blinks based on the derivative of the vertical EOG signal.

Joint Approximate Diagonalization of Eigen-matrices [59], JADE, like FICA is an Independent Components Analysis correction method that assumes that the recorded signal is composed of underlying components which are mutually independent.

Principal Components Analysis [36], PCA, is perhaps the most basic components analysis method. Instead of independency, PCA assumes that components underlying a recorded signal are uncorrelated.

Multiple Linear Regression [39], MLR, is a standard mathematical tool that is used for many purposes. When applied to EEG research, simultaneously recorded EOG is scaled and subtracted from the raw EEG.

Second order blind identification [51;52], SOBI, is a components-based method that like PCA only uses second-order statistics, i.e., correlations. Whereas PCA assumes merely that components are mutually uncorrelated at one moment in time (instantaneously), SOBI also assumes that components are mutually uncorrelated at other moments in time, dubbed lags. These lags should be carefully selected to optimize correction accuracy as was demonstrated in [124]. In the current implementation we used lags similar to those in Chapter 2.

Regression with an Auto-Regressive Error structure [46], RARE, is a special implementation of MLR, in which the cerebral electrical activity that is seen in the EEG is assumed to be spectrally colored. While the scaling factors of EOG propagation to EEG, as in MLR, are determined, this spectral content in considered.

These methods were selected in part because prior studies, including the evaluation Chapter 2, suggested their appropriateness for ocular artifact correction [15;16;73;98] and in part because they are amongst the most frequently used correction methods to date.

5.4 Quantifying ocular artifacts in EEG

For each participant, the experimental data is segmented in a number, M, of trials. A trial represents all samples close to a STOP-stimulus, starting 0.5 s prior to this stimulus (t=0) and ending 1.5 s afterwards (t=2). In our experiment M=395. The GO-stimulus of each trial is thus located in the first 0.5 s of the trial. To (roughly) set the time-averaged amplitude of the trials to zero, the average voltage of the 0.5 s EEG prior to the GO-stimulus is determined for each trial and subtracted from each sample within that trial.

The resulting data will be denoted as $r_m(t)$ with $m=[1:M]$ the specific trial number and t a time index. Each trial contains electrical brain activity, $f_m(t)$, related to the m^{th} stimulus as well as other non-stimulus related electrical brain activity, $b_m(t)$, which is referred to as background EEG. The stimulus related electrical brain activity, $f_m(t)$, is assumed to be of similar morphology, $f(t)$, for all trials, varying inter-trial only in ERP amplitude, A_m, and ERP delay, δ_m,

$$f_m(t) = A_m \cdot f(t + \delta_m). \qquad (5.1)$$

Additionally some trials may contain electrical activity, $e_m(t)$, due to ocular artifacts. Thus

$$r_m(t) = f_m(t) + b_m(t) + e_m(t). \tag{5.2}$$

For each trial $r_m(t)$, the trial-power $P(..)$ is defined as

$$P(r_m) = \frac{1}{2}\int_{t=0}^{2} r_m(t)^2 dt. \tag{5.3}$$

By assuming that $f_m(t)$, $b_m(t)$, and $e_m(t)$ are orthogonal, this leads to

$$P(r_m) = P(f_m) + P(b_m) + P(e_m). \tag{5.4}$$

To quantify the amount of ocular artifact in a trial, an indication of the contribution of $P(e_m)$ to $P(r_m)$ is needed. Unfortunately, $P(r_m)$ is the only observable term in equation (5.4). The contribution of $P(e_m)$ can only be estimated when $P(f_m)$ and $P(b_m)$ either are assumed constant, or are in some way removed from $P(r_m)$.

- The power $P(f_m)$ is not constant over trials because ERPs can vary in amplitude and latency. Caution should thus be taken not to mistake inter-trial ERP variations for ocular artifacts. To estimate the inter-trial ERP variations, we first estimate the trial-averaged ERP, $\hat{f}(t)$, together with the amplitudes, $\hat{A}_m$, and delays, $\hat{\delta}_m$ of the separate trials using a maximum likelihood estimator described by [142]. These estimates can be used to estimate the single trial ERPs, $\hat{f}_m(t)$, in a way similar to (5.1). Next, the estimated $\hat{f}_m(t)$ is subtracted from $r_m(t)$ prior to calculating $P(r_m - \hat{f}_m)$. Using (5.4) we get

$$\begin{aligned} P(r_m - \hat{f}_m) &= P(b_m + e_m + (f_m - \hat{f}_m)) \\ &\approx P(b_m + e_m) = P(b_m) + P(e_m). \end{aligned} \tag{5.5}$$

- The power $P(b_m)$ can be assumed constant for a period of several minutes and hence over multiple trials if measurements are performed in a controlled, and stabile, environment. For trials without ocular artifacts, $P(e_m)$ is zero and $P(r_m - \hat{f}_m)$ is approximately equal to $P(b_m)$ according to (5.5). Therefore, to estimate $P(b_m)$ we carefully select trials without ocular artifacts as described below, and determine $P(r_m - \hat{f}_m)$ for these trials. Averaging over the resulting $P(r_m - \hat{f}_m)$ leads to the trial-averaged estimate for background EEG power, which will be referred to as P_{REF}.

Accordingly, we obtain an estimate for the power of the ocular artifact, $\hat{P}(e_m)$, in each trial as

$$\hat{P}(e_m) = P(r_m - \hat{f}_m) - P_{REF}. \quad (5.6)$$

In the process of determining P_{REF}, it is required that trials without ocular artifacts are separated from trials with ocular artifacts. To this end, we monitored eye tracker recordings simultaneously with each trial in order to mark trials based on whether or not they contain blinking artifacts and eye movement artifacts. Whenever the eye tracker lost track of the pupil, we marked the trial during which this happened. This loss of tracking is typical for blinking, as the eyelid briefly covers the pupil. Marking trials with eye movement artifacts requires a more delicate detection. An eye tracker can detect very small eye movements which cause potential changes in the EEG that are even smaller than ERPs. Clearly, a threshold based on which amplitude of the corresponding eye movement artifacts is considered significant, should be set for the eye-tracker recording. Based on extrapolation of artifacts for large eye movements in other experimental data, and on small eye movements in a simulation model, we found that a change in ocular orientation of app. 0.3° will cause an artifact of comparable amplitude as an ERP. This 0.3° threshold is used as the eye movement detection threshold. Applying this threshold to the eye tracker recordings aided in dividing the M trials in three categories,

- OA^0 No blinks, < 0.3° change in ocular orientation,
- OA^- No blinks, ≥ 0.3° change in ocular orientation,
- OA^+ Blinks.

The fact that a fixation mark is visually presented to the participant during all trials, does not imply that no eye movements are made. Literature [143] shows that changes in ocular orientation during fixation occur, and that vertical changes in gaze direction during fixation have a standard-deviation of less than 0.23^o.

Trials in the OA^0 category are used for determining P_{REF} since for this category $P(e_m)$ is zero. For the OA^- and the OA^+ trials, $P(r_m - \hat{f}_m)$ is expected to be larger than P_{REF}. We will denote $P(r_m - \hat{f}_m)$, averaged over all trials in these categories as P_- and P_+. Similarly, P_0 indicates $P(r_m - \hat{f}_m)$ for the OA^0 category.

Combining these expectations, we can define a measure j that indicates the amount of ocular artifact in all three categories combined,

$$j = |P_0 - P_{REF}| + |P_- - P_{REF}| + |P_+ - P_{REF}|. \quad (5.7)$$

It is straightforward to see that j is nonnegative and equals zero only if the trial-averaged powers for all three categories are equal to P_{REF}. Although it is

expected that $P_0 \approx P_{REF}$, $P_- > P_{REF}$, and $P_+ > P_{REF}$, the use of absolute values in (5.7) ensures that both too large and too small trial-averaged powers will increase j. Later this will be shown useful for corrected data.

Because both the properties of background EEG and ocular artifacts can vary between subjects, P_-, P_+, P_0, P_{REF}, and j may show inter-subject variability. We define one final overall yardstick J for the amount of ocular artifact in data as

$$J = \frac{1}{9}\sum_{k=1}^{9} j(k), \tag{5.8}$$

with k the participant-number. An overview of the steps discussed above is given in Figure 5.1.

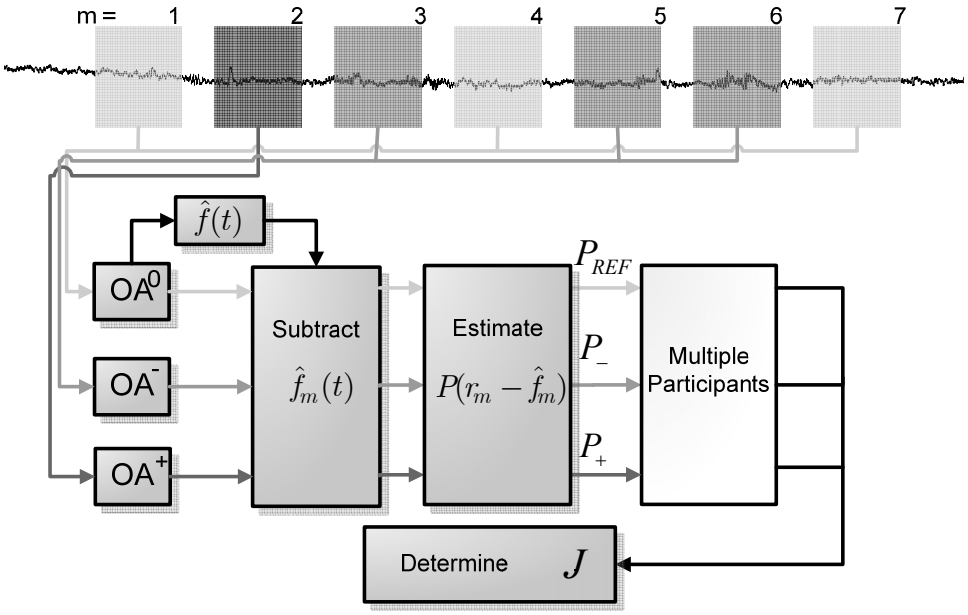

Figure 5.1: Illustration of the sequence of steps for determining yardstick J from raw EEG data. Relevant trials in the raw data are selected and categorized based on what sort of ocular artifacts they contain. Subsequently, the ERP estimate $\hat{f}_m(t)$ is subtracted from each trial and the power of the remaining signals, $P(r_m - \hat{f}_m)$, is determined. After repeating these steps for all nine participants, the yardstick J which represents the amount of ocular artifact in data is determined. For illustrative purposes, seven relevant trials are closely spaced in time. In reality, these trials will be separated by fragments of raw EEG that do not contain a STOP-stimulus. Only 30% of all GO stimuli are followed by a STOP-stimulus.

Ocular artifact correction is supposed to remove $e_m(t)$ from $r_m(t)$, without affecting both $f_m(t)$ and $b_m(t)$. We will denote corrected data by a superscript, e.g., $r_m^*(t)$. Because ocular artifact correction removes $e_m(t)$, $P(r_m^* - \hat{f}_m)$ should ideally equal P_{REF} regardless of whether or not a trial contained ocular

artifacts prior to correction. For corrected data it is therefore expected that P_+^*, P_-^* and P_0^* are all equal to P_{REF}. Note that equality of P_0^* and P_{REF} is not trivial even though they both relate to data without ocular artifacts. A correction method might erroneously affect trials without ocular artifacts and therefore we included the $|P_0 - P_{REF}|$ term to (5.7).

5.5 Results & discussion

The number of trials in each category is given in Table 5.1. Trials in which a STOP-stimulus was given, but in which a response did occur, or in which other, non-ocular, artifacts occurred were not used for further analysis.

Table 5.1: Number of trials in each category

	1	2	3	4	5	6	7	8	9
OA^0	51	104	42	61	39	20	36	58	46
OA^-	28	36	31	76	61	22	11	125	5
OA^+	69	26	53	44	22	29	49	11	129

In (5.8) , results for all participants are weighted equally, regardless of the number of trials they have in the different categories. If a trial category for a participant contains only a very limited number of trials, the accuracy of $P(r_m - \hat{f}_m)$ for this category is limited as r_m^* is (partly) stochastic. For this reason, participant 9 was excluded.

For each category, one trial of participant 4 is illustrated in Figure 5.2. The bottom subfigure shows $\hat{f}(t)$. Clearly visible in the OA^+ trial is the blink artifact at t=1.3 s, whereas in both the OA^0 and OA^+ trials visual detection of any ocular artifact is difficult. In $\hat{s}(t)$, an ERP shape can be seen after the STOP-stimulus at t=0.5 s. This ERP shows typical characteristics associated with ERPs of stop signal tasks, namely a negative peak app. 0.2 s after the STOP-stimulus and a positive peak app. 0.3 s after the STOP-stimulus.

The power $P(r_m - \hat{f}_m)$ for these trials is indicated.

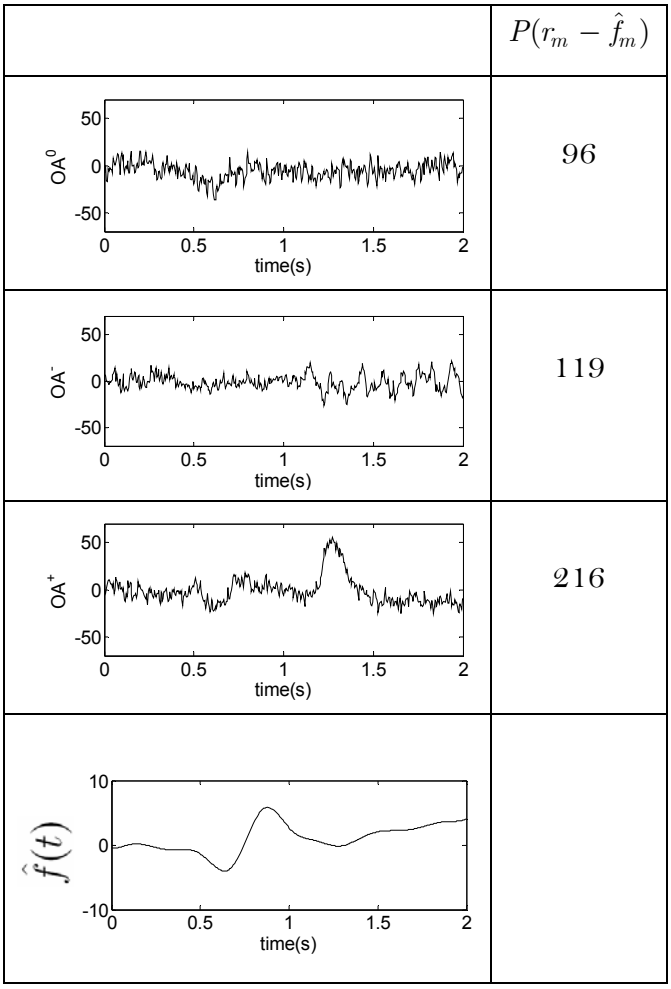

Figure 5.2: Examples of trials in the three categories, OA⁰, OA⁻, and OA⁺, with their corresponding $P(r_m - \hat{f}_m)$*. Lower plot shows the estimated, stimulus-related and trial-averaged, ERP potential* $\hat{f}(t)$*. All y-axis scalings are in μV.*

For this participant, the results averaged over multiple trials lead to $P_0 = P_{REF} = 101$, $P_- = 118$, and $P_+ = 194$ for the uncorrected data. After correction by EYE it is found that $P_0^* = 96$ $P_-^* = 117$ and $P_+^* = 102$. As expected $(P_0 < P_- < P_+)$, $\left(P_-^* < P_-\right)$, $\left(P_+^* < P_+\right)$ and $\left(P_0^* \approx P_0 \approx P_+^*\right)$. Contrary to the expectations, $\left(P_-^* \approx P_- \neq P_0\right)$, which indicates that resemblance between OA⁻ trials before and after correction is larger than the resemblance between corrected OA⁻ trials and uncorrected OA⁰ trials. Surprisingly, for the OA⁻ trials of this participant similar results were also observed when other correction methods were used. A possible explanation for this would be that the background EEG for these trials is significantly different from the background EEG of the OA⁰ trials. A visual inspection of Figure 5.2, suggests that this is a plausible explanation. This explanation contradicts the assumption

(constant $P(b_m)$) that we made for background EEG in Section 5.4. The consequences of this would be that the optimal j and J values are (slightly) above zero, and overcorrection can erroneously be overlooked. Because this unexpected result was only found in one participant, no actions are taken.

Similar calculations of trial-, and corrected trial powers are performed for all participants. The resulting *J*-scores are shown in Figure 5.3.

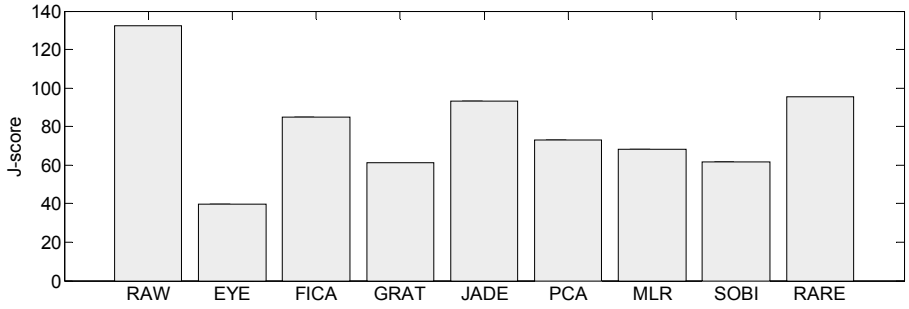

Figure 5.3: Correction accuracy determined for seven different ocular artifact correction methods. The y-axis indicates J-score, as defined in (5.8), which is a non-negative measure that is zero for optimal correction. High J-score relates to low correction accuracy.

To verify whether results on a single trial appear to be in line with the general result presented in Figure 5.3, the result of correcting three single trials is shown for all correction methods in Figure 5.4. These particular trials, prior to correction are identical to those already shown in Figure 5.2. The left column of Figure 5.4 shows $r_m(t)$ and $r_m{}^*(t)$. For all three categories of trials, the $r_m{}^*(t)$ corresponding to the different correction methods appear to be similar. Accuracy of the different correction methods apparently is hard to distinguish based on the corrected signal because the relatively high amplitude of background EEG obscures them. Therefore, the right column of Figure 5.4 shows the estimate of the ocular artifact, $r_m{}^*(t) - r_m(t)$. Differences between correction methods are visually much more apparent in this right column.

OA0

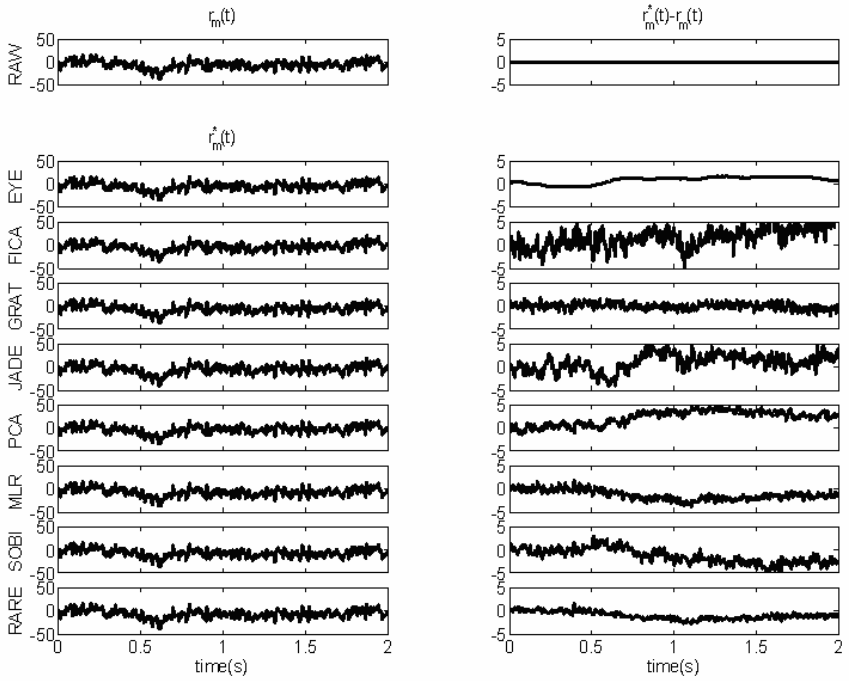
$r_m(t)$
$r_m^*(t)-r_m(t)$
$r_m^*(t)$
RAW
EYE
FICA
GRAT
JADE
PCA
MLR
SOBI
RARE
time(s)

OA-

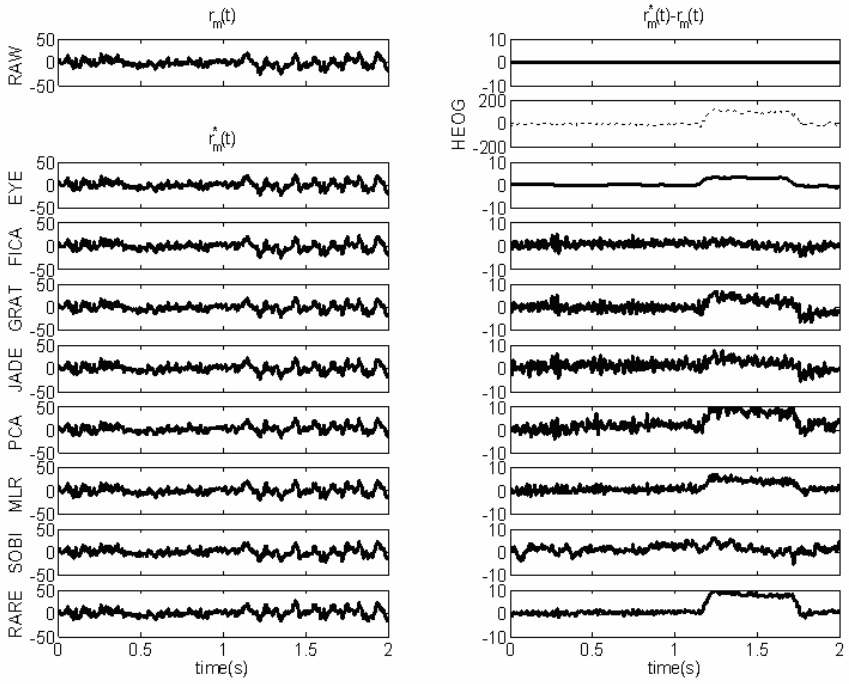
$r_m(t)$
$r_m^*(t)-r_m(t)$
$r_m^*(t)$
RAW
HEOG
EYE
FICA
GRAT
JADE
PCA
MLR
SOBI
RARE
time(s)

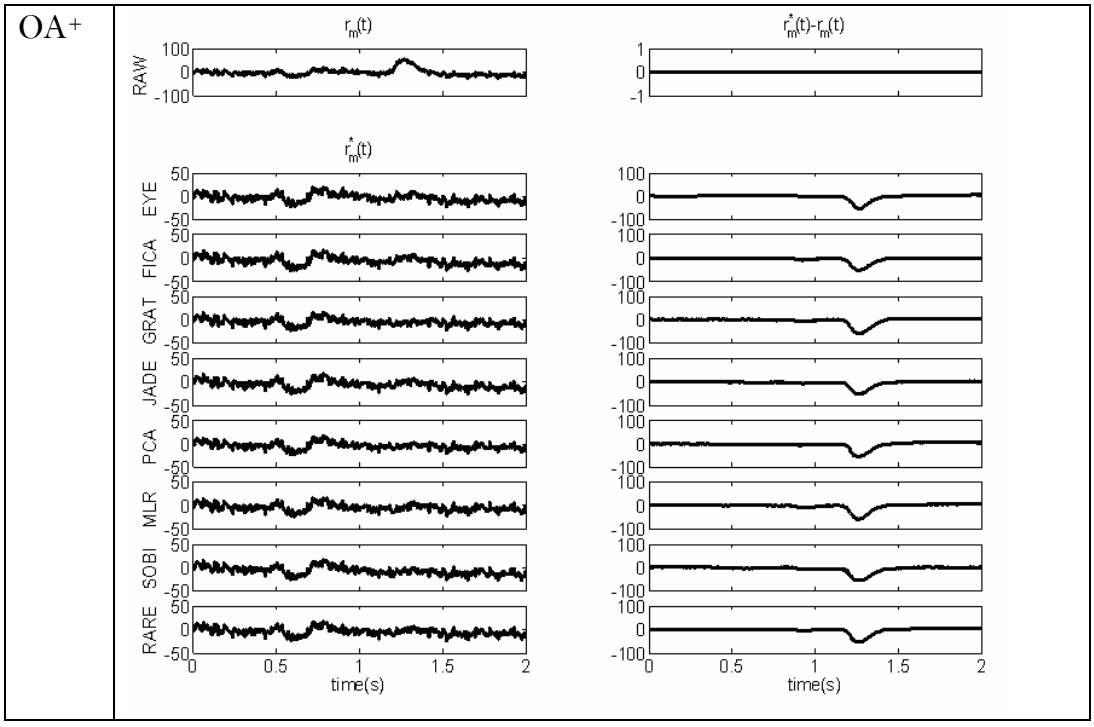

Figure 5.4: Left column: Raw and corrected data for trials with and without ocular artifacts. Right column: estimated ocular artifact. Rows correspond to different correction methods, indicated ate the left. For OA+, the HEOG is also shown. All y-axis scalings are in μV.

It can be seen that the estimated ocular artifact is, for all correction methods, largest in the OA^+, trials and smallest in the OA^0 trials, as was expected. All of the correction methods estimate some ocular artifact in all trial categories. Even for the OA^0 category, which is assumed to be free of ocular artifact, $r_m{}^*(t) - r_m(t)$ is not zero. Based on our assumptions, this implies that none of the correction methods is fully accurate.

For all correction methods except EYE, $r_m{}^*(t) - r_m(t)$ in the OA^0 category shows low amplitude, high frequency fluctuations. These fluctuations are either caused by

1. brain activity or electrode noise in EOG channels, and in the case of components-based methods, other EEG channels, or by
2. very small, high frequency, eye movements during fixation.

If these fluctuations would be mainly due to the first cause, they are not part of the ocular artifact and they should not be removed from $r_m(t)$, which would indicate in accordance with Figure 5.3 that EYE is most accurate. If the fluctuations would be mainly due to the second cause, they are artifactuous, and they should be removed, which would indicate that EYE is least accurate.

It is known that eye movements during fixation merely exhibit a slow drift and occasional micro-saccades [143], resetting the point of focus. This suggests that erroneously removed brain activity is the cause of these fluctuations and that the effect seen in Figure 5.4 is thus not of ocular origin and should not be seen as part of the ocular artifact.

Representing OA^- trials, a trial is shown during which a participant made a brief horizontal eye movement. This can be seen in the HEOG that is shown in the right column. In $r_m(t)$, the ocular artifact due to this eye movement is nearly impossible to detect, but $r_m{}^*(t) - r_m(t)$ illustrates that all correction methods detect a step-like artifact. The correction methods do not agree on the amplitude of this step-like artifact. Which of the methods estimates the artifact amplitude best, cannot be concluded based solely on this trial's corrected data. Similar to the OA^0 category, EYE is the only method that lacks high frequencies in the estimated ocular artifact.

For the OA^+ trial category, a trial with an obvious blink artifact is corrected. Again, differences between correction methods are difficult to detect in $r_m{}^*(t)$. Again, EYE is the only method that lacks high frequencies in the estimated ocular artifact, although in Figure 5.4 this is obscured by the high amplitude of the estimated blinking artifact.

5.6 Conclusions

This chapter estimates the correction accuracy of eight ocular artifact correction methods. For EEG that is recorded during a stop-signal task, it is essential that ocular artifacts are accurately corrected to be able to extract the low amplitude ERP waveforms. We therefore test for correction accuracy on trials that are recorded during a stop-signal task. The trials are categorized in three groups, based on which artifacts they contain, and subsequently corrected and evaluated. As expected, all methods succeed in removing (part of) the ocular artifacts from the data. All correction methods in Figure 5.3 have an accuracy yardstick J which is lower than the J calculated for raw data.

The overall ranking of the estimated accuracies of the eight methods, in Figure 5.3, corresponds very well with the correction accuracy of these methods on simulated data in Chapter 4. To illustrate this, Figure 5.5 shows the SNR_1 performance measure of the simulated data of Chapter 4, and the yardstick J of the experimental data of this chapter for those correction methods that are evaluated in both chapters. There is a clear correlation between the two measures.

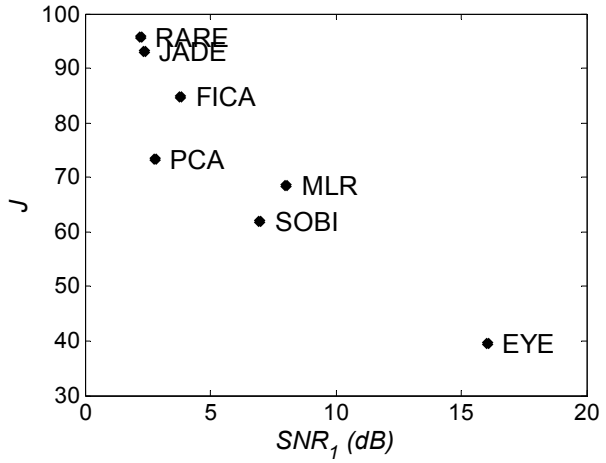

Figure 5.5: Performance measure SNR_1 and yardstick J for several correction methods. This figure combines the results shown in Figure 5.3 with the results shown in Figure 4.3 for random eye movements at a blinking rate of 0.1 blinks/s.

For raw data the first right hand-side term in (5.7) by definition equals zero, whereas for corrected data this term is only zero if these trials are not affected by correction. The improvements in J due to correction methods therefore cannot be attributed to unexpected effects in artifact free trials, but are the result of ocular artifact removal from the OA^-, and OA^+ categorized trials.

In the single-trial correction comparison, in Figure 5.4, we find that all correction methods except EYE consistently estimate an ocular artifact that contains low amplitude high frequency fluctuations. Because no high frequency eye movements are expected to occur during fixation, these fluctuations are probably due to non-ocular influences, like brain-activity or electrode noise. Thus, such fluctuations should not be removed by ocular artifact correction methods. The fact that both the EOG-based and the components-based correction methods do remove some of these fluctuations, illustrates their susceptibility to overcorrection, whereas EYE does not appear to overcorrect the data.

The EYE method again appears to be most suited for ocular artifact correction, which was expected because it is the only method that exploits the extra eye tracker recordings in the process of correction. The GRAT method that was not tested in Chapter 4, is similarly accurate as the SOBI correction method. Interestingly, the SOBI method requires multi-channel EEG recordings, whereas GRAT requires only one EEG channel but requires the use of multiple EOG electrodes and accurate trial alignment. MLR performs remarkably well considering the simplicity of merely scaling and subtracting EOGs. The result that simple EOG-based techniques can outperform ICA methods was also reported in [16;144]. The PCA correction performs better

than the ICA-based correction methods JADE and FICA in this experiment. Although this complies with results of some studies [16], this result may appear strange given the amount of attention that ICA-based methods are currently receiving. It also contradicts results of other studies [98]. However, in [98], an implementation of ICA other than JADE and FICA was used [57], and the validation of correction of ocular artifacts is based solely on a visual inspection of the extracted components. All components-based methods have the advantage that they can easily be used for a much wider range of applications than specialized ocular artifact correction methods like EYE and GRAT. They estimate ocular artifact simultaneously to a variety of other artifacts, e.g., [77], whereas EYE can only be used for this single application. Furthermore, components-based methods have also been demonstrated to be able to accurately extract task-specific EEG activity from raw EEG signals [145]. This versatility of components-based correction methods aids to their user-friendliness and will assure that they will continue to be improved further. The ICA methods that are currently widely used, and are therefore selected for evaluation here, were developed already in 1993 (JADE) and 1999 (FICA). Probably there have already been improvements to these methods that will result in improved ocular artifact correction accuracy that simply have not yet found their way to mainstream EEG-research.

Chapter 6

Conclusions, recommendations & perspectives

6.1 Conclusions and recommendations

This thesis concerns the correction of ocular artifacts in EEG recordings. To aid in estimating the accuracies of various existing correction methods, the thesis introduces a model of the human head that can simultaneously simulate eye movement artifacts, blinking artifacts and EEGs in a realistic way. This model is used in the process of validating correction methods throughout the thesis. For all these model-based validations, similar evaluations on experimental data were performed to check for inconsistencies between simulated and experimental data. The comparisons between the correction of simulated and experimental data did not reveal any significant inconsistencies and hence the model appears to incorporate the most essential elements of EEG and artifact signal generation. Despite this, model refinements are desirable to further increase agreement with reality. Potentially relevant refinements include

- the use of more accurate skull modeling, especially concerning the eyeball sockets,
- the use of a more refined mesh for the tissue boundaries, and
- providing an analytic, yet realistic, description of various eye movement patterns. This will eliminate the need for the eye tracker as a basis for simulated eye movement patterns.

Another major improvement would be the modeling of eyelid movements, using the same model as the model for eye movement modeling. Such an improvement will yield an analytic description of blink-artifact patterns and will eliminate the need for the EOG recording as a basis for blink-artifact patterns. This would require the use of a head model that allows changes in morphology over time. Considering that the boundary element method does not allow for such changes, a finite element modeling approach may be more suitable for this.

For the correction of ocular artifacts, this thesis introduces a radically new approach. Whereas previous correction methods used only the EEG and/or the EOG in order to estimate ocular artifacts, the newly introduced EYE method uses an eye tracker for this purpose, as illustrated in Figure 6.1.

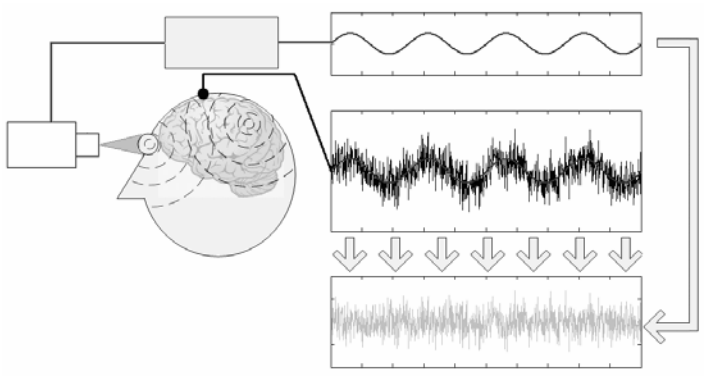

Figure 6.1: Illustration of the eye-tracker solution to the correction of ocular artifacts in the EEG, with an impression of signal morphology on the right. The eye tracker only records ocular information, which can be converted to an accurate estimate of the ocular artifact. Combined with the electrode recording which contained both EEG and artifact, an accurate estimate of the EEG is derived.

Because an eye tracker's recording simply cannot reflect electrical brain activity, traditionally troublesome issues like forward/backward propagation play no role in the EYE method.

In this thesis it is shown on simulated data, that the EYE method consistently estimates the ocular artifact more accurately than other methods.

For the EYE method, it is expected that results can be further improved by altering the assumptions concerning the structure of the EEG. In the current implementation, the procedure that is used for the tracking of parameters of the Kalman filter uses the assumption that the corrected EEG has a white spectrum. A more accurate estimate for the spectrum of the corrected EEG, implemented via a noise whitening filter, should further improve the accuracy of correction. The EYE method could also be extended to cope with unstable lighting conditions during experiments. As mentioned in Section 1.3, the difference in electrical charge between cornea and retina depends on the lighting conditions. A recording of the luminance signal by the eye tracker, can be used as an additional parameter in the estimation of ocular artifacts.

Next to this methodological improvement, some practical improvements related to the eye tracker will also result in better correction accuracy, namely

- the use of an eye tracker with a higher sampling rate (e.g. 256 Hz), will give more accurate estimates for fast saccadic movements,

- the development and use of different eye tracker software to provide information on pupil position in a recorded image,
- the use of a head mounted eye tracker to eliminate the effects of head movements in the detection of pupil position. For this improvement, it is required that the head mounted eye tracker does not interfere (either mechanically or electronically) with the EEG recording. Placing a light weight eye tracker on the frame of a pair of glasses could be an elegant solution to this.

One remaining disadvantage, even if all the suggestions above are implemented and an advanced eye tracker would be used, is the fact that the pupil position cannot be detected by the eye tracker when the eyelids are closed. During a blink this causes a brief interruption in the pupil position detection. This problem could be countered by using an estimated small shift in pupil position that is known to occur during blinking. More seriously, the inability to record pupil position when the eyes are closed disqualifies the use of the EYE method in combination with eye tracker recordings for EEG recordings that are taken while the eyes remain closed. A possible alternative in this situation could be the use of the EYE method with magnets or magnetic coils. Magnets attached to eyeball and eyelid can be used to obtain information on pupil and eyelid position that is essentially the same as the information as provided by an eye tracker. However, even when the eyes are closed separate information on eyeball and eyelid movement can be obtained by monitoring the magnetic field surrounding these magnets.

For some applications the consequences of (slightly) lower accuracy, of rejecting data with ocular artifacts, and even of not correcting data will be tolerable, and an eye tracker will be considered merely as an extra burden in the recording setup. In contrast, many modern EEG-based applications require highly accurate correction. For such challenging applications, it is demonstrated on experimental data regarding response inhibition, that the accuracy of correction is highest when an eye tracker and the EYE correction method are used.

6.2 Perspectives

When in the near future more and more EEG-based applications are improved and newly introduced, it is to be expected that many of these application will depend (even more than today) on a highly accurate separation of the electrical effects of brain activity from other electrical activities.

A good example of an already existing application is the brain computer interface. With such an interface, the brain of a person is linked to a computer in order to control computer driven processes. Some of these brain computer

interfaces attempt to 'read' the brain's natural processes e.g., involved in decision making or motor control. They use information on these processes to control the computer. As these (often subtle) processes are obscured by other brain processes that occur simultaneously, one major challenge still is to accurately extract the relevant process from the background EEG. It will evidently be essential that no *other* factors, like ocular artifacts, further complicate this process. Ultimately, real-time operation in which a single thought is enough to control the computer process may be the goal of future experiments.

If all requirements for an ocular artifact correction method would be listed, the following two requirements will probably be most important:

- Accuracy,
  as it is clearly essential that "the corrected EEG is the correct EEG".
- Usability,
  as the method used to correct for ocular artifacts should not impose serious limitations to the environment in which the EEG is recorded and should not be time consuming in that it requires lengthy installment and calibration of equipment or lengthy calibration trials.

In addition to these requirements it is also essential that there is a 'need for correction'. Section 1.5 showed that for some studies the simplest solutions (artifact rejection) are often preferred if accurate correction is not considered to be essential. The need for correction is beyond the focus of the correction method itself, but is likely to increase with future applications such as the brain computer interfaces described above.

The accuracy of EYE was shown in this thesis to be already superior to the accuracy of several frequently used other correction methods, and can be improved even further with the suggestions given in Section 6.1. The usability of the EYE method currently is limited. Adding an eye tracker in an experimental protocol, synchronizing eye tracker recordings with EEG recordings, and time consuming calibration of the eye tracker are all undesirable features in an optimal correction method.

The development of easy-to-use hardware, such as an eye tracker mounted on a pair of glasses as suggested in Chapter 4, as well as the development of advanced (supporting) software for synchronization and eyelid position detection, will be needed, but seems all together feasible. Thus the EYE method that is proposed in this thesis could further develop to meet the accuracy and usability requirements, and hence be a good starting point in the search for the ultimate correction method.

Appendix A

Eye tracker recordings

The eye tracking system that is used throughout this thesis is video-based. It consists of a camera, an infra-red light source, and accompanying image processing software.

The camera focuses on one of the eyes and records its orientation as the observed person is observing a screen or a monitor which is placed in front of him. In Figure A.1 this is illustrated for a remote eye tracking device, where the camera is not attached to the subject and placed at a distance of approximately one meter. The chin of the participant is supported during the experiments to reduce head movements. Other eye tracking devices can be head-mounted, which means that they are attached to the head, e.g., by means of a helmet, and that they move whenever the head moves.

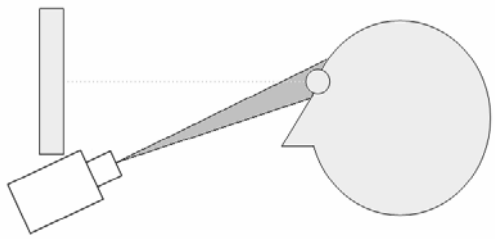

Figure A.1: Illustration of the positioning of screen, eye tracker, and participant during experiments.

The camera records images that are subsequently analyzed by image processing software. A brightness threshold is employed to detect the darkest area in these images. This threshold is adjusted manually until the darkest area coincides with the pupil of the eye. Next, the center of the darkest area is determined, which represents the center of the pupil, as is illustrated in Figure A.2.

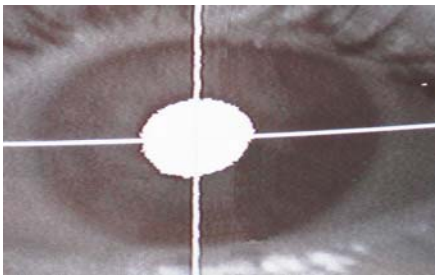

Figure A.2: Example of the image as recorded by the eye tracker. The white circular shape in the center corresponds to all points below the brightness threshold; the cross marks the center of this shape.

The coordinates of the center-point are usually expressed on a pixel-based scale which depends on the resolution of the camera. A calibration protocol is employed to determine how these pixel-values can be related to the position of a marker on the screen, expressed in m.

Typical parameters that can be determined from the image in real-time are

- the horizontal position of the pupil, $p_1(t)$,
- the vertical position of the pupil, $p_2(t)$, and
- the diameter of the pupil, $d_p(t)$, expressed in arbitrary units.

To illustrate the changes in these three parameters during eye movement, Figure A.3 illustrates these parameters when recorded during a visual tracking task. The participant was asked to focus his eyes on a dot that followed a circular path on the screen. Light intensity in the room remained constant throughout this experiment.

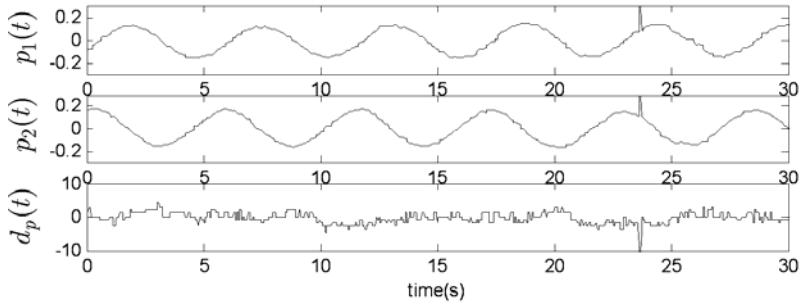

Figure A.3: Eye tracker data recorded during a 30 s visual tracking task.

Note that the 'spike' in Figure A.3 that occurs in all three parameters after approximately 23 s is caused by blinking.

Appendix B

Methodological backgrounds to Section 1.5

Appendix B1 (MLR)

Equation (1.2) can be used to obtain

$$\begin{aligned} \underline{n}^T\underline{n} &= \left(\underline{y} - \alpha \cdot \underline{x}\right)^T \left(\underline{y} - \alpha \cdot \underline{x}\right) \\ &= \underline{y}^T\underline{y} + \alpha^2 \cdot \underline{x}^T\underline{x} - 2\alpha \cdot \underline{x}^T\underline{y} \; . \end{aligned} \tag{B.1}$$

Regression assumes that vector $\underline{n}$ is zero mean, white, of normal distribution, and independent of $\underline{x}$. Now $\hat{\alpha}$ is the estimate for α that minimizes the noise sum of squares as given by (B.1). This leads to

$$\hat{\alpha} = \left(\underline{x}^T\underline{x}\right)^{-1} \left(\underline{x}^T\underline{y}\right). \tag{B.2}$$

By using $\hat{\alpha}$, it is now possible to estimate $\underline{n}$ according to

$$\hat{\underline{n}} = \underline{y} - \hat{\alpha} \cdot \underline{x}. \tag{B.3}$$

Similarly for MLR it is found that

$$\hat{\underline{\alpha}} = \left(\underline{\underline{X}}^T\underline{\underline{X}}\right)^{-1} \left(\underline{\underline{X}}^T\underline{y}\right). \tag{B.4}$$

Appendix B2 (PCA)

Assume for now that a blinking artifact is recorded at all electrodes, and at the same time there is no prominent other electrical activity at any of the N electrodes. In matrix $\underline{\underline{Y}}$, all columns contain some information on the changes in electric potential due to this blinking. If PCA is successful in identifying the exact blinking artifact as a single component $\underline{z}_n$, then just this one component together with its corresponding row in $\underline{\underline{W}}_{\mathrm{PCA}}$ captures all information on the artifact. In effect this reduces the dimensionality of the system from N to one.

PCA first estimates the covariance between different electrodes. With N electrodes this results in a covariance matrix

$$\underline{\underline{\Sigma}}_Y = \frac{1}{T}\underline{\underline{Y}}^T\underline{\underline{Y}}. \tag{B.5}$$

Because the ocular artifacts are detected at all electrodes, all elements in matrix $\underline{\underline{\Sigma}}_Y$ tend to be non-zero. If all information on the artifacts is isolated in one column, $\underline{z}_n$, of $\underline{\underline{Z}}$, then calculating a similar matrix

$$\underline{\underline{\Sigma}}_Z = \frac{1}{T}\underline{\underline{Z}}^T\underline{\underline{Z}}, \tag{B.6}$$

will only have a non-zero variance for the element in $\underline{\underline{C}}_Z$ which corresponds to $\underline{z}_n{}^T \underline{z}_n$. All other elements, reflecting $\underline{z}_{...}{}^T \underline{z}_{...}$, are approximately equal to zero.

By combining (1.9), (B.5) and (B.6) it follows that

$$\underline{\underline{\Sigma}}_Z = \underline{\underline{W}}_{PCA}{}^{-1} \underline{\underline{\Sigma}}_Y \underline{\underline{W}}_{PCA}{}^{-1^T}, \qquad \text{(B.7)}$$

and thus matrix $\underline{\underline{W}}_{\text{PCA}}{}^{-1}$ should transform a fully filled matrix $\underline{\underline{\Sigma}}_Y$ into a diagonal matrix $\underline{\underline{\Sigma}}_Z$.

Note now that this also holds for situations with more than one electrically active source. Assuming that their electrical activities are uncorrelated, PCA can identify them by simply minimizing covariances.

Because $\underline{\underline{\Sigma}}_Y$ is symmetric, an orthogonal matrix $\underline{\underline{W}}_{\text{PCA}}$ that can perform the diagonalization as described in (B.7) exists [146] (Theorem 5.8). Two specific properties of such an orthogonal transformation are that $\underline{\underline{W}}_{\text{PCA}}{}^T = \underline{\underline{W}}_{\text{PCA}}{}^{-1}$, and that the Eigen values of matrix $\underline{\underline{\Sigma}}_Y$ appear, ordered in magnitude, on the diagonal of matrix $\underline{\underline{\Sigma}}_Z$. After $\underline{\underline{W}}_{\text{PCA}}$ is determined, the principal components matrix $\underline{\underline{Z}}_{\text{PCA}}$ follows from (1.9).

Other implementations

In (B.5), matrix $\underline{\underline{\Sigma}}_Y$ is taken as a starting point for deriving the principal components. This matrix contains the covariances of vectors $\underline{y}_1$, $\underline{y}_{..}$, $\underline{y}_N$.

Instead of using covariances between different electrodes when determining $\underline{\underline{\Sigma}}_Y$ as in (B.5), it is also possible to use covariances between different samples, based on $\underline{\underline{Y}}\underline{\underline{Y}}^T$ instead of $\underline{\underline{Y}}^T\underline{\underline{Y}}$. This way the main assumption is no longer that different components have uncorrelated time-series (temporal-PCA), but that different components have uncorrelated scalp topographies (spatial-PCA). A more thorough description about differences between these two implementations can be found e.g., in [147]. Instead of using covariances, matrix $\underline{\underline{\Sigma}}_Y$ can be replaced by a correlation matrix. This alternative implementation also results in uncorrelated components [117].

Appendix B3 (sphering)

It is easy to demonstrate how the orthogonal components can be converted to orthonormal components. Note that (1.9) does not strictly define the magnitudes of $\underline{\underline{Z}}$ and $\underline{\underline{W}}$ because a scaling matrix $\underline{\underline{A}}$ can change them both as

$$\begin{aligned} \underline{\underline{Z}}^T &= \underline{\underline{W}}^{-1} \cdot \underline{\underline{Y}}^T \\ \underline{\underline{A}}\,\underline{\underline{Z}}^T &= \underline{\underline{A}}\,\underline{\underline{W}}^{-1} \cdot \underline{\underline{Y}}^T, \end{aligned} \qquad \text{(B.8)}$$

with $\underline{\underline{A}}$ being a full rank matrix (NxN). Determining covariances similar to (B.6) leads to

$$\underline{\underline{\Sigma}}_{AZ} = \frac{1}{T}\underline{\underline{A}}\,\underline{\underline{Z}}^T\underline{\underline{Z}}\,\underline{\underline{A}}^T = \underline{\underline{A}}\,\underline{\underline{\Sigma}}_Z\,\underline{\underline{A}}^T. \qquad \text{(B.9)}$$

Because $\underline{\underline{\Sigma}}_Z$ is diagonal with Eigen values $\lambda_1, \lambda_2, .., \lambda_N$ on the diagonal, it follows that when $\underline{\underline{A}}$ is a diagonal matrix with $\frac{1}{\sqrt{\lambda_1}}, \frac{1}{\sqrt{\lambda_2}}, \ldots, \frac{1}{\sqrt{\lambda_N}}$ on its diagonal, matrix $\underline{\underline{\Sigma}}_{AZ}$ equals $\underline{\underline{I}}$.

Appendix B4 (SOBI)

The matrix $\underline{\underline{Y}}$ is transformed using PCA and sphering. This leads to the component-space of PCA, $\underline{\underline{Z}}_{\mathrm{PCA}_2}$, defined as

$$\underline{\underline{Z}}_{\mathrm{PCA}_2} = \left(\underline{\underline{W}}_{\mathrm{PCA}_2}{}^{-1} \cdot \underline{\underline{Y}}^T\right)^T. \qquad \text{(B.10)}$$

The next steps will use $\underline{\underline{Z}}_{\mathrm{PCA}_2}$ as a starting point for finding $\underline{\underline{Z}}_S$.

In effect SOBI thus performs a new components analysis to the components that were obtained by PCA. A new mixing matrix $\underline{\underline{W}}_{S2}$ is derived in this extra components analysis,

$$\underline{\underline{Z}}_S{}^T = \underline{\underline{W}}_{S2}{}^{-1} \cdot \underline{\underline{Z}}_{\mathrm{PCA}_2}{}^T = \underline{\underline{W}}_{S2}{}^{-1} \cdot \left(\underline{\underline{W}}_{\mathrm{PCA}_2}{}^{-1} \cdot \underline{\underline{Y}}^T\right). \qquad \text{(B.11)}$$

The full mixing matrix $\underline{\underline{W}}_S$ which is required to relate $\underline{\underline{Z}}_S$ directly to $\underline{\underline{Y}}$ is defined as

$$\underline{\underline{W}}_S = \left(\underline{\underline{W}}_{S2}{}^{-1} \cdot \underline{\underline{W}}_{\mathrm{PCA}_2}{}^{-1}\right)^{-1} = \underline{\underline{W}}_{\mathrm{PCA}_2} \cdot \underline{\underline{W}}_{S2} \qquad \text{(B.12)}$$

When shifting all rows of a matrix, e.g., $\underline{\underline{Z}}$, the notation $(\underline{\underline{Z}})_\tau$ will be used to reflect the fact that all components in this matrix are delayed in time. By combining (1.13) and (1.14), a time shifted covariance matrix of SOBI components $\underline{\underline{\Sigma}}_{Z_S}(\tau)$ is found,

$$\underline{\underline{\Sigma}}_{Z_S}(\tau) = \frac{1}{T}\underline{\underline{Z}}_S{}^T\left(\underline{\underline{Z}}_S\right)_\tau = \begin{bmatrix} \rho_1(\tau) & 0 & 0 & 0 \\ 0 & \rho_2(\tau) & 0 & 0 \\ 0 & 0 & ... & 0 \\ 0 & 0 & 0 & \rho_N(\tau) \end{bmatrix}. \qquad \text{(B.13)}$$

Similar to (B.7), there exists some diagonalization operation for the delayed covariance matrix that transforms $\underline{\underline{\Sigma}}_{Z_{PCA2}}(\tau)$ to $\underline{\underline{\Sigma}}_{Z_S}(\tau)$,

$$\underline{\underline{\Sigma}}_{Z_S}(\tau) = \underline{\underline{W}}_{S2}\ \underline{\underline{\Sigma}}_{Z_{PCA2}}(\tau)\ \underline{\underline{W}}_{S2}{}^T. \qquad \text{(B.14)}$$

Clearly, different delays will result in different matrices $\underline{\underline{\Sigma}}_{Z_{PCA2}}(\tau)$ and $\underline{\underline{\Sigma}}_{Z_S}(\tau)$.

SOBI determines one mixing matrix $\underline{\underline{W}}_{S2}$ which optimizes the joint diagonalization of all matrices $\underline{\underline{\Sigma}}_{Z_S}(\tau)$ that are obtained at different delays. Matrix $\underline{\underline{W}}_{S2}$ is obtained by minimizing the sum of all off-diagonal elements

over all matrices $\underline{\underline{\Sigma}}_{Z_S}(\tau)$. A way to iteratively estimate this minimum, and find the jointly diagonalizing matrix $\underline{\underline{W}}_{S2}$ is given in [51].

Bibliography

[1] H. Berger, "Uber das elektrenkephalogramm des menschen", *Archif fur psychiatrie*, vol. 87 pp. 527-570, 1929.

[2] P. E. Voorhoeve, *Leerboek der neurofysiologie*, Amsterdam: Elsevier, 1984.

[3] R. J. Barry, S. J. Johnstone, and A. R. Clarke, "A review of electrophysiology in attention-deficit/hyperactivity disorder: II. Event-related potentials", *Clinical Neurophysiology*, vol. 114, no. 2, pp. 184-198, 2003.

[4] J. Duff, "The usefulness of quantitative EEG (QEEG) and neurotherapy in the assessment and treatment of post-concussion syndrome", *Clinical Eeg and Neuroscience*, vol. 35, no. 4, pp. 198-209, 2004.

[5] O. E. Mendez and R. P. Brenner, "Increasing the yield of EEG", *Journal of clinical neurophysiology*, vol. 23, no. 4, pp. 282-293, 2006.

[6] E. J. Novotny, "The role of clinical neurophysiology in the management of epilepsy", *Journal of clinical neurophysiology*, vol. 15, no. 2, pp. 96-108, 1998.

[7] T. Ebrahimi, J. M. Vesin, and G. Garcia, "Brain-computer interface in multimedia communication", *IEEE Sig.Proc.Mag.*, vol. 20, no. 1, pp. 14-24, 2003.

[8] R. J. Croft and R. J. Barry, "Removal of ocular artifact from the EEG: a review", *Neurophysiologie clinique*, vol. 30, no. 1, pp. 5-19, 2000.

[9] I. I. Goncharova, D. J. McFarland, T. M. Vaughan, and J. R. Wolpaw, "EMG contamination of EEG: spectral and topographical characteristics", *Clinical Neurophysiology*, vol. 114 pp. 1580-1593, 2003.

[10] J. P. Lanquart, M. Dumont, and P. Linkowski, "QRS artifact elimination on full night sleep EEG", *Medical Engineering & Physics*, vol. 28, no. 2, pp. 156-165, 2006.

[11] P. C. Lo and J. S. Leu, "Adaptive baseline correction of meditation EEG", *American Journal of Electroneurodiagnostic Technology*, vol. 41, no. 2, pp. 142-155, 2001.

[12] M. v. d. Velde, *Signal validation in electroencephalography research*, PhD Thesis, Eindhoven University of Technology, Eindhoven: Universiteitsdrukkerij TUE, 2000.

[13] R. J. M. Somsen and B. van Beek, "Ocular artifacts in children's EEG: selection is better than correction", *Biological Psychology*, vol. 48, no. 3, pp. 281-300, 1998.

[14] J. Malmivuo and R. Plonsey, *Bioelectromagnetism : principles and applications of bioelectric and biomagnetic fields*, New York, N.Y., Oxford University Press, 1995.

[15] L. C. Parra, C. D. Spence, A. D. Gerson, and P. Sajda, "Recipes for the linear analysis of EEG", *Neuroimage*, vol. 28, no. 2, pp. 326-341, 2005.

[16] G. L. Wallstrom, R. E. Kass, A. Miller, J. F. Cohn, and N. A. Fox, "Automatic correction of ocular artifacts in the EEG: a comparison of regression-based and component-based methods", *Int.J.Psychophysiol.*, vol. 53, no. 2, pp. 105-119, July 2004.

[17] L. Vigon, M. R. Saatchi, J. E. W. Mayhew, and R. Fernandes, "Quantitative evaluation of techniques for ocular artefact filtering of EEG waveforms", *IEE proceedings Science, Measurement and Technology*, vol. 147, no. 5, pp. 219-228, 2000.

[18] P. Olejniczak, "Neurophysiologic Basis of EEG", *Journal of clinical neurophysiology*, vol. 23, no. 3, pp. 186-189, 2006.

[19] P. L. Nunez and R. D. Katznelson, *Electric fields of the brain : the neurophysics of EEG*, New York: Oxford University Press, 1981.

[20] W. Barry and G. M. Jones, "Influence of eye lid movement upon electro-oculographic recording of vertical eye movement", *Aerospace medicine*, pp. 855-858, 1965.

[21] M. Iwasaki, C. Kellinghaus, A. V. Alexopoulos, R. C. Burgess, A. N. Kumar, Y. H. Han, H. O. Luders, and R. J. Leigh, "Effects of eyelid closure, blinks, and eye movements on the electroencephalogram", *Clinical Neurophysiology*, vol. 116, no. 4, pp. 878-885, 2005.

[22] B. W. Jervis, E. C. Ifeachor, and E. M. Allen, "The removal of ocular artifacts from the electroencephalogram - a review", *Medical & biological engineering & computing*, vol. 26, no. 1, pp. 2-12, 1988.

[23] E. Marg, "Development of electro-oculography", *A.M.A.Archives of opthalmology*, vol. 45 pp. 169-185, 1951.

[24] J. D. Bronzino, *The biomedical engineering handbook*, London: CRC Press, 1995.

[25] D. Regan, *Human brain electrophysiology : evoked potentials and evoked magnetic fields in science and medicine*, Amsterdam: Elsevier, 1989.

[26] H. Jasper, "The ten twenty electrode system of the international federation", *Electroencephalography and Clinical Neurophysiology*, vol. 10 pp. 371-375, 1958.

[27] G. E. Chatrian, E. Lettich, and P. L. Nelson, "Ten percent electrode system for topographic studies of spontaneous and evoked EEG activities", *American journal of EEG technology*, vol. 25 pp. 83-92, 1985.

[28] R. Oostenveld and P. Praamstra, "The five percent electrode system for high-resolution EEG and ERP measurements", *Clinical Neurophysiology*, vol. 112, no. 4, pp. 713-719, Apr. 2001.

[29] S. L. G. Andino, R. D. P. Marqui, P. A. V. Sosa, R. B. Lirio, C. Machado, G. Diaz, P. F. Rodriguez, and C. C. Torrez, "Brain electrical-field measurements unaffected by linked earlobes reference", *Electroencephalography and Clinical Neurophysiology*, vol. 75, no. 3, pp. 155-160, 1990.

[30] S. L. G. Andino, "Is a linked ears reference adequate for topographic eeg analysis - reply", *Electroencephalography and Clinical Neurophysiology*, vol. 76, no. 4, pp. 374-375, 1990.

[31] E. Rodin, "Is a linked ears reference adequate for topographic eeg analysis", *Electroencephalography and Clinical Neurophysiology*, vol. 76, no. 4, pp. 373-374, 1990.

[32] C. Joyce and B. Rossion, "The face-sensitive N170 and VPP components manifest the same brain processes: The effect of reference electrode site", *Clinical Neurophysiology*, vol. 116, no. 11, pp. 2613-2631, 2005.

[33] S. Vanhatalo, J. Voipio, and K. Kaila, "Full-band EEG (FbEEG): an emerging standard in electroencephalography", *Clinical Neurophysiology*, vol. 116, no. 1, pp. 1-8, 2005.

[34] J. E. Desmedt, *Attention, voluntary contraction and event-related cerebral potentials*, Karger, 1977.

[35] G. Gratton, M. G. H. Coles, and E. Donchin, "A new method for off-line removal of ocular artifact", *Electroencephalography and Clinical Neurophysiology*, vol. 55 pp. 468-484, 1983.

[36] I. T. Jolliffe and I. NetLibrary, *Principal component analysis [electronic resource]*, New York: Springer, 2002.

[37] C. Jutten and J. Herault, "Blind separation of sources .1. An adaptive algorithm based on neuromimetic architecture", *Signal Processing*, vol. 24, no. 1, pp. 1-10, 1991.

[38] C. H. M. Brunia, J. Mocks, M. M. C. van den Berg-Lenssen, M. Coelho, M. G. H. Coles, T. Elbert, T. Gasser, G. Gratton, E. C. Ifeachor, B. W. Jervis, W. Lutzenberger, L. Sroka, A. W. van Blokland Vogelesang, G. Van Driel, J. C. Woestenburg, P. Berg, W. C. McCallum, P. D. Tuan, P. V. Popock, and W. T. Roth, "Correcting ocular artifacts in the EEG: a comparison of several methods", *Journal of psychophysiology*, vol. 3 pp. 1-50, 1989.

[39] E. C. Ifeachor, B. W. Jervis, E. M. Allen, E. L. Morris, D. E. Wright, and N. R. Hudson, "Investigation and Comparison of some models for removing ocular artefacts from EEG signals", *Medical & biological engineering & computing*, vol. 26 pp. 584-590, 1988.

[40] T. Elbert, W. Lutzenberger, B. Rochstroh, and N. Birbaumer, "Removal of Ocular artifacts from the EEG - A biophysical approach to the EOG", *Electroencephalography and Clinical Neurophysiology*, vol. 60 pp. 455-463, 1985.

[41] V. Hakkinen, K. Hirvonen, J. Hasan, M. Kataja, A. Varri, P. Loula, and H. Eskola, "The effect of small differences in electrode position on eog signals - application to vigilance studies", *Electroencephalography and Clinical Neurophysiology*, vol. 86, no. 4, pp. 294-300, 1993.

[42] R. J. Croft and R. J. Barry, "EOG correction of blinks with saccade coefficients: a test and revision of the aligned-artefact average solution", *Clinical Neurophysiology*, vol. 111, no. 3, pp. 444-451, 2000.

[43] G. Barrett, "Correcting ocular artefact in electrophysiological data: new approaches to old problems", *Journal of psychophysiology*, vol. 14, no. 4, pp. 203, 2000.

[44] R. J. Croft and R. J. Barry, "Issues relating to the subtraction phase in EOG artefact correction of the EEG", *Int.J.Psychophysiol.*, vol. 44, no. 3, pp. 187-195, 2002.

[45] D. A. Pierce, "Testing normality in autoregressive models", *Biometrika*, vol. 72, no. 2, pp. 293-297, 1985.

[46] M. M. C. van den Berg-Lenssen, C. H. M. Brunia, and J. A. Blom, "Correction of ocular artifacts in EEGs using an autoregressive model to describe the EEG; a pilot study", *Electroencephalography and Clinical Neurophysiology*, vol. 73 pp. 72-83, 1989.

[47] L. H. Zetterberg, "A mathematical model for analysis of eeg", *Electroencephalography and Clinical Neurophysiology*, vol. 26, no. 3, pp. 338-&, 1969.

[48] M. M. C. van den Berg-Lenssen, J. A. M. van Gisbergen, and B. W. Jervis, "Comparison of two methods for correcting ocular artefacts in EEGs", *Medical & biological engineering & computing*, vol. 32 pp. 501-511, 1994.

[49] G. Gratton, "Dealing with artifacts: the EOG contamination of the event-related brain potential", *Behavior Research Methods, instruments & computers*, vol. 30, no. 1, pp. 44-53, 1998.

[50] R. J. Croft, J. S. Chandler, R. J. Barry, N. R. Cooper, and A. R. Clarke, "EOG correction: A comparison of four methods", *Psychophysiology*, vol. 42, no. 1, pp. 16-24, 2005.

[51] A. Belouchrani, K. Abed-Meraim, J. F. Cardoso, and E. Moulines, "A blind source separation technique using second order statistics", *IEEE Transactions on Signal Processing*, vol. 45, no. 2, pp. 434-444, 1997.

[52] A. C. Tang, J. Y. Liu, and M. T. Sutherland, "Recovery of correlated neuronal sources from EEG: The good and bad ways of using SOBI", *Neuroimage*, vol. 28, no. 2, pp. 507-519, 2005.

[53] C. Bauer, *Independent Component Analysis of Biomedical Signals. Modern Data Analysis Techniques Can Assist Medical Decision Making*, PhD Thesis, Regensburg University, Regensburg: Logos Verlag Berlin, 2001, pp. 1-224.

[54] S. Amari, A. Cichocki, and H. H. Yang, "A new learning algorithm for blind signal separation", *Advances in neural information processing systems*, vol. 8 pp. 757-763, 1996.

[55] S. Amari, A. Cichocki and H. H. Yang. "Recurrent neural networks for blind separation of sources", *Proc. Int. Symp. Nonlinear Theory and its Applications, NOLTA-95*, 37-42. 1995.

[56] A. K. Barros, A. Cichocki and N. Ohnishi, "Extraction of statistically dependent sources with temporal structure", *Proc.of the VI Brazilian Symp.on Neural Networks, SBRN '00*, 61-65. 2000.

[57] A. J. Bell and T. J. Sejnowski, "An information-maximization approach to blind separation and blind deconvolution", *Neural computation*, vol. 7 pp. 1129-1159, 1995.

[58] T. Blaschke and L. Wiskott. "An improved cumulant based method for independent component analysis", *ICANN2002*. 2002.

[59] J. F. Cardoso and A. Souloumiac, "Blind beamforming for non-Gaussian signals", *IEE Proceedings F radar and signal processing*, vol. 140, no. 6, pp. 362-370, 1993.

[60] J. F. Cardoso, "Multidimensional independent component analysis", *Acoustics, Speech, and Signal Processing, 1998.ICASSP '98.Proceedings of the 1998 IEEE International Conference on*, 1941-1944. 1998.

[61] J. F. Cardoso, "High-order contrasts for independent component analysis", *Neural computation*, vol. 11, no. 1, pp. 157-192, 1999.

[62] P. Comon, "Independent Component Analysis, A new concept?", *Signal Processing*, vol. 36 pp. 287-314, 1994.

[63] D. Erdogmus, K. E. Hild, and J. C. Principe, "Blind source separation using Renyi's α-marginal entropies", *neurocomputing*, vol. 49 pp. 25-38, 2002.

[64] A. Hyvarinen and E. Oja, "A fast fixed-point algorithm for independent component analysis", *Neural computation*, vol. 9 pp. 1483-1492, 1997.

[65] A. Hyvarinen, "Fast and robust fixed point algorithms for independent component analysis", *IEEE Transactions on Neural Networks*, vol. 10, no. 3, pp. 626-634, 1999.

[66] Y. Inouye and K. Hirano, "Cumulant-based blind identification of linear multi-input-multi-output systems driven by colored inputs", *IEEE Transactions on Signal Processing*, vol. 45, no. 6, pp. 1543-1552, 1997.

[67] T. P. Jung, C. Humphries, T. W. Lee, S. Makeig, M. J. McKeown, V. Iragui, and T. J. Sejnowski, "Extended ICA removes artifacts from Electroencephalographic recordings", *Advances in neural information processing systems*, vol. 10 pp. 894–900, 1998.

[68] E. G. Miller and J. W. Fisher III. "Independent component analysis by direct entropy minimization", *UCB/CSD-03-1221*, 1-25. 2003. University of California at Berkeley.

[69] A. Ziehe, P. Laskov, G. Nolte, and K.-R. Muller, "A fast algorithm for joint diagonalization with non-orthogonal transformations and its application to blind source separation", *journal of machine learning research*, vol. 5 pp. 777-800, 2004.

[70] J. Anemuller, T. J. Sejnowski, and S. Makeig, "Complex independent component analysis of frequency-domain electroencephalographic data", *Neural networks*, vol. 16, no. Special issue, pp. 1311-1323, 2003.

[71] G. D. Brown, S. Yamada, and T. J. Sejnowski, "Independent component analysis at the neural cocktail party", *Trends in Neurosciences*, vol. 24, no. 1, pp. 54-63, 2001.

[72] I. F. Gorodnitsky and A. Belouchrani, "Joint cumulant and correlation based signal separation with application to EEG data analysis", *Third International Conference on Independent Component Analysis and Signal Processing*. 2001.

[73] C. A. Joyce, I. F. Gorodnitsky, and M. Kutas, "Automatic removal of eye movement and blink artifacts from EEG data using blind component separation", *Psychophysiology*, vol. 41, no. 2, pp. 313-325, 2004.

[74] T. P. Jung, S. Makeig, C. Humphries, T. W. Lee, M. J. McKeown, V. Iragui, and T. J. Sejnowski, "Removing electroencephalographic artifacts by blind source separation", *Psychophysiology*, vol. 37, no. 2, pp. 163-178, 2000.

[75] S. Makeig, A. J. Bell, T. P. Jung, and T. J. Sejnowski, "Independent Component Analysis of Electroencephalographic Data", *Advances in neural information processing systems*, vol. 8 1996.

[76] A. C. Tang, B. Pearlmutter, D. B. Phung, and S. A. Carter, "Independent Components of magnetoencephalography, Part I: Localization", *Neural computation*, vol. 14, no. 8, pp. 1827-1858, 2002.

[77] S. Tong, A. Bezerianos, J. Paul, Y. Zhu, and N. Thakor, "Removal of ECG interference from the EEG recordings in small animals using independent component analysis", *Journal of neuroscience methods*, vol. 108, no. 1, pp. 11-17, July 2001.

[78] R. N. Vigario, "Extraction of ocular artefacts from EEG using independent component analysis", *Electroencephalography and Clinical Neurophysiology*, vol. 103, no. 3, pp. 395-404, 1997.

[79] L. Zhukov, D. Weinstein, and C. Johnson, "Independent component analysis for EEG source localization", *IEEE Engineering in Medicine and Biology Magazine*, vol. 19, no. 3, pp. 87-96, 2000.

[80] A. Hyvärinen, J. Karhunen, and E. Oja, *Independent component analysis*, New York: Wiley, 2001.

[81] L. Mattner, "What are cumulants?", *Documenta Mathematica*, vol. 4 pp. 601-622, 1999.

[82] N. P. Castellanos and V. A. Makarov, "Recovering EEG brain signals: Artifact suppression with wavelet enhanced independent component analysis", *Journal of neuroscience methods*, vol. 158, no. 2, pp. 300-312, 2006.

[83] R. Q. Quiroga, "Obtaining single stimulus evoked potentials with wavelet denoising", *Physica D-Nonlinear Phenomena*, vol. 145, no. 3-4, pp. 278-292, 2000.

[84] T. Zikov, S. Bibian, G. A. Dumont and M. Huzmezan, "A wavelet based de-noising technique for ocular atrifact correction of the electroencephalogram", *24th international conference of the IEEE Engineering in medicine and biology society, Huston, Texas.* 2002.

[85] A. Kandaswamy, V. Krishnaveni, S. Jayaraman, N. Malmurugan, and K. Ramadoss, "Removal of ocular artifacts from EEG - A survey", *Iete Journal of Research*, vol. 51, no. 2, pp. 121-130, 2005.

[86] S. M. Haas, M. G. Frei, I. Osorio, B. Pasik-Duncan, and J. Radel, "EEG ocular artifact removal through armax model system identification using extended least squares", *Communications in information and systems*, vol. 3, no. 1, pp. 19-40, 2003.

[87] P. Berg and M. Scherg, "Dipole modeling of eye activity and its application to the removal of eye artifacts from the eeg and meg", *Clinical Physics and Physiological Measurement*, vol. 12 pp. 49-54, 1991.

[88] G. Nolte and M. S. Hamalainen, "Partial signal space projection for artefact removal in MEG measurements: a theoretical analysis", *Physics in medicine and biology*, vol. 46, no. 11, pp. 2873-2887, 2001.

[89] R. R. Gharieb and A. Cichocki, "Segmentation and tracking of the electro-encephalogram signal using an adaptive recursuve bandpass filter", *Medical & biological engineering & computing*, vol. 39 pp. 237-248, 2001.

[90] W. Philips, "Adaptive noise removal from biomedical signals using warped polynomials", *IEEE Transactions on biomedical engineering*, vol. 43, no. 5, pp. 480-492, 1996.

[91] P. K. Sadasivan and D. N. Dutt, "ANC schemes for the enhancement of EEG signals in the presence of EOG artifacts", *Computers and biomedical research*, vol. 29, no. 1, pp. 27-40, 1996.

[92] S. Selvan and R. Srinivasan, "Removal of ocular artifacts from EEG using an efficient neural network based adaptive filtering technique", *Ieee Signal Processing Letters*, vol. 6, no. 12, pp. 330-332, 1999.

[93] R. R. Gharieb and A. Cichocki, "Noise reduction in brain evoked potentials based on third-order correlations", *IEEE Transactions on biomedical engineering*, vol. 48, no. 5, pp. 501-512, 2001.

[94] M. R. Ford, S. Sands, and H. L. Lew, "Overview of artifact reduction and removal in evoked potential and event-related potential recordings", *Physical Medicine and Rehabilitation Clinics of North America*, vol. 15 pp. 1-17, 2004.

[95] T. W. Picton, P. van Roon, M. L. Armilio, P. Berg, N. Ille, and M. Scherg, "The correction of ocular artifacts: a topographic perspective", *Clinical Neurophysiology*, vol. 111, no. 1, pp. 53-65, 2000.

[96] P. He, M. Kahle, G. Wilson and C. Russel, "Removal of ocular artifacts grom EEG: A comparison of adaptive filtering method and regression method using simulated data", *Proceedings of the 2005 IEEE Engineering in medicine and biology 27th annual conference* . 2005.

[97] J. L. Kenemans, P. C. M. Molenaar, M. N. Verbaten, and J. L. Slangen, "Removal of ocular artefacts from the EEG: A comparison of time and frequency domain methods with simulated and real data", *Psychophysiology*, vol. 28, no. 1, pp. 114-121, 1991.

[98] T. P. Jung, C. Humphries, T. W. Lee, S. Makeig, M. J. McKeown, V. Iragui, and T. J. Sejnowski, "Removing Electroencephalographic artifacts: Comparison between ICA and PCA", *Neural Networks for signal processing*, pp. 63-72, 1998.

[99] G. Ivanova, M. E. Kirlangic, D. Perez, M. Kisser and G. Henning, "Method of ocular artifact correction of cognitive electrophysiological signals", *Proceedings of the 25th annual international conference of the IEEE-EMBS*, 2499-2502. 2003.

[100] A. C. Tang, M. T. Sutherland, and C. J. McKinney, "Validation of SOBI components from high-density EEG", *Neuroimage*, vol. 25, no. 2, pp. 539-553, 2005.

[101] H. J. Wieringa, *MEG, EEG and the integration with magnetic resonance images*, PhD Thesis, Twente University, Enschede: 1993.

[102] J. J. M. Kierkels, G. J. M. van Boxtel, and L. L. M. Vogten, "A model-based objective evaluation of eye movement correction in EEG recordings", *IEEE Transactions on biomedical engineering*, vol. 53, no. 2, pp. 246-253, 2006.

[103] J. J. M. Kierkels, J. Riani, J. W. M. Bergmans, and G. J. M. van Boxtel, "Using an eye tracker for accurate eye movement artifact correction", *IEEE Transactions on biomedical engineering*, vol. 54, no. 7, pp. 1256-1267, 2007.

[104] P. Berg and M. Scherg, "Dipole models of eye movements and blinks", *Electroencephalography and Clinical Neurophysiology*, vol. 79 pp. 36-44, 1991.

[105] M. S. Hamalainen, R. Hari, R. J. Ilmoniemi, J. Knuutila, and O. V. Lounasmaa, "Magnetoencephalography - theory, instrumentation, and applications to noninvasive studies of the working human brain", *Reviews on Modern Physics*, vol. 65, no. 2, pp. 413-497, 1993.

[106] R. Verleger, "Should we really use different estimates for correcting EEG artefacts produced by blinks and by saccades?", *Journal of psychophysiology*, vol. 14, no. 4, pp. 204-206, 2000.

[107] T. F. Oostendorp and A. van Oosterom, "Source parameter estimation in inhomogeneous volume conductors of arbitrary shape", *IEEE Transactions on biomedical engineering*, vol. 36, no. 3, pp. 382-391, 1989.

[108] C. Bradley and A. Pullan, "Application of BEM in biopotential problems", *Engineering Analysis with Boundary Elements*, vol. 26 pp. 391-403, 2002.

[109] R. Hoekema, G. H. Wieneke, F. S. S. Leijten, C. W. M. van Veelen, P. C. van Rijen, G. J. M. Huiskamp, J. Ansems, and A. C. van Huffelen, "Measurement of the conductivity of skull, temporarily removed during epilepsy surgery", *Brain topography*, vol. 16, no. 1, pp. 29-38, 2003.

[110] J. B. Nixon, P. E. Rasser, M. D. Teubner, C. R. Clark, and M. J. Bottema, "Numerical model of electrical potential within the human head", *International journal for numerical methods in engineering*, vol. 56 pp. 2353-2366, 2003.

[111] Advanced Source Analysis Software, ANT-software. [Online], Available: http://www.ant-software.nl. 2007.

[112] M. F. Marmor and E. Zrenner, "Standard for clinical electrooculography", *Documenta Ophthalmologica*, vol. 85, no. 2, pp. 115-124, 1993.

[113] S. de Brouwer, D. Yuksel, G. Blohm, M. Missal, and P. Lefevre, "What triggers catch-up saccades during visual tracking?", *Journal of neurophysiology*, vol. 87, no. 3, pp. 1646-1650, 2002.

[114] C. W. Hesse, E. Seiss, R. M. Bracewell, and P. Praamstra, "Absence of gaze direction effects on EEG measures of sensorimotor function", *Clinical Neurophysiology*, vol. 115, no. 1, pp. 29-38, Jan. 2004.

[115] A. Hyvarinen, "Survey on independent component analysis", *Neural computing surveys*, vol. 2 pp. 94-128, 1999.

[116] S. Chatterjee and A. S. Hadi, "Influential observations, high leverage points, and outliers in linear regression", *Statist. Sci.* 1986, pp. 379-416.

[117] G. J. M. van Boxtel, "Computational and statistical methods for analyzing event-related potential data", *Behavior Research Methods, instruments & computers*, vol. 30, no. 1, pp. 87-102, 1998.

[118] A. Hyvarinen and E. Oja, "Independent component analysis: A tutorial", *Neural networks*, 1999.

[119] Z. Akalin-Acar and N. G. Gencer, "An advanced bounary element method (BEM) implementation for the forward problem of electromagnetic source imaging", *Physics in medicine and biology*, vol. 49 pp. 5011-5028, 2004.

[120] F. Matsuo, J. F. Peters, and E. L. Reilly, "Electrical phenomena associated with movements of the eyelid", *Electroencephalography and Clinical Neurophysiology*, vol. 38 pp. 507-511, 1975.

[121] K. G. Rottach, V. E. Das, W. Wohlgemuth, A. Z. Zivotofsky, and R. J. Leigh, "Properties of horizontal saccades accompanied by blinks", *Journal of neurophysiology*, vol. 79, no. 6, pp. 2895-2902, 1998.

[122] D. Simon, "Kalman Filtering", *Embedded Systems Programming*, vol. 14, no. 6, pp. 72-79, 2001.

[123] R. G. Brown and P. Y. C. Hwang, *Introduction to random signals analysis and applied Kalman filtering : with MATLAB exercises and solutions*, New York: Wiley, 1997.

[124] M. T. Sutherland, J. Y. Liu and A. C. Tang, "Temporal delays in blind identification of primary somatosensory cortex", *Proceedings of the third international conference on machine learning and cybernetics* . 2004.

[125] S. A. Hillyard and R. Galambos, "Eye movement artifact in the CNV", *Electroencephalography and Clinical Neurophysiology*, vol. 28 pp. 173-182, 1970.

[126] H. V. Semlitsch, P. Anderer, P. Schuster, and O. Presslich, "A solution for reliable and valid reduction of ocular artifacts, applied to the P300 ERP", *Psychophysiology*, vol. 23, no. 6, pp. 695-703, 1986.

[127] R. Verleger, T. Gasser, and J. Mocks, "Correction of eog artifacts in event-related potentials of the eeg - aspects of reliability and validity", *Psychophysiology*, vol. 19, no. 4, pp. 472-480, 1982.

[128] A. Schlogl, C. Keinrath, D. Zimmermann, R. Scherer, R. Leeb, and G. Pfurtscheller, "A fully automated correction method of EOG artifacts in EEG recordings", *Clinical Neurophysiology*, vol. 118 pp. 98-104, 2007.

[129] E. Donchin, "A multivariate approach to analysis of average evoked potentials", *IEEE Transactions on biomedical engineering*, vol. 13, no. 3, pp. 131-139, 1966.

[130] R. N. Vigario, "Extraction of ocular artefacts from EEG using independent component analysis", *Electroencephalography and Clinical Neurophysiology*, vol. 103, no. 3, pp. 395-404, 1997.

[131] A. O. DiScenna, V. Das, A. Z. Zivotofsky, S. H. Seidman, and R. J. Leigh, "Evaluation of a video tracking device for measurement of horizontal and vertical eye rotations during locomotion", *Journal of neuroscience methods*, vol. 58, no. 1-2, pp. 89-94, 1995.

[132] M. Takagi, M. Katoh, K. Mohri, and S. Yoshino, "Magnet displacement sensor using MI elements for eyelid movement sensing", *Ieee Transactions on Magnetics*, vol. 29, no. 6, pp. 3340-3342, 1993.

[133] F. VanderWerf, P. Brassinga, D. Reits, M. Aramideh, and B. O. de Visser, "Eyelid movements: Behavioral studies of blinking in humans under different stimulus conditions", *Journal of neurophysiology*, vol. 89, no. 5, pp. 2784-2796, 2003.

[134] R. Naatanen, S. Pakarinen, T. Rinne, and R. Takegata, "The mismatch negativity (MMN): towards the optimal paradigm", *Clinical Neurophysiology*, vol. 115 pp. 140-144, 2004.

[135] E. D. Guestrin and M. Eizenman, "General theory of remote gaze estimation using the pupil center and corneal reflections", *IEEE Transactions on biomedical engineering*, vol. 53, no. 6, pp. 1124-1133, 2006.

[136] J. M. Findlay, "Magnitude of translational head movements", *Optica Acta*, vol. 16, no. 1, pp. 65-&, 1969.

[137] W. P. M. v. d. Wildenberg, *Perspectives on stopping behavior : process analyses of stop-signal inhibition*, PhD Thesis, Universiteit van Amsterdam, Amsterdam: Printpartners Ipskamp B.V., 2003.

[138] G. J. M. van Boxtel, M. W. van der Molen, J. R. Jennings, and C. H. M. Brunia, "A psychophysiological analysis of inhibitory motor control in the stop-signal paradigm", *Biological Psychology*, vol. 58 pp. 229-262, 2001.

[139] K. H. Knuth, A. S. Shah, W. A. Truccolo, M. Z. Ding, S. L. Bressler, and C. E. Schroeder, "Differentially variable component analysis: Identifying multiple evoked components using trial-to-trial variability", *Journal of neurophysiology*, vol. 95, no. 5, pp. 3257-3276, 2006.

[140] G. D. Logan and W. B. Cowan, "On the ability to inhibit thought and action - a theory of an act of control", *Psychological Review*, vol. 91, no. 3, pp. 295-327, 1984.

[141] M. Schmajuk, M. Liotti, L. Busse, and M. G. Woldorff, "Electrophysiological activity underlying inhibitory control processes in normal adults", *Neuropsychologia*, vol. 44, no. 3, pp. 384-395, 2006.

[142] P. Jaskowski and R. Verleger, "Amplitudes and latencies of single-trial ERP's estimated by a maximum-likelihood method", *IEEE Transactions on biomedical engineering*, vol. 46, no. 8, pp. 987-993, 1999.

[143] M. Morisita and T. Yagi, "The stability of human eye orientation during visual fixation and imagined fixation in three dimensions", *Auris Nasus Larynx*, vol. 28, no. 4, pp. 301-304, 2001.

[144] L. Parra, C. Alvino, A. Tang, B. Pearlmutter, N. Yeung, A. Osman, and P. Sajda, "Linear spatial integration for single-trial detection in encephalography", *Neuroimage*, vol. 17, no. 1, pp. 223-230, 2002.

[145] T. P. Jung, S. Makeig, M. Westerfield, J. Townsend, E. Courchesne, and T. J. Sejnowski, "Analyzing and Visualising Single-Trial Event-Related Potentials", *Advances in neural information processing systems*, vol. 11 pp. 118-124, 1999.

[146] B. Kolman and D. R. Hill, *Introductory linear algebra : with applications*, 6 ed. New York: Macmillan, 1997.

[147] V. D. Calhoun, T. Adali, G. D. Pearlson, and J. J. Pekar, "Spatial and temporal independent component analysis of functional MRI data containing a pair of task-related waveforms", *Hum.Brain Mapp.*, vol. 13, no. 1, pp. 43-53, 2001.

Symbols

Symbol		First appears in Chapter
α	'propagation factor', relating $y(t)$ to $x(t)$	1
$\hat{\alpha}$	estimate of α	1
$\underline{\alpha}$	vector with several α_i e.g., $[\alpha_1, \alpha_2, \alpha_3]^T$	1
$\hat{\underline{\alpha}}$	estimate of $\underline{\alpha}$	3
β	contribution of a cerebral source to r	1
γ	contribution of an artifact source to r	1
$\hat{\gamma}$	estimate of γ	1
$\hat{\Gamma}_b(t)$	asymmetric peak approximation of the b^{th} blink in the EOG	4
$\varepsilon(t)$	artifact electrical activity	1
$\eta(t)$	noise signal	1
$\underline{\kappa}(t)$	Kalman gains	3
λ	Eigen value	1
μ	auto-correlation between elements of $\underline{n}$	1
$\hat{\mu}$	estimate of μ	1
${\xi^1}_b, {\xi^2}_b, {\xi^3}_b, {\xi^4}_b$	four parameters defining the shape of the b^{th} blink in $\hat{\Gamma}_b(t)$	4
$\underline{\underline{\Pi}}(t)$	a posteriori estimate error covariance of $\underline{\phi}(t)$	3
σ	conductivity	2
${\sigma_{\underline{X}}}^2$	diag($\underline{\underline{Q}}$)	3
${\sigma_{X3}}^2$	third diagonal element of $\underline{\underline{Q}}$	3
$\underline{\underline{\Sigma}}$	covariance matrix	1
$\underline{\underline{\Sigma}}(\tau)$	covariance matrix for delay signals	1
τ	delay	1
τ_w	constant delay	3

$\phi_1(t)$, $\phi_2(t)$,....	parameters 1,2, ... in relation between $e(t)$ and $\underline{p}(t)$	3
$\underline{\phi}(t)$	vector with parameters $\phi_1(t), \phi_2(t)$,....	3
$\underline{\hat{\phi}}(t)$	estimate of $\underline{\phi}(t)$	3
$\underline{\underline{\Phi}}$	Matrix defining expected changes in $\underline{\phi}(t)$	3
$\underline{\Psi}$	Vector containing representations of $\underline{p}(t)$	3
ω	angular frequency	3
$\underline{\underline{A}}$	scaling matrix, used for sphering	1
b	blink index number	4
B	total number of blinks in recording	4
B_T	threshold value for blink detection	4
$b_m(t)$	background electrical brain activity during m^{th} stimulus	5
$c(t)$	cerebral electrical activity	1
$\underline{\hat{c}}$	vector with estimates of cerebral electrical activity	1
$\underline{\underline{\hat{C}}}$	matrix with several $\underline{\hat{c}}_i$	1
d_m	maximum amplitude of $\underline{p}(t)$	3
D	noise order in AR model	1
$e(t)$	ocular electrical activity	3
$\underline{\hat{e}}$	vector with estimates of artifact electrical activity	1
$\underline{\underline{\hat{E}}}$	matrix with several $\underline{\hat{e}}_i$	1
$f_m(t)$	electrical brain activity related to the m^{th} stimulus	5
$\hat{f}_m(t)$	estimate of $f_m(t)$	5
$\hat{f}(t)$	trial-averaged ERP	5
F_b	blink frequency	4
g	SNR gain	2
G	indicator for performance of a correction algorithm	2
i	electrode number (subscript)	1
$\underline{\underline{I}}$	identity matrix	1

j	single-person measure for amount of ocular artifact	5
J	multi-person yardstick for the amount of ocular artifact	5
K	number of ocular artifact sources	1
M	number of trials	5
$n(t)$	noise signal	1
$\underline{n}$	vector with multiple $n(t)$ values	1
$\hat{\underline{n}}$	estimate of $\underline{n}$	1
N	number of electrodes	1
$p_1(t)$	pupil position (horizontal)	3
$p_2(t)$	pupil position (vertical)	3
$p_3(t)$	eyelid position	4
$\hat{p}_3(t)$	EOG-based estimate of eyelid position	4
$\underline{p}(t)$	vector with pupil (and eyelid) positions	3
$\hat{\underline{p}}(t)$	vector with pupil and EOG-based eyelid	4
$P(..)$	trial-power	5
P_0	$P(r_m - \hat{f}_m)$, averaged over all trials in the OA^0 category	5
P_-	$P(r_m - \hat{f}_m)$, averaged over all trials in the OA^- category	5
P_+	$P(r_m - \hat{f}_m)$, averaged over all trials in the OA^+ category	5
P_{REF}	trial-averaged estimate for background EEG power	5
$\underline{\underline{Q}}$	expected co-variances of $\underline{w}(t)$	3
R	expected variance of $c(t)$	3
$r(t)$	raw EEG	1
$r_m(t)$	raw EEG during trial m	5
$s(t)$	signal of interest	3
S_{BA}	set of blink artifact time indices	4
SNR_r	signal-to-noise ratio based on $r(t)$	2
SNR_c	signal-to-noise ratio based on $\hat{c}(t)$	2

SNR_1	signal-to-noise ratio measure	4
SNR_2	signal-to-noise ratio measure for blinks	4
t	time index	1
T	maximum value of t in an interval/recording	1
t_1	start of recording	3
T_w	duration of dataset	3
$u(t)$	short notation for $c(t) - \hat{c}(t)$	3
$\underline{w}(t)$	fluctuations in $\underline{\phi}(t)$	3
$\underline{\underline{W}}$	mixing matrix for components analysis	1
$\underline{\underline{W}}^{\#}$	changed mixing matrix for artifact removal	1
$x(t)$	signal	1
$\underline{x}$	vector with multiple $x(t)$ values	1
$\underline{\underline{X}}$	matrix with several $\underline{x}_i$, e.g., $[\underline{x}_1, \underline{x}_2, \underline{x}_3]$	1
$y(t)$	signal	1
$\underline{y}$	vector with multiple $y(t)$ values	1
$\underline{\underline{Y}}$	matrix with several $\underline{y}_i$	1
$z(t)$	component	1
$\underline{z}$	vector with multiple $z(t)$ values	1
$\underline{\underline{Z}}$	matrix with several $\underline{z}_i$, e.g., $[\underline{z}_1, \underline{z}_2, \underline{z}_3]$	1
*	referring to data *after* correction	5

Summary

Validating and Improving the Correction of Ocular Artifacts in Electro-encephalography

For modern applications of electro-encephalography, including brain computer interfaces and single-trial Event Related Potential detection, it is becoming increasingly important that artifacts are accurately removed from a recorded electro-encephalogram (EEG) without affecting the part of the EEG that reflects cerebral activity.

Ocular artifacts are caused by movement of the eyes and the eyelids. They occur frequently in the raw EEG and are often the most prominent artifacts in EEG recordings. Their accurate removal is therefore an important procedure in nearly all electro-encephalographic research. As a result of this, a considerable number of ocular artifact correction methods have been introduced over the past decades. A selection of these methods, which contains some of the most frequently used correction methods, is given in Section 1.5.

When two different correction methods are applied to the same raw EEG, this usually results in two different corrected EEGs. A measure for the accuracy of correction should indicate how well each of these corrected EEGs recovers the part of the raw EEG that truly reflects cerebral activity. The fact that this accuracy cannot be determined directly from a raw EEG is intrinsic to the need for artifact removal. If, based on a raw EEG, it would be possible to derive an exact reference on what the corrected EEG should be, then there would not be any need for adequate artifact correction methods.

Estimating the accuracy of correction methods is mostly done either by using models to simulate EEGs and artifacts, or by manipulating the experimental data in such a way that the effects of artifacts to the raw EEG can be isolated.

In this thesis, modeling of EEG and artifact is used to validate correction methods based on simulated data. A new correction method is introduced which, unlike all existing methods, uses a camera to monitor eye(lid) movements as a basis for ocular artifact correction. The simulated data is used to estimate the accuracy of this new correction method and to compare it against the estimated accuracy of existing correction methods. The results of this comparison suggest that the new method significantly increases correction accuracy compared to the other methods. Next, an experiment is performed,

based on which the accuracy of correction can be estimated on raw EEGs. Results on this experimental data comply very well with the results on the simulated data. It is therefore concluded that using a camera during EEG recordings provides valuable extra information that can be used in the process of ocular artifact correction.

In Chapter 2, a model is introduced that assists in estimating the accuracy of eye movement artifacts for simulated EEG recordings. This model simulates EEG and eye movement artifacts simultaneously. For this, the model uses a realistic representation of the head, multiple dipoles to model cerebral and ocular electrical activity, and the boundary element method to calculate changes in electrical potential at different positions on the scalp. With the model, it is possible to simulate different data sets as if they are recorded using different electrode configurations. Signal to noise ratios are used to assess the accuracy of these six correction methods for various electrode configurations before and after applying six different correction methods. Results show that out of the six methods, second order blind identification, SOBI, and multiple linear regression, MLR, correct most accurately overall as they achieve the highest rise in signal to noise ratio.

The occurrence of ocular artifacts is linked to changes in eyeball orientation. In Chapter 2 an eye tracker is used to record pupil position, which is closely linked to eyeball orientation. The pupil position information is used in the model to simulate eye movements.

Recognizing the potential benefit of using an eye tracker not only for simulations, but also for correction, Chapter 3 introduces an eye movement artifact correction method that exploits the pupil position information that is provided by an eye tracker. Other correction methods use the electro-oculogram (EOG) and/or the EEG to estimate ocular artifacts. Because both the EEG and the EOG recordings are susceptive to cerebral activity as well as to ocular activity, these other methods are at risk of overcorrecting the raw EEG. Pupil position information provides a reference that is linked to the ocular artifact in the EEG but that cannot be affected by cerebral activity, and as a result the new correction method avoids having to solve traditionally problematic issues like forward/backward propagation and evaluating the accuracy of component extraction.

By using both simulated and experimental data, it is determined how pupil position influences the raw EEG and it is found that this relation is linear or quadratic. A Kalman filter is used for tuning of the parameters that specify the relation. On simulated data, the new method performs very well, resulting in an SNR after correction of over 10 dB for various patterns of eye movements. When compared to the three methods that performed best in the evaluation of

Chapter 2, only the SOBI method which performed best in that evaluation shows similar results for some of the eye movement patterns. However, a serious limitation of the correction method is its inability to correct blink artifacts.

In order to increase the variety of applications for which the new method can be used, the new correction should be improved in a way that enables it to correct the raw EEG for blinking artifacts. Chapter 4 deals with implementing such improvements based on the idea that a more advanced eye-tracker should be able to detect both the pupil position and the eyelid position. The improved eye tracker-based ocular artifact correction method is named EYE. Driven by some practical limitations regarding the eye tracking device currently available to us, an alternative way to estimate eyelid position is suggested, based on an EOG recorded above one eye. The EYE method can be used with both the eye tracker information or with the EOG substitute.

On simulated data, accuracy of the EYE method is estimated using the EOG-based eyelid reference. This accuracy is again compared against the six other correction methods. Two different SNR-based measures of accuracy are proposed. One of these quantifies the correction of the entire simulated data set and the other focuses on those segments containing simulated blinking artifacts. After applying EYE, an average SNR of at least 9 dB for both these measures is achieved. This implies that the power of the corrected signal is at least eight times the power of the remaining noise. The simulated data sets contain a wide range of eye movements and blink frequencies. For almost all of these data sets, 16 out of 20, the correction results for EYE are better than for any of the other evaluated correction method. On experimental data, the EYE method appears to adequately correct for ocular artifacts as well. As the detection of eyelid position from the EOG is in principle inferior to the detection of eyelid position with the use of an eye tracker, these results should also be considered as an indicator of even higher accuracies that could be obtained with a more advanced eye tracker. Considering the simplicity of the MLR method, this method also performs remarkably well, which may explain why EOG-based regression is still often used for correction.

In Chapter 5, the simulation model of Chapter 2 is put aside and, alternatively, experimentally recorded data is manipulated in a way that correction inaccuracies can be highlighted. Correction accuracies of eight correction methods, including EYE, are estimated based on data that are recorded during stop-signal tasks. In the analysis of these tasks it is essential that ocular artifacts are adequately removed because the task-related ERPs, are located mostly at frontal electrode positions and are low-amplitude. These data are corrected and subsequently evaluated. For the eight methods, the overall ranking of estimated accuracy in Figure 5.3, corresponds very well with the

correction accuracy of these methods on simulated data as was found in Chapter 4. In a single-trial correction comparison, results suggest that the EYE corrected EEG, is not susceptible to overcorrection, whereas the other corrected EEGs are.

Samenvatting

Validating and Improving the Correction of Ocular Artifacts in Electro-encephalography

Voor moderne toepassingen van elektro-encefalografie, zoals brain-computer interfaces en single-trial analyses, is het van groot belang dat artefacten uit het elektro-encefalogram (EEG) verwijderd kunnen worden zonder dat de gemeten hersenactiviteit hierdoor wordt beïnvloed.

Oogartefacten worden veroorzaakt door bewegingen van de ogen en van de oogleden en komen veelvuldig voor in EEG-registraties. Het nauwkeurig verwijderen van deze artefacten uit registraties is daarom een belangrijk aspect van vrijwel ieder EEG-onderzoek. Er zijn in de afgelopen jaren dan ook vele oogartefactcorrectiemethodes geïntroduceerd. De meest gangbare correctiemethodes worden behandeld in Sectie 1.5 van dit proefschrift.

Wanneer twee verschillende correctiemethodes worden gebruikt om dezelfde EEG registratie te corrigeren, zal dit meestal leiden tot twee verschillend gecorrigeerde EEGs. Om aan te kunnen geven welke van deze EEGs het beste de elektrische activiteit van de hersenen weergeeft, is een maatstaf nodig. Het feit dat deze maatstaf niet eenvoudig is af te leiden uit het gemeten EEG is intrinsiek aan het probleem van artefact correctie. Immers, wanneer het op basis van een gemeten EEG mogelijk zou zijn om een exacte maatstaf af te leiden, dan zou oogartefact correctie overbodig zijn. Het bepalen van zo'n maatstaf voor de nauwkeurigheid van verschillende correctiemethodes gebeurt meestal door gebruik te maken van gesimuleerde data, of door gemeten data dusdanig te manipuleren dat de aanwezigheid van artefacten naar voren gebracht wordt.

In dit proefschrift worden EEG-data gesimuleerd, om vervolgens correctiemethodes te valideren. Hierna wordt een geheel nieuwe correctiemethode geïntroduceerd die, in tegenstelling tot alle bestaande methodes, gebruik maakt van een eye-tracker om oog- en ooglidbewegingen te registreren. Deze registraties bieden waardevolle informatie bij het corrigeren van oogartefacten. Door gebruik te maken van gesimuleerde data wordt de nauwkeurigheid van de nieuwe correctiemethode vergeleken met de reeds bestaande methodes. De nieuwe correctiemethode blijkt significant nauwkeuriger dan bestaande methodes te zijn. Ook op (gemanipuleerde) gemeten EEG-data leidt de nieuwe correctiemethode tot aantoonbaar betere

correctie, waaruit wordt geconcludeerd dat de met een eye-tracker verkregen data een belangrijke bron van informatie vormen in het correctieproces.

In hoofdstuk 2 wordt een model gepresenteerd waarmee hersenactiviteit en oogbewegingen tegelijkertijd kunnen worden gesimuleerd. Hiertoe wordt gebruik gemaakt van een realistisch model van het hoofd, van een aantal dipool bronnen die de elektrische gevolgen van hersenactiviteit en oogbewegingen simuleren en van de 'boundary element method' waarmee de elektrische potentialen op de hoofdhuid als gevolg van de dipool bronnen kunnen worden bepaald. Met behulp van dit model kunnen EEG-metingen worden gesimuleerd voor verschillende elektrode-configuraties. Enkele experimenten zijn uitgevoerd waarbij een eye-tracker is gebruikt om de pupil-positie te registreren. De zo verkregen informatie over oogbewegingspatronen is gebruikt om realiteitsgetrouwe oogbewegingen en artefacten te simuleren.

De gesimuleerde data worden vervolgens met diverse correctiemethodes opgeschoond. Hierna wordt voor iedere correctiemethode bepaald wat de signaal-ruis verhouding na opschoning is. Hieruit blijkt dat de second order blind identification methode (SOBI) en de multiple linear regression (MLR) methode de grootste stijging in signaal-ruis verhouding opleveren ten opzichte van het ongecorrigeerde signaal en dus het nauwkeurigst corrigeren.

Aangezien een eye-tracker in potentie niet alleen voor simulatie van data, maar ook voor correctie van data gebruikt kan worden, wordt in hoofdstuk 3 een correctiemethode geïntroduceerd die gebaseerd is op het meten van de pupil-positie. Aan de hand van de pupil-positie wordt de amplitude en de vorm het artefact in het EEG geschat. In tegenstelling tot het elektro-oculogram wat door bestaande correctiemethodes vaak wordt gebruikt om oogbewegingsartefacten te detecteren en corrigeren, kan de meting van pupil-positie niet worden beïnvloed door de elektrische gevolgen van hersenactiviteit. Hierdoor heeft een op pupil-positie gebaseerde correctiemethode als voordeel dat klassieke moeilijkheden die samenhangen met oogartefact correctie, bijvoorbeeld ten gevolge van forward/backward propagatie en component selectie, kunnen worden omzeild. Voor zowel gesimuleerde als voor gemeten EEGs wordt vervolgens vastgesteld dat de relatie tussen artefact-amplitude en pupil-positie kan worden beschreven met een eerste of tweede graads vergelijking. De parameters die bij deze vergelijkingen horen worden met behulp van een Kalman filter geschat. Wanneer de correctieresultaten worden vergeleken met de correctieresultaten voor de methodes uit hoofdstuk 2, blijkt dat alleen de SOBI methode een vergelijkbaar resultaat behaalt. Tevens wordt de nauwkeurigheid van verschillende correctiemethodes voor experimenteel verkregen data bekeken, waarbij een vergelijkbare correctie nauwkeurigheid wordt gevonden.

Een tekortkoming van de tot dusverre beschreven nieuwe correctiemethode is het feit dat oogknipperartefacten niet gecorrigeerd kunnen worden. In hoofdstuk 4 wordt de correctiemethode daarom uitgebreid en wordt de mogelijkheid om oogknipperartefacten te corrigeren toegevoegd. Deze toevoeging is gebaseerd op het idee dat het in de nabije toekomst mogelijk zal zijn om met meer geavanceerde eye-trackers ook de ooglid-positie te registreren. Gedwongen door de beperkingen van onze huidige eye-tracker, wordt een alternatieve manier voor detectie van ooglidbewegingen aangedragen. Dit alternatief is gebaseerd op registratie van oogknippers door gebruik te maken van een EOG elektrode, geplaatst boven het oog. De nieuwe correctiemethode, EYE, kan ofwel worden gebruikt met de eye-tracker, ofwel met de EOG elektrodes, om de ooglidpositie te detecteren. Met behulp van gesimuleerde data wordt de nauwkeurigheid van de EYE methode, met gebruik van de EOG elektrode, bepaald. Deze nauwkeurigheid wordt wederom vergeleken met die van zes bestaande methodes. Hiertoe worden twee verschillende maatstaven gedefinieerd. De eerste hiervan is gebaseerd op de signaal-ruis verhouding van het gehele gecorrigeerde EEG en de tweede is alleen gebaseerd op de signaal-ruis verhouding van die segmenten uit het EEG waarin een oogknipperartefact gedetecteerd wordt. Na correctie met EYE is de signaal-ruis verhouding volgens beide maatstaven minimaal 9 dB, wat aangeeft dat in het gecorrigeerde signaal het vermogen van de ruis acht keer lager is dan het vermogen van het relevante signaal.

Meerdere datasets, met verschillende typen oogbewegingen en met verschillende oogknipper frequentie, zijn gesimuleerd en voor vrijwel al deze datasets, 16 uit 20, is de uiteindelijke signaal-ruis verhouding na EYE-correctie hoger dan na toepassing van de reeds bestaande correctiemethodes. Aangezien EOG-gebaseerde detectie van ooglid positie in principe minder accuraat is dan eye-tracker gebaseerde detectie, zal de nauwkeurigheid van correctie waarschijnlijk nog verder toenemen indien een geavanceerde eye-tracker voor detectie wordt gebruikt.

In hoofdstuk 5 worden experimentele data gebruikt om de correctiemethodes te valideren. Voor acht verschillende correctiemethodes, waaronder EYE, wordt de nauwkeurigheid van correctie bepaald aan de hand van EEG-data gemeten tijdens stop-taken. Aangezien de aan deze taak gerelateerde hersenactiviteit en event-related-potentials (ERPs) vooral frontaal optreden en slechts een lage amplitude hebben, is het juist voor deze ERPs essentieel dat alle oogartefacten nauwkeurig worden verwijderd. De gevonden correctie nauwkeurigheid voor de acht correctiemethodes, te zien in Figuur 5.3, komt overeen met de in Hoofdstuk 4 gevonden nauwkeurigheden op gesimuleerde data. In een vergelijking van de correctienauwkeurigheid op single-trial niveau

is te zien dat de EYE methode, in tegenstelling tot andere methodes, niet overcorrigeert en dus de ERPs in tact laat bij de correctie.

Dankwoord

Aan het eind gekomen van mijn promotietraject, een voltooid proefschrift en veel ervaring rijker, wil ik graag iedereen bedanken die mij gedurende dit traject heeft gesteund.

Allereerst wil ik uiteraard mijn copromotor dr. Geert van Boxtel en mijn promotor prof. dr. ir. Jan Bergmans bedanken. Geert, jij liet mij kennis maken met de psychofysiologie en wist altijd met groot enthousiasme uit te weiden over de processen die aan de EEG metingen ten grondslag liggen. Wat me ook zeker zal bijblijven is de grote wirwar van kabels die tijdens de experimenten ontstond wanneer we alle computers op de juiste manier wilden aansturen. Jan, telkens weer stond ik ervan te kijken hoe snel tijdens onze besprekingen een lastig voorkomend probleem plotseling veranderde in een mooi gestructureerd schema met diverse oplossingen. Jouw kennis en sturing zijn zeker gedurende de tweede helft van mijn promotietraject onmisbaar geweest. In aanvulling hierop wil ik ook dr.ir. Leo Vogten bedanken die, tot zijn afscheid op de TU/e, bijna wekelijks kritisch mijn vorderingen volgde.

Soms was het lastig om experimenten in te plannen omdat meetapparatuur niet altijd beschikbaar was. Ik wil dr. ir. Pierre Cluitmans bedanken voor het beschikbaar stellen van apparatuur, voor de inhoudelijke discussies die we hadden én voor zijn hulp bij het slepen van tafels, stoelen, computers enzovoorts. Uiteraard bedank ik ook alle proefpersonen, voor het belangeloos 'beschikbaar stellen' van hun hersenactiviteit.

Een goede werksfeer is natuurlijk essentieel om gedurende meerdere jaren enthousiast onderzoek te blijven doen. Alle vaste medewerkers en afstudeerders van de SPS groep wil ik dan ook bedanken voor hun betrokkenheid, hulp en gezellige gesprekken tijdens de lunch en tijdens werktijd. Een apart groepje wordt al snel gevormd door collega-promovendi, met wie de fake-SPS events vaak uitdraaiden op late avonden in de kroeg. Andrej, Arijit, Chiara, Emanuël, Jamal, Massimo, Suzanne, Tamara en ook Harald en Pedro, jullie waren fantastische collega's! Collega promovendus en kamergenoot Tanya mag in dit rijtje ook zeker niet ontbreken. Ruim drie jaar lang hadden we vele discussies over de meest uiteenlopende onderwerpen, van gezondheidszorg tot teckels, gezichtsoliën en reisbestemmingen. Ik had geen betere kamergenoot kunnen treffen!

Naast het onderzoek en de universiteit was er gelukkig ook nog tijd voor vrienden, sport, muziek en ontspanning. Linda, Evelyne, Pim, Leon, bedankt voor de gezellige etentjes en koffiebreaks. Promotie perikelen kunnen delen

was vaak een opluchting. Mathijs, Hubert, Bas, Roel, Geert S, Geert V, Mark V en Joep, bedankt voor de gezellige weekenden, barbecues en voetbalwedstrijden. Mark M zorgde, net als de leden van BC Geldrop, altijd voor een sportieve uitdaging, waarbij de drang om te presteren werd vergroot door de verwedde flessen bier. Jules wil ik natuurlijk bedanken voor zijn steun en voor zijn bijdrage aan de lay-out van dit proefschrift.

Bijna aan het eind gekomen van dit dankwoord wil ik ook pap, mam en Tom bedanken voor hun steun en vertrouwen, niet alleen tijdens dit promotietraject maar een leven lang.

En tenslotte Paulien, natuurlijk zijn de laatste regels in dit dankwoord voor jou. Zonder jou waren de afgelopen jaren veel zwaarder geweest. Bedankt voor alle liefde, kritiek, hulp, aanmoedigingen en opbeuringen, bedankt voor ... alles!!

Curriculum Vitae

Joep Kierkels was born on June 18th, 1979 in Baexem, the Netherlands. After finishing secondary school (VWO) in Horn in 1997, he moved to Eindhoven to study Biomedical Engineering at the Eindhoven University of Technology (TU/e). In 2000, he received the B.Sc. degree in Biomedical Engineering and later, in 2002, the M.Sc. degree in Biomedical engineering from the TU/e. During his studies, in 2001, he did an internship on 'trend-detection in EEG recordings during cardiac surgery' at CITY University in London, UK, which sparked his interest in EEG measurements and analysis. His M.Sc. graduation project focussed on the 'measurement and modeling of muscle motor-unit conduction velocity', and was performed in the Control Systems group of the department the Electrical Engineering at the TU/e. From 2002 to 2007, he pursued his Ph.D. degree in the Signal Processing Systems group at the department of Electrical Engineering at the TU/e. The Ph.D. project, which is reported in this thesis, was carried out in close collaboration with the department of Psychology and Health at the University of Tilburg (UvT). At the end of this Ph.D. project, he worked as a visiting researcher at the Biomedical Engineering department of Zhejiang University, China.